UNIVERSITEIT VAN PRETORIA
UNIVERSITY OF PRETORIA
YUNIBESITHI YA PRETORIA

Antibacterial activity of synthetic peptide W_5(Os-C) against *Staphylococcus epidermidis* ATCC 35984

By

Lize Janeska van Heerden

13061934

Supervisor: Prof Anabella RM Gaspar (Division Biochemistry)

Co-supervisor: Prof Megan J Bester (Department of Anatomy)

Submitted in fulfilment of the degree

MSc (Biochemistry)

in the Faculty of Natural and Agricultural Sciences

University of Pretoria

Date: 15 February 2024

Declaration

I, Lize Janeska van Heerden, declare that this dissertation, which I hereby submit for the degree MSc (Biochemistry), at the University of Pretoria, is my own work and has not been previously submitted for a degree at this or any other tertiary institution.

..... 24/05/2023.....

SIGNATURE **DATE**

Plagiarism declaration:

UNIVERSITY OF PRETORIA

FACULTY OF NATURAL AND AGRICULTURAL SCIENCES

DEPARTMENT OF BIOCHEMISTRY, GENETICS AND MICROBIOLOGY

Full name: Lize Janeska van Heerden Student number: 13061934

Title of the work: Antibacterial activity of synthetic peptide W_5(Os-C) against *Staphylococcus epidermidis* ATCC 35984

1. I understand what plagiarism is and am aware of the University's policy is in this regard.
2. I declare that this dissertation is my own original work. Where other people's work has been used (either from a printed source, Internet or any other source), this has been properly acknowledged and referenced in accordance with departmental requirements.
3. I have not used work previously produced by another student or any other person to hand in as my own.
4. I have not allowed and will not allow anyone to copy my work with the intention of passing it off as his or her own work.

SIGNED:  **DATE:** 24/05/2023

Acknowledgements

I would like to thank the following:

- My supervisors, Prof ARM Gaspar and Prof MJ Bester, for their wisdom, patience, guidance, and encouragement to strive for excellence. They have stood alongside me every step of the way and facilitated personal and scientific growth and discovery**.** They have been the best mentors any student could ask for. I am forever grateful for their help.

- Ms Sandra van Wyngaardt and Ms Sonya September for their assistance and training in the use of technical equipment. Also, for their dedication to the upkeep of the equipment and creating a safe, clean lab environment to work in.

- Dr J Serem and Dr H Taute for their advice, suggestions and encouragement to improve my work.

- All members of the Biotherapeutics research group, especially Mr CK Chiramba, for his advice and being a soundboard to discuss my progressing research with. Also Prof. Chris Lorenz and his team in the King's College London Department of Physics, as well as Ms M van der Walt and Mr D Möller for their assistance with the Molecular Dynamic Simulations.

- The National Research Foundation of South Africa and the University of Pretoria for funding of the research project.

- My family, especially my grandparents for their unwavering support, love, and financial contributions that made my completion of this project possible.

- My fellow scientist, Mr Reinhard Swart, for his facilitation of discussions of all matters to ensure this project is completed.

- My dear friend, Ms Tamzin J. Glass, for her encouragement, support, and for believing in me. Without her standing by my side, I would never have been able to achieve my goals.

- Above all I would like to thank God the Almighty who blessed me with the opportunity, the means, and the people that I would need to achieve this.

Table of Contents

Declaration i
Plagiarism declaration: i
Acknowledgements ii
Summary v
List of Tables vii
List of Figures viii
List of Abbreviations xi
1. INTRODUCTION 1
1.1. *Staphylococcus epidermidis* 3
1.1.1. Clinically relevant *S. epidermidis* drugs and antimicrobial resistance 4
1.1.2. Trends in antimicrobial resistance of *Staphylococcus spp* 7
1.1.3. Role of *S. epidermidis* in antimicrobial resistance 7
1.2. Biofilms 8
1.2.1. Biofilm structure and development in *Staphylococcus spp* 8
1.2.2. Combined biofilms 9
1.2.3. *S. epidermidis* biofilm development and contributions to antimicrobial resistance 10
1.3. Antimicrobial peptides 10
1.3.1. Structures of antimicrobial peptides 11
1.3.2. Antimicrobial peptides target cellular membranes 12
1.3.3. Other targets of antimicrobial peptides 14
1.3.4. Antimicrobial peptides as attractive antimicrobial agents against *S. epidermidis* 15
1.3.5. Antimicrobial resistance against antimicrobial peptides 15
1.3.6. Antimicrobial peptides used in combination therapies 16
1.4. Molecular dynamics simulations in antimicrobial research 18
1.5. Background information 20
1.6. Aim of the study 22
1.7. Objectives of the study 22
CHAPTER 2: MATERIALS AND METHODS 23
2.1. MATERIALS 23
2.1.1. *Staphylococcus epidermidis* (ATCC 35984) cultures 23
2.1.2. HaCat cell cultures 23
2.1.3. Biofilm promoting media (BPM) 23
2.1.4. Bacterial cell culture medium 23
2.1.5. Antimicrobial agents 24
2.1.5.1. W_5(Os-C) and melittin 24
2.1.5.2. Vancomycin 25
2.2 Methods 25
2.2.1 Growth curves of *S. epidermidis* (ATCC 35984) in different media 25
2.2.2 Anti-planktonic activity 25
2.2.2.1 Growth inhibition assays 25
2.2.2.2 Vancomycin and peptide combination anti-planktonic assay 26
2.2.3 Anti-biofilm activity 27
2.2.3.1 Optimisation of biofilm growth conditions 27
2.2.3.2 Biofilm inhibition assays 29
2.2.3.3 Vancomycin and W_5(Os-C) combination anti-biofilm assay 30
2.2.4 HaCat cytotoxicity 31
2.2.5 *In silico p*eptide characterisation 32

2.2.6 Statistical analysis 35
CHAPTER 3: RESULTS 36
3.1 Growth curve determination of *S. epidermidis* (ATCC 35894) 36
3.2 Antimicrobial activity 37
3.2.1 Anti-planktonic activity of W_5(Os-C) 37
3.2.2 Synergism studies of W_5(Os-C) and vancomycin against planktonic cells 39
3.3 Anti-biofilm activity 41
3.3.1 Biofilm growth optimisation and characterisation 41
3.3.2 Biofilm inhibitory activity of W_5(Os-C) 43
3.3.3 Synergism studies: W_5(Os-C) and vancomycin - biofilm inhibition 45
3.4 Keratinocyte (HaCat) Cytotoxicity 50
3.5 Peptide characterisation 51
3.5.1 Peptide structure and folding 51
3.5.2 Peptide to peptide interactions in the presence of a Gram-positive membrane 53
3.5.3 Peptide interactions with the Gram-positive membrane 56
3.5.4 Peptide dynamics in presence of a Gram-positive membrane 57
CHAPTER 4: DISCUSSION 60
4.1 Antimicrobial activity of W_5(Os-C) 60
4.2 Cytotoxicity of W_5(Os-C) against human keratinocytes 65
4.3 Molecular dynamics of W_5(Os-C) 65
CHAPTER 5: 69
CONCLUSION AND FUTURE PERSPECTIVES 69
REFERENCES 74

Summary

Nosocomial or healthcare associated infections (HAI) are of growing concern as antimicrobial resistance continues to increase globally. Nosocomial infections are increasingly caused by methicillin resistant *Staphylococcus epidermidis* (MRSE). Although most infections respond to vancomycin, vancomycin resistant *S. epidermidis* (VRSE) strains have been reported. Furthermore, methicillin resistance can be transferred between different *Staphylococcus* strains and these bacteria grow as biofilms on intravascular and urinary catheters, wound sites, as well as on medical implants. A need for new antibiotics to combat resistant infections is driving development of antimicrobial peptides (AMPs) as antibacterial drugs.

Current research strategies involve modifying existing antimicrobial drugs, shotgun screening compound libraries, rational drug design, and combinatory therapies. Antimicrobial peptides are viable options as antimicrobial drugs, due to broad spectrum of activity, low rate of resistance development, and multifunctionality. A challenge associated with the development of clinically relevant AMPs is loss of activity in physiological environments, which can be overcome by structural modifications such as tryptophan (Trp) end-tagging.

Prior to this study, synthetic peptide Os-C was derived from the C-terminal of the AMP, defensin OsDef2, identified in the soft tick *Ornithodoros savignyi*. Os-C was further tagged with five N-terminal Trp residues to overcome loss of activity in physiological environments, producing W_5(Os-C). The aim of this study was to determine for W_5(Os-C), the antimicrobial and anti-biofilm activity against Gram-positive *S. epidermidis* (ATCC 35984), potential synergism with vancomycin, cytotoxicity, and lastly to evaluate the interaction of W_5(Os-C) with a model Gram-positive membrane. For the antibacterial and anti-biofilm assays, vancomycin and melittin were used as positive controls. Vancomycin is a clinically relevant tricyclic antimicrobial agent used against *Staphylococcus*, *Streptococcus*, and *Enterococcus* infections. Melittin is a bee venom derived AMP, active against a wide range of bacterial and cancer cells *in vitro*, although it is not commonly used *in vivo* due to high cytotoxicity against host cells.

Against planktonic *S. epidermidis*, the minimum concentration of maximum inhibition (MIC_{max}) of vancomycin, melittin, and W_5(Os-C) were 3.83 µM, 8.67 µM, and 2.44 µM respectively. The MIC_{max} of W5(Os-C) was found to be significantly lower than that of vancomycin ($p<0.05$), with both vancomycin and W5(Os-C) MIC_{max} values significantly lower than that of melittin ($p<0.0001$). The minimum concentration of maximum biofilm inhibition (BIC_{max}) of vancomycin, melittin, and W_5(Os-C) were 3.81 µM, 9.04 µM, and 3.06 µM respectively for biomass

associated cell viability. The BIC_{max} values in terms of biomass development inhibition were 3.76 µM, undeterminable, and 3.07 µM respectively. Vancomycin, melittin, and W_5(Os-C) maximum inhibition of biomass and viable cells were >95%, >95%, and >80% respectively. Synergism was investigated for vancomycin and W_5(Os-C) at various ratios to increase vancomycin activity at less toxic concentrations but no synergism was observed. Neither vancomycin nor W_5(Os-C) exhibited cytotoxicity against human keratinocytes (HaCat) cells while melittin reduced viability by 70%.

Molecular dynamics simulations (MDSims) were used to better understand the interactions of the peptide with a model Gram-positive POPG membrane in physiologically relevant (0.15 M) and higher, *in vitro* relevant (0.30 M) NaCl environments. Increasing salt concentrations induced conformational changes in the peptide. In an aqueous environment, the peptide remained in an extended conformation at both 0.15 M and 0.30 M salt concentrations. Conformational changes were facilitated by glycine (Gly) residues and hydrophobic residue interactions. Peptide-peptide interactions decreased when salt concentrations increased which destabilized aggregates. At higher salt concentrations, W_5(Os-C) molecules alternated between no-, dipeptide-, and tripeptide aggregation while more stable dipeptide aggregates were formed in a lower salt environment. Peptide-POPG membrane interactions were characterized by Trp-tagged N-terminals inserting into the membrane and remaining fixed in an α-helical structure while the rest of the peptide moved freely outside the membrane in an extended conformation. Peptide insertion was facilitated by hydrogen bonding of the N-terminal amine group of lysine (Lys) and occasionally arginine (Arg) residues. Higher salt concentrations resulted in more hydrogen bonding and deeper insertion into the POPG membrane.

In conclusion, W_5(Os-C) was found to inhibit >90% of planktonic cell growth, but could not inhibit >90% biomass formation or biomass associated cell viability. These results should be confirmed in a wider range of sensitive and resistant strains of Gram-positive bacteria. Preliminary synergism studies with vancomycin and W_5(Os-C) indicated a decrease in anti-planktonic and -biofilm activity of vancomycin as the concentration of W_5(Os-C) increased. Thus the interactions between vancomycin and W_5(Os-C) as well as the modes of action of both antimicrobials should be investigated to improve synergism focused drug design. In addition, the MDSims as used in this study indicated few differences in peptide-peptide and peptide-membrane interactions at 0.15 M vs 0.30 M NaCl concentrations and can be used to design analogues of W_5(Os-C) with improved activity.

List of Tables

Table 1.1: Properties of defensins from *O savignyi*, OsDef1 and OsDef2, and derived AMPs. 21
Table 2.1: Properties of antimicrobial agents used in this study 24
Table 2.2: Preparation of combinations of vancomycin and W_5(Os-C). 27
Table 3.1: Analysis of the growth curves of *S. epidermidis* under various conditions used in this study. 37
Table 3.2: MIC_{50} and MIC_{max} values of vancomycin, melittin, and W_5(Os-C). 39
Table 3.3: MIC_{50} and MIC_{max} values of vancomycin, W_5(Os-C), and vancomycin and W_5(Os-C) in combination ratios 3V:1W, 2V:2W and 1V:3W. 41
Table 3.4: BIC_{50} and BIC_{max} values of vancomycin, melittin, and W_5(Os-C) in terms of cell viability inhibition (CTB) and biomass development inhibition (CV). 45
Table 3.5: BIC_{50} and BIC_{max} values of vancomycin, W_5(Os-C), and vancomycin and W_5(Os-C) in combination ratios 3V:1W, 2V:2W; and 1V:3W in terms of cell viability inhibition (CTB) and biomass development inhibition (CV). 49
Table 5.1: Summary of *in silico* investigation results. 73
Table 5.2: Summary of *in silico* investigation results. 73

List of Figures

Figure 2.1: Chemical structure of crystal violet. CV is a positively charged (basic), purple dye binding to negative charges on cell components (DNA, RNA, proteins, and phosphate groups) and is commonly used in biomass quantification. Structure drawn using ChemSketch (ACD/Labs). 28

Figure 2.2: Chemical reaction of resazurin and NADH. Cell titre blue (resazurin) is reduced by NADH, a product of metabolically active cells, to pink resorufin. This redox reaction is often used to test for cell viability after exposure to a potential antimicrobial agent. Structures drawn using ChemSketch (ACD/Labs). 29

Figure 2.3: The reaction of MMT with NADH. Yellow MTT is reduced by NADH, a product of metabolically active cells, to purple, insoluble formazan. Structures drawn using ChemSketch (ACD/Labs). 31

Figure 3.1: The growth curves of *S. epidermidis* under various conditions. A -80˚C stock culture inoculum was incubated in TSB (▪). Two overnight (16h) 1/200 inoculums were prepared from this initial culture and incubated in BPM (●) or TSB (▲). Results are from two independent experiments each with three technical repeats. 36

Figure 3.2: Inhibitory effect of (A) vancomycin, (B) melittin, and (C) W_5(Os-C) against planktonic *S. epidermidis* (ATCC 35984) cultures. The final concentration range for vancomycin, melittin and W_5(Os-C) were 0.31 µM to 40 µM for vancomycin, 0.78 µM to 50 µM for melittin, and 0.63 µM to 20 µM respectively. Error bars indicate mean ± SEM. Results are from three independent experiments each with three technical repeats. 38

Figure 3.3: Growth inhibitory activity of (A) vancomycin, (B) W_5(Os-C), and vancomycin and W_5(Os-C) in combination ratios (C) 3V:1W, (D) 2V:2W, and (E) 1V:3W against planktonic *S. epidermidis* (ATCC 35984). Serial doubling dilutions of the combinations were prepared so that the final antimicrobial agent concentration ranged from 0.31 µM - 20 µM and plotted in terms of the concentration of vancomycin (0.16 µM - 15 µM). Error bars indicate mean ± SEM. Results are from three independent experiments each with three technical repeats. 40

Figure 3.4: Mature, crystal violet stained 24 hr old biofilms prepared from (A) 1/100, (B) 1/200, (C) 1/400, and 1/800 cell dilutions cultured in BPM. Magnification 20x evaluated with inverted microscopy. 42

Figure 3.5: Time based study of biomass development of *S. epidermidis* (ATCC 35984) incubated in BPM at a cell dilution 1/200. Magnification 10x under inverted microscopy with crystal violet staining. 43

Figure 3.6: Percentage inhibition of *S. epidermidis* (ATCC 35984) cell viability (^{v}) and biomass accumulation (^{bm}) from 24 h old biofilms developed in the presence of (A) vancomycin, (B)

melittin, and (C) W_5(Os-C). Final concentrations are 0.31 µM to 50 µM. Results are from three independent experiments each with three technical repeats. Error bars indicate mean ± SEM. 44

Figure 3.7: Percentage inhibition of *S. epidermidis* ATCC 35984 cell viability (^{v}) from 24 hour old biofilms developed in the presence of (A) vancomycin, (B) W_5(Os-C), and vancomycin and W_5(Os-C) in combination ratios (C) 3V:1W, (D) 2V:2W, and (E) 1V:3W. Serial doubling dilutions of the combinations were prepared so that the final antimicrobial agent concentration ranged from 0.31 µM - 20 µM and plotted in term of the concentration of vancomycin (0.16 µM - 15 µM). Results are from three independent experiments each with three technical repeats. Error bars indicate mean ± SEM. 47

Figure 3.8: Percentage inhibition of *S. epidermidis* ATCC 35984 biomass development (^{bm}) from 24 hour old biofilms developed in the presence of (A) vancomycin, (B) W_5(Os-C), and vancomycin and W_5(Os-C) in combination ratios (C) 3V:1W, (D) 2V:2W, and (E) 1V:3W. Serial doubling dilutions of the combinations were prepared so that the final antimicrobial agent concentration ranged from 0.31 µM - 20 µM and plotted in term of the concentration of vancomycin (0.16 µM - 15 µM). Results are from three independent experiments each with three technical repeats. Error bars indicate mean ± SEM. 478

Figure 3.9: Relative biofilm formation of *S. epidermidis* ATCC 35984 from 24 hour old biofilms developed in the presence of and vancomycin and W_5(Os-C) in combination ratios (A) 3V:1W, (B) 2V:2W, and (C) 1V:3W. Horizontal axis indicates final vancomycin concentration in the antibiotic combination relative the BIC. Results are from three independent experiments each with three technical repeats. Error bars indicate mean ± SEM. 50

Figure 3.10: Effects of melittin, vancomycin and W_5(Os-C), on cell viability in HaCat keratinocytes. Error bars indicate mean ± SEM. Results are from three independent experiments each with three technical repeats. 51

Figure 3.11: Structure of a single W_5(Os-C) molecule showing the backbone cartoon with side chain stick representations following simulations in (A) PEP-FOLD to be submitted for molecular dynamic simulations, (B) pure TIP3P water, (C) water box containing a POPG membrane and physiological salt concentration (0.15 M), and (D) water box containing a POPG membrane and high salt concentration (0.30 M). Red indicates hydrophobicity and white indicates hydrophilicity. Glycine residues shaded yellow are hydrophobic. Images were processed in PyMOL 53

Figure 3.12: Peptide-peptide interactions from *in silico* simulation in POPG membrane (A-C) with physiological salt concentration (0.15 M), and (D-F) high salt concentration (0.30 M). Average Cα-Cα between residues of two W_5(Os-C) molecules in (A) physiological, and (D) high

salt concentration presented as a heatmap. Number of aggregates formed, and number of peptides involved in each aggregate over 1000 ns in (B and C) physiological, and (E and F) high salt concentration. 55
Figure 3.13: Analysis of W_5(Os-C) secondary structure obtained from *in silico* molecular dynamic simulations in physiological salt concentration. The (A) average psi angle, (B) average phi angle, and circular variance for (C) psi angle, and (D) phi angle indicating dynamic changes in conformation of residues during interaction with POPG membrane. 56
Figure 3.14: Analysis of W_5(Os-C) secondary structure obtained from *in silico* molecular dynamic simulations in high salt concentration. The (A) average psi angle, (B) average phi angle, and circular variance for (C) psi angle, and (D) phi angle indicating dynamic changes in conformation of residues during interaction with POPG membrane. 57
Figure 3.15: Analysis of W_5(Os-C) interaction with a POPG membrane obtained from *in silico* molecular dynamic simulations. In physiological salt concentration (A) number of hydrogen bonds with the membrane per residue, (B) average Z position indicating insertion into membrane, and in high salt concentration (C) number of hydrogen bonds with the membrane per residue, (D) average Z position indicating insertion into membrane. 58
Figure 3.16: Top view snapshot after 1000 ns showing peptide-POPG membrane where (A) W_5(Os-C) trimer formed in physiological salt concentration, and (B) dimer formed in high salt concentration. 59

List of Abbreviations

A	
AHLs	*N*-acyl homoserine lactones
∑FIC	Fractional inhibitory concentration
AI	Auto-inducers
AIP	Auto-inducing peptide
AMPs	Antimicrobial peptides
aps	Antimicrobial peptide-sensing
Arg	Arginine
B	
BIC	Biofilm inhibitory concentration
BIC_{50}	Concentration at which 50% inhibition of cell viability or biomass development is observed
BIC_{max}	Concentration at which tangents to slope and to maximum cell viability or biomass development intersect
^{bm}BIC	Biofilm inhibitory concentration related to biomass
BPM	Biofilm promoting media
C	
C2DA	Cis-2-decenoic acid (fatty acid based messenger molecule produced by bacterial cells)
CAMP	Cationic antimicrobial peptides
CD	Circular dichroism
CFU	Colony forming units
CHARMM	Chemistry at Harvard macromolecular mechanics (program applied for biochemical simulation)
CHARMM-GUI	Graphical user interface used to generate input files for molecular dynamics simulations
CRAMP	Cathelicidin-related antimicrobial peptide
CTB	CellTitre Blue®
CV	Crystal violet (gentian violet)
D	
ddsH_2O	Double distilled, sterilized, filtered water
DHBA	Dihydroxybenzoic acid
DMSO	Dimethyl sulfoxide
DNA	Deoxyribonucleotides
E	

ECM	Extracellular matrix
eDNA	Extracellular DNA
EDTA	Ethylenediaminetetraacetic acid
EPS	Extracellular polymeric substances
EtOH	Ethanol
G	
Gly	Glycine
H	
HaCaT	Cultured immortalized human keratinocytes (human adult low calcium high temperature)
HAI	Healthcare associated infections
hBD-3	Human β-defensin 3
HPLC	High performance Liquid Chromatography
L	
Lys	Lysine
M	
MDSims	Molecular dynamics simulations
MIC	Minimum inhibitory concentration (of planktonic cells)
MIC_{50}	Concentration at which 50% inhibition of a planktonic cell population is observed
MIC_{max}	Concentration at which tangents to slope and to maximum inhibition of a planktonic inhibition curve intersect
MRSA	Methicillin resistant *Staphylococcus aureus*
MRSE	Methicillin resistant *Staphylococcus epidermidis*
MSSE	Methicillin resistant *Staphylococcus epidermidis*
MTT	3-(4,5-dimethylthiazol-2-yl)-2,5-diphenyltetrazolium bromide
N	
NAD^+	Nicotinamide adenine dinucleotide
NADH	
NAG	*N*-acetylglucosamine
NAM	*N*-acetylmuramic acid
NMR	Nuclear Magnetic Resonance
NVT	Thermodynamic state with constant volume, temperature, and number of atoms
O	
OD	Optical density
OsDef	*Ornithodoros savignyi* defensin AMP
P	

PBPs	Penicillin-binding proteins
PBS	Phosphate buffered solution
PIA proteins	Polysaccharide intercellular adhesion proteins
PME	Particle mesh Ewald
POPG	1-palmitoyl-2-oleoyl-sn-glycero-3-phospho-(1'-rac-glycerol)
R	
RD	Radial diffusion
RNA	Ribonucleotides
S	
SEM	Standard error of the mean
T	
TIP3P	Transferable intermolecular potential 3P water
Trp	Tryptophan
TSB	Tryptic soy broth
V	
^{v}BIC	Biofilm inhibitory concentration related to viability
VRSE	Vancomycin resistant *Staphylococcus epidermidis*
W	
w/v	Weight per volume (g/100 mL)
WHO	World Health Organisation

CHAPTER 1: LITERATURE REVIEW

INTRODUCTION

Nosocomial or healthcare associated infections (HAI) are of increasing concern as antimicrobial resistance continues to increase globally. Infections of *Staphylococcus epidermidis* are of special concern as these infections develop biofilms on intravascular and urinary catheters, wound sites, as well as on medical implants (1). Biofilms consist of a variety of bacterial and fungal microorganisms attached to a living or non-living surface and covered by an extracellular matrix (ECM) which provides protection from the immediate environment, including antimicrobial agents. Once biofilm development is initiated, even healthy immune systems fail to overcome infection without toxic doses of antibiotics (2, 3). Chessa *et al* (2016) reported 63% of *S. epidermidis* infections following breast implants were caused by biofilm developing strains (4). However, this and all reports presumably underrepresent infection rates as many countries do not have the proper resources to identify infections.

Although most strains of *S. epidermidis* still respond to vancomycin, and to a lesser extent methicillin, reports of both vancomycin resistant *Staphylococcus epidermidis* (VRSE) and methicillin resistant *Staphylococcus epidermidis* (MRSE) isolates are increasing rapidly (5, 6). However, *S. epidermidis* exhibits increasingly similar resistance profiles to that of *Staphylococcus aureus* (7). Once VRSE becomes more wide-spread, gene transfer between *S. epidermidis* and *S. aureus* is expected to occur for vancomycin resistant genes (8-12). Whether an infection is due to naturally present *S. epidermidis*, or acquired from strains present on hospital equipment and personnel, action needs to be taken to prevent the increase and spread of MRSE and VRSE.

Antimicrobial peptides are short-sequence proteins or peptides synthesised by most biological cells as part of the innate immune system with a wide variety of antimicrobial activities. The AMPs are used either as a defence mechanism against infection in eukaryotes, or to outcompete other microbes among prokaryotes. The structures of AMPs are varied, but most considered for development as antibacterial drugs have several common characteristics. This includes a net positive charge; and both hydrophobic and hydrophilic portions in order to dissolve in aqueous environments, interact with charged cell membrane surfaces, and modify or pass through the lipid bilayer spanning the hydrophobic portion of the cell membrane (13, 14).

As AMPs target the cellular membrane and act through neutralisation, pore formation or other membrane disrupting mechanisms, the risk of developing antimicrobial resistance is reduced. Additionally, AMPs exhibit broad spectrum activity against bacteria, fungi, viruses, and certain types of cancer cells through rapid killing at relatively low concentrations compared to traditional antimicrobial agents (15-21). Furthermore, AMPs may neutralize endotoxins when combined with other antimicrobial agents without exhibiting notable toxicity themselves (15, 17, 18). Limitations of AMPs are few, but significant. Antimicrobial peptides are sensitive to proteolysis in the digestive tract due to low pH and peptide digesting enzymes, restricting treatments mainly to topical and intravenous administration. Some peptides may even be sensitive to proteolytic enzymes in the bloodstream or cause haemolysis, further limiting use to topical administration (18, 22, 23). Antimicrobial peptides are generally not stable long term, and require costly synthesis strategies due to the antimicrobial activity of AMPs against most microbes used for recombinant DNA biosynthesis (24). Although less likely than with traditional antimicrobial agents, AMPs may also induce antimicrobial resistance (25, 26)

Once identified, naturally occurring AMPs are characterized and screened for antimicrobial potential. These AMPs are then modified to create a library of derivatives which are analysed via high-throughput screening for antimicrobial activity (14, 27, 28). Antimicrobial peptides can be altered through one or more of the following approaches: reducing length by creating all possible truncation variations of the AMP to isolate the minimum sequence required for antimicrobial activity (29-31); systematic substitution of key residues to improve activity and stability while reducing toxicity of the AMP (32-34); sequence scrambling by changing the amino acid sequence order while maintaining peptide length, charge, and composition (35-37); altering existing or designing new peptide sequences to strategically place amino acids with specific characteristics e.g. changing the order of charged vs non-charged amino acids (alternate charged and non-charged, or two charged followed by two non-charged etc.) (38); or applying combinatorial chemistry in which a group of similar sequences are edited to create variants (39-41).

In the endeavour to design more active and stable peptides, bioinformatics such as predictive models of molecular dynamics simulations (MDSims) are used. This provides a cost effective method to identify candidate peptides based on the modelling of the interaction of the AMP with a model membrane (42-44). In addition, MDSims can be used to predict the mode of action and the effects of other molecules such as cations and pH on peptide-membrane interactions (45, 46).

One approach to overcome resistance and decrease toxicity is the combination of antibiotics with other compounds. Although some AMPs exhibit little to no antimicrobial activity, synergistic activity with known antibiotics or other AMPs are often reported with either the AMP increasing the activity of the antibiotic, the antibiotic increasing the activity of the AMP, or both. The most common reason for synergy is the combination of antimicrobial agents with different targets, limiting the ability of microbes to evade or survive treatments (47-50). Combination therapies increase antimicrobial activity while simultaneously decreasing therapeutic doses needed as well as the risk of antimicrobial resistance mutagenesis.

The aim of this study was to determine for W_5(Os-C), the antimicrobial and anti-biofilm activity, potential synergism with vancomycin against *S. epidermidis*, and lastly to evaluate the interaction of W_5(Os-C) with a model Gram positive membrane.

1.1. *Staphylococcus epidermidis*

Staphylococcus epidermidis is a coagulase negative, Gram-positive bacterium that thrives on moist host niches including the epidermis of the armpits, pelvic region, nasal cavities, and in the eyes along with many other *Staphylococci* as pathobionts (51-53).

The human innate immune system inhibits growth of *S. epidermidis* into the upper airway of healthy individuals through the release of nitric oxide by the sino-nasal epithelium. Nitric oxide activates signalling pathways leading to increased movement of cilia to clear infected mucus faster. Antimicrobial peptides and enzymes present in the host mucus, together with nitric oxide damage bacterial membranes, DNA, and enzymes (54, 55).

Staphylococcus epidermidis is a key component of the healthy skin biome. Growth of *S. epidermidis* on the skin of healthy individuals prevents infection from pathogens. *Staphylococcus epidermidis* has been shown to inhibit the formation of *S. aureus* biofilms through the synthesis and release of glutamyl endopeptidase, a serine protease. This protease is able to degrade proteins required by *S. aureus* during biofilm adhesion and proliferation. Interestingly, glutamyl endopeptidase is selectively expressed, although the conditions inducing expression still require further investigation (56-59).

Staphylococcus epidermidis infections most commonly occur during implantation of medical devices. Among all coagulase negative *Staphylococcus* species, *S. epidermidis* is one of the most likely to cause infections following implantation surgery (60, 61). Intravascular catheters,

vascular grafts, prosthetic cardiac valves, pacemakers, prosthetic joints, and central nervous system shunts are all associated with a coagulase negative *Staphylococcus* infection rate of 5% or more and most are caused by *S. epidermidis*. Increasingly, hospitals report 35 – 40% of infection induced revision surgeries for biomedical implants, especially joint replacements due to *S. epidermidis* infection (62-64). In many cases, septicaemia may develop which drastically increases the risk of mortality (65-69). Infections caused by *S. epidermidis* are very common in the clinical setting due to its natural occurrence on human skin. Investigation of clinical *Staphylococcus* isolates are complicated by the natural occurrence of this genus in the human skin flora (4). It is difficult to discern whether the presence of a *S. epidermidis* bacterium in a sample is the causative agent of infection, or peripheral contamination from the human biome. Current diagnosis relies on a complex system incorporating multiple blood samples taken over a period of time (60). *Staphylococcus epidermidis* infections are difficult to detect before biofilm formation and other antimicrobial evasion mechanisms are active.

1.1.1. Clinically relevant *S. epidermidis* drugs and antimicrobial resistance

Methicillin, oxacillin, penicillin G, and other penicillin-derived antimicrobials were the first line of defence against most *Staphylococcus* infections. However, due to the rapid evolution of plasmid based β-lactamase enzymes (70, 71) and peptidoglycan polymerization enzymes called penicillin-binding proteins (PBPs) with lowered affinity for β-lactam antimicrobials (72), vancomycin is the only remaining effective treatment against *S. epidermidis* infections (10, 12, 73, 74). Vancomycin (**Figure 1.1**) is a glycopeptide derived from *Streptococcus orientalis* with multiple cyclic structures. It is clinically relevant against MRSA, as well as various *Enterococcus* and *Streptococcus* species infections, but must be used with caution due to nephrotoxicity and/or risk of developing resistance against vancomycin (75-77). Vancomycin is only effective when the patient's immune system is adequately functioning and if given within a very narrow time window post infection (78).

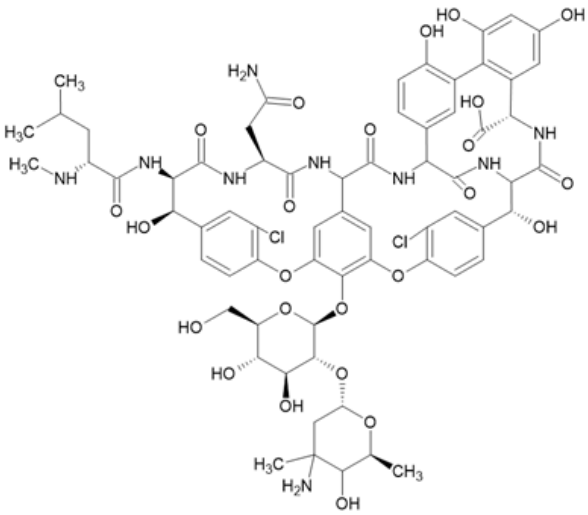

vancomycin

Figure 1.1: Chemical structure of vancomycin.

The most common target for antibiotics is cell wall biosynthesis. Bacterial cell walls consist of peptidoglycans crosslinked via amide bonds as depicted in **Figure 1.2.** Peptidoglycan polymers consist of alternating *N*-acetylglucosamine (NAG) and *N*-acetylmuramic acid (NAM) monomers with β-1→4 linkages and substitution of the NAM *D*-lactoyl groups for peptide stems. These peptides stems may vary, but predominantly consist of *L*-Ala-γ-*D*-Glu-*L*-Lys-*D*-Ala-*D*-Ala peptide chains with the most common variation a substitution of the *L*-Lys substitution for *meso*-2,6-diaminopimelic acid (Azpm) in which case the amide bond is between the carboxylic acid group of Azpm and the amine group of the subsequent *D*-Ala (1, 79, 80).

Cell wall biosynthesis starts in the cytoplasm where NAG and NAM are synthesised and joined together to form dimers. The dimers are transferred across the membrane where peptidoglycan assembly is controlled by PBPs with transpeptidase and peptidoglycan polymerisation activities. There are two classes of PBPs: aPBPs contain both transglucosylase and transpeptidase activity while bPBPs contain only transpeptidase activity. The transglucosylase domain of this enzyme is responsible for adding peptidoglycan dimers to the growing sugar chains (81, 82). The transpeptidase domain is responsible for amide bond formation during which the second *D*-Ala is cleaved and a crosslink amide bond is formed between the *L*-Lys R-group amine and the *D*-Ala carboxyl group of two different peptidoglycan peptide stems. Cell walls become increasingly resistant to osmotic lysis as the number of amide bonds increase (82-84). Glycopeptides like vancomycin and teicoplanin bind to the *D*-Ala-*D*-Ala amide bond, making this bond the target for resistance evolution. Resistance can occur when the amide

bond is replaced with an ester bond and the second *D*-Ala is replaced with a *D*-lactate group which eliminates a hydrogen bonding point for vancomycin (85, 86). This differs from the activity of β-lactam antimicrobials which covalently bond to the PBP transpeptidase domains directly and compete for the *D*-Ala-*D*-Ala substrate (87, 88).

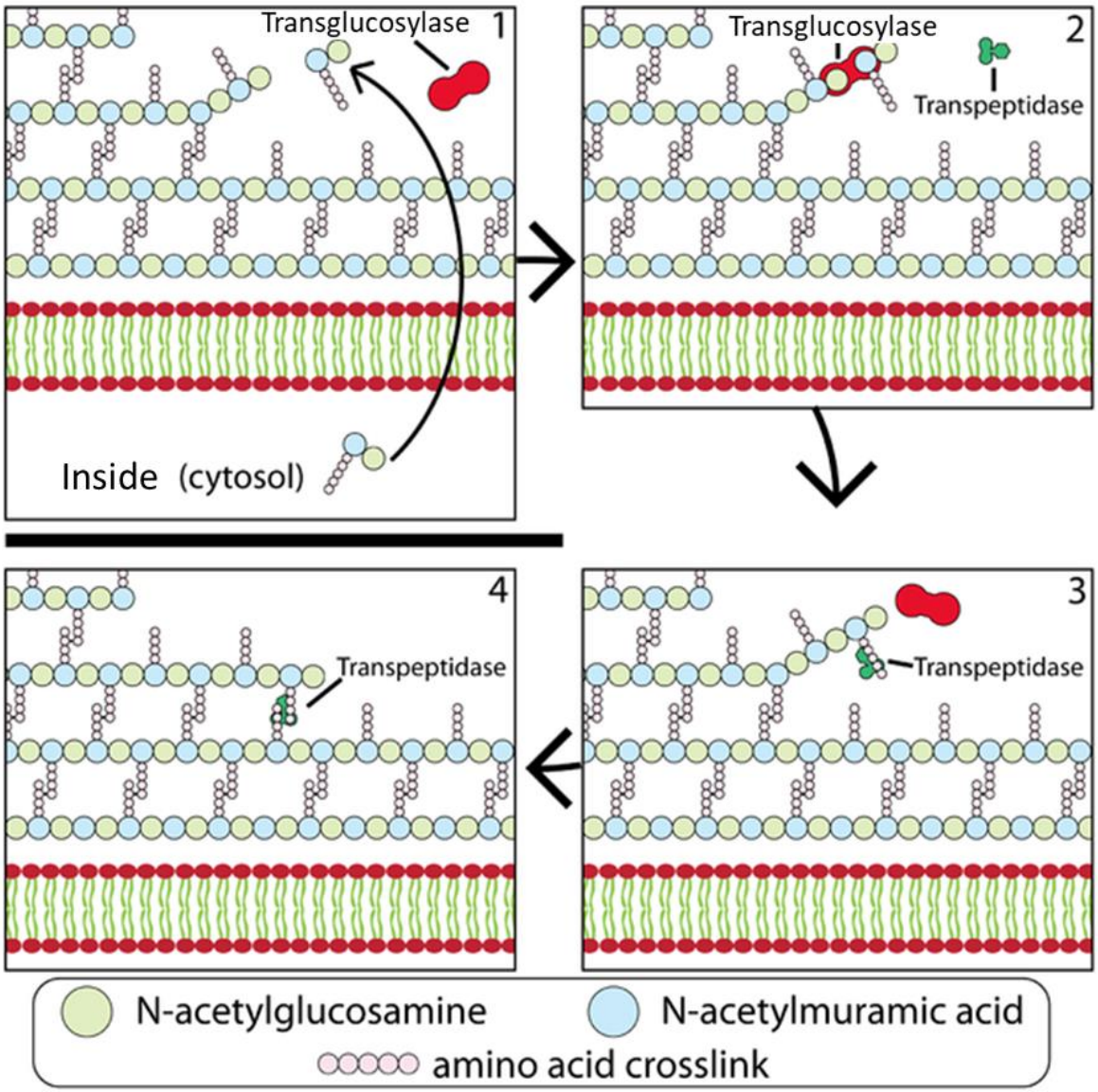

Figure 1.2: Structure and synthesis of the peptidoglycan cell wall in Gram-positive bacteria. (1) NAG-NAM dimers are formed in the cytosol and transferred across the membrane. (2) Transglucosylase incorporates dimers into established cell wall. (3) Transpeptidase binds to amino acid portion of newly incorporated NAM. (4) Transpeptidase forms peptide bond to cross link newly incorporated dimer to existing cell wall components. Adapted from commons.wikimedia.org.

1.1.2. Trends in antimicrobial resistance of *Staphylococcus spp*

Staphylococcus aureus is one of the most well studied *Staphylococcus* species. This is due to its pathogenic nature as well as its ability to rapidly evolve antimicrobial resistance. In 1942, within one year of the discovery and use of penicillin G for *S. aureus* infections, the first reports of resistance was reported (89). By 1945, multiple *Staphylococcus* species exhibited resistance to penicillin through the action of penicillinase, the first discovered β-lactamase (90, 91) and by 1996, estimates of methicillin resistance was reported as 75% (92). In 2019, the World Health Organization (WHO) reported a median rate of methicillin-resistant bloodstream *S. aureus* infections of 12.11% as reported by 25 countries (93). These statistics, however, do not accurately represent infection rates due to the difficulty in discerning between contamination and infection from samples, as well as the lack of access to equipment in underdeveloped and developing countries.

1.1.3. Role of *S. epidermidis* in antimicrobial resistance

Albeit at a slower rate than that of *S. aureus*, *S. epidermidis* is evolving antimicrobial resistance in a similar pattern. *Staphylococcus epidermidis* expresses the gene products of the *mec* gene family, namely PBPs. The proteins encoded by the *mec* genes are the target of β-lactam antimicrobials (5, 7, 8, 12, 74). As an alternative to the production of β-lactamase enzymes, many microbes including *S. epidermidis* have evolved modified PBPs called PBP2a, to which penicillin derived antimicrobial agents have a reduced affinity (72, 74). In recent years, more multi-drug resistant *S. epidermidis* strains with PBP variations have been identified, with more antibiotics being rendered ineffective against infection every year (67, 94, 95).

Many *Staphylococcus spp* achieve resistance via gene transfer from other bacterial species, for example, the methicillin-resistance gene, *mec*, is often reported to transfer from *Enterococcus spp* or *S. epidermidis* to *S. aureus* (9, 96, 97). Rifampin, linezolid, and vancomycin are currently in clinical use against MRSE. At present, clinicians avoid administration of rifampin unless in combination with other antimicrobial agents due to the high risk of rifampin resistance (94, 95). Although still considered rare, linezolid resistant *S. epidermidis* infections are increasingly reported (98-100). Vancomycin resistance is also rare but of increasing concern (10, 12, 101). Not only is *S. epidermidis* at the brink of evolving vancomycin resistance, but may also act as an antimicrobial resistance gene repository for more severe pathogens.

Staphylococcus epidermidis is not only evolving resistance against most clinically relevant antimicrobial agents, but can also transfer its resistance properties to more harmful microbes, or develop biofilms which can impede antimicrobial access to all microbes forming part of the biofilm communities.

1.2. Biofilms

1.2.1. Biofilm structure and development in *Staphylococcus spp*

Bacterial biofilms consist of cells and a mixture of extracellular DNA (eDNA), as well as secreted proteins and polysaccharides (adhesins) that interact to form the ECM (102, 103). The ECM acts as physical barrier, preventing antibiotic access to the bacterial cells, and providing an hypoxic environment filled with nutrients necessary for growth (102-104). Efflux pumps within the biofilm are able to remove antibiotics that are able to pass through the ECM (105). Exposure to low concentrations of antibiotics may increase antibiotic resistance through selection for antibiotic resistant cells (106-108).

Biofilm formation is dependent on quorum sensing and consists of four steps: adherence, proliferation, maturation, and dispersal (**Figure 1.3**) (107, 109, 110). Quorum sensing refers to the regulation of physiological processes and precise gene expression using chemical communication between cells, allowing optimal cell differentiation in order for cells to adhere to a suitable surface (110-113). Once quorum sensing provides the correct sequence of signals, biofilm development is initiated. First, an auto-inducing peptide (AIP) is produced in response to environmental signals. The AIP activates the accessory gene regulator operon which contains the genes for extracellular adhesins and autolysins. In turn, these proteins facilitate the release of eDNA, which allow for initial adherence and aggregation of *S. epidermidis* cells (109, 114-116). Within two hours of the first quorum sensing signals, cells have formed adhered colonies exhibiting biofilm properties. During this proliferation stage, most *S. epidermidis* strains produce polysaccharide intercellular adhesion proteins (PIA) in addition to ECM components. The PIA proteins form fibres to which the ECM can adhere and accommodate proteins associated with innate immune system evasion (117, 118). The presence of PIA in *S. epidermidis* biofilms also facilitates bacterial cell aggregation as well as haemagglutination within the host (119). Therefore, PIA contributes significantly to virulence in *S. epidermidis*. However, it is important to note that some PIA deficient *Staphylococcus spp* strains form biofilms in a PIA independent manner (108). Adhered cells proliferate and alter metabolic processes in order to produce and secrete ECM components. Within 24 hours, the

secreted ECM has accumulated to form a mature biofilm. Cells involved in mature biofilms exhibit altered gene expression and morphology to allow for sessile colonies able to persist in low pH environments associated with biofilms (114, 117, 120). Finally, mature biofilm covered cells inhibit further ECM development, and some adhered cells may be released back into the environment to initiate new infection (121, 122).

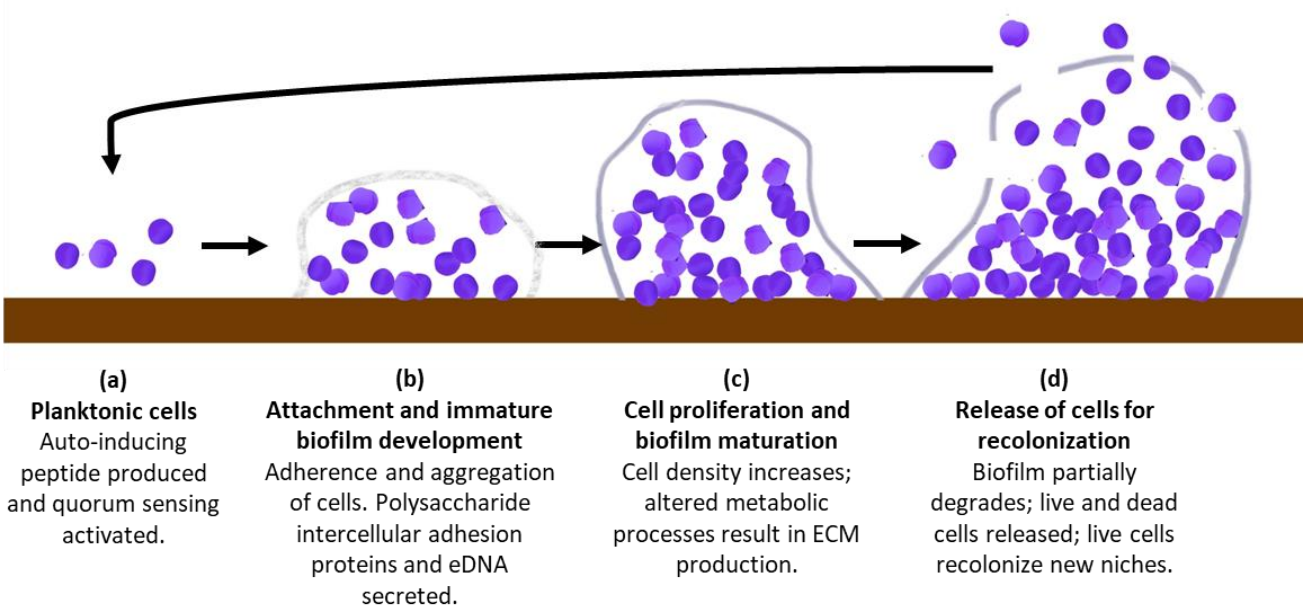

Figure 1.3: Process of biofilm formation in *Staphylococcus epidermidis*. (a) Planktonic cells produce auto-inducing peptide and quorum sensing is activated. (b) Attachment and aggregation of cells signals secretion of polysaccharide intercellular adhesion proteins and eDNA. (c) Cells proliferate and biofilm matrix matures. (d) Biofilm can no longer sustain all cells and partially degrades/breaks apart to allow cells to escape and colonize new niches. Image produced using Canva.com.

1.2.2. Combined biofilms

Biofilms can also form as a mixture of secretions from multiple microorganisms. Fox *et al.* (2014) discovered that *Candida albicans* biofilms create an anoxic environment in which anaerobic members of the normal human microbiome can grow (123). *S. epidermidis* routinely forms mixed biofilms with *C. albicans*. Adam *et al.* (2002) observed extensive *Staphylococcus* adherence to *C. albicans* in cellular yeast as well as hyphal morphologies. These interactions lead to a more robust, antibiotic resistant biofilm (123, 124). Identifying a drug exhibiting biofilm inhibition and eradication activity against both microorganisms would reduce the cost and toxicity of treating infections. However, *Staphylococcus* species do not often form combined biofilms with each other due to quorum sensing based inhibition of virulence factors (125, 126). Thus, for the purposes of this study, combined biofilms are not of immediate interest.

1.2.3. *S. epidermidis* biofilm development and contributions to antimicrobial resistance

Compared to *S. aureus*, *S. epidermidis* has very few exotoxins or exo-enzymes. Exotoxins are known to elicit host immune responses including antibody production and inflammation (127-129). Consequently, implant associated infections are often only identified once biofilm development is well underway (110). Lack of exotoxins and other virulence factors make biofilm development one of the most important virulence determinants for *S. epidermidis* infections (105, 112, 130, 131).

S. epidermidis is able to implement genome-wide changes during biofilm development that slow down biosynthetic processes within some cells to produce persister cells, or small colony variants. Antimicrobial agents target proteins or other molecules only abundant in metabolically active cells and as a result, the susceptibility of the persister cells to the antibiotics are reduced (132-134).

The high prevalence of biofilm formation among *S. epidermidis* strains further boosts the emergence of antimicrobial resistance (71, 135). When an established *S. epidermidis* biofilm is treated with an antimicrobial agent, efflux pumps expression is upregulated and decreases antimicrobial agent concentrations below the biofilm layer, often to sub-inhibitory concentrations, resulting in accelerated evolution of antimicrobial resistance (136, 137).

The increasing development of resistance, the decrease in the number of effective antimicrobial drugs and the challenges associated with the treatment of biofilms, make the discovery and the development of new antimicrobial drugs essential. Antimicrobial peptides, target cell membranes, are increasingly being investigated as antibiotic substitutes for the treatment of infections.

1.3. Antimicrobial peptides

From as early as 1880, AMPs were discovered in a variety of fluids produced by most living organisms. Antimicrobial peptides are highly effective antibacterial agents with low risk of antimicrobial resistance, and are active against a broad spectrum of pathogens and exhibit high selectivity (98, 138-140). Antimicrobial peptides secreted by a host organism exploit the weaknesses of pathogenic microbes, modulate the host immune system to elicit a response or

neutralize endotoxins. A number of AMPs found in animals and humans function as part of the host innate immune system (141-144).

1.3.1. Structures of antimicrobial peptides

AMPs are short, usually cationic (CAMP), amphipathic peptide sequences with widely varied secondary and tertiary structures. Secondary structures commonly found in AMPs include α-helical, β-pleated, extended, or combinations thereof as shown in **Figure 1.4**. Activity strictly depends on their environment e.g. some AMPs selectively exhibit antimicrobial activity in a reducing or oxidising environment while others are activated in an acidic environment (49, 145, 146). Mammalian AMPs tend to have notable direct antimicrobial activity under low salt conditions but the activity significantly decreases under physiological conditions. As such, mammalian AMPs mainly function through modulation of the innate immune system rather than direct antimicrobial activity (147-149). Overall, AMPs efficiency and function varies according to the immediate environment.

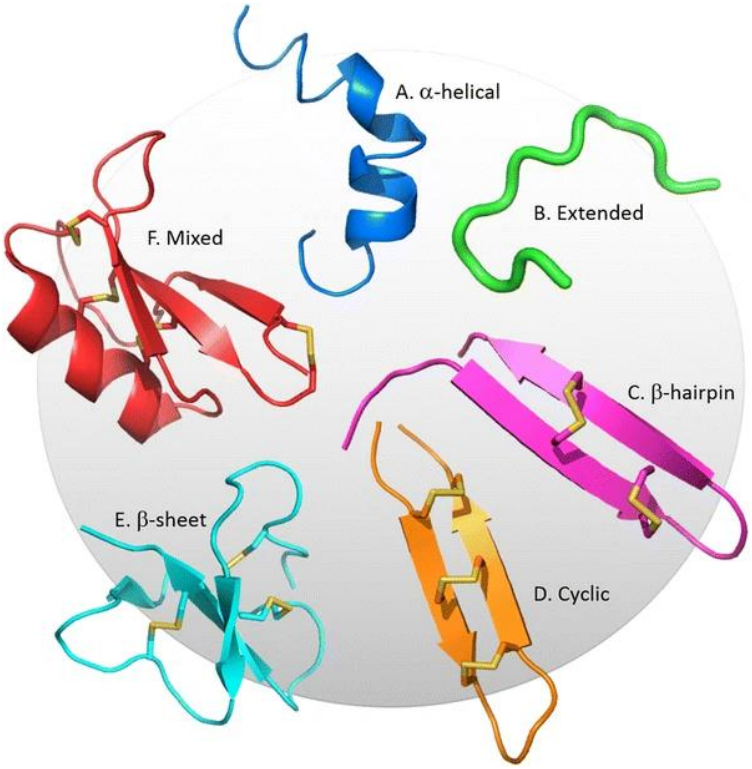

Figure 1.4: Possible secondary structures of AMPs. (A) standard α-helical conformation with some linking sequences; (B) extended with helical and sheet characteristics absent; various β-sheet conformations with either (C) two disulphide bond stabilisation, (D) three disulphide bond stabilization, or (E) more than two sheets parallel with sulphide bond stabilisation; and (F) a combination of the other conformations. Image used with permission from Springer International Publishing AG (150).

There are three main families of mammalian AMPs: cathelicidins, defensins, and histatins: Cathelicidins play an important role in innate immunity during initial infection. All cathelicidins have a highly conserved signal sequence at the N-terminal, followed by a conserved cathelin domain, but vary along the C-terminal (151-153). Histatins are positively charged, small AMPs characterised by many histidine residues. Histatin AMPs are secreted by mammalian salivary glands as part of oral defence against microbes (154, 155). Defensins comprise the largest group of characterised AMPs. They contain positively charged residues, resulting in a net positive charge, and six or more cysteine residues that form three or more disulphide bridges (13). Besides the conserved arginine and cysteine residues, defensin structures are greatly varied among and within organisms, conferring activity against a selection of Gram-positive and -negative bacteria, fungi, viruses, and tumour cells. Defensins are involved in the innate and adaptive immunity of animals (156-159). Although difficult to classify, AMPs of interest fall into one of three broad categories, each with some identifiable characteristics as well as highly variable sequences, origins, and activities.

As with many other therapeutic drugs, clinically relevant AMPs considered for use as antibiotics are usually chemical derivatives of AMPs isolated from biological sources. The derived AMPs are modified using strategies that aim to provide chemical stability in physiological environments (resistant to proteolysis), improve antimicrobial activity at lower concentrations while reducing toxicity and reduce the cost of production. These strategies include amidation, glycosylation, isomerisation, halogenation, truncation, cyclisation, acetylation, and/or other chemical modifications (139, 144, 160-163).

1.3.2. Antimicrobial peptides target cellular membranes

Antimicrobial peptides interact with the negatively charged cell wall components (electrostatic attraction) before passing through the cell wall and other protective layers surrounding microbial cells e.g. the lipoteichoic acid infused peptidoglycan layer in Gram-positive bacteria, and the lipopolysaccharide layer in Gram-negative bacteria (98, 164). Once AMPs reach and interact electrostatically with the cell membrane, the AMPs can form membrane pores and pass through into the cells. Pore formation can occur via several mechanisms as shown in **Figure 1.5** and an AMP may employ more than one mechanism simultaneously. Most interactions of AMPs with cellular membranes induce conformational changes of the AMPs, membrane, or both. The resulting conformations may be transient or fixed to induce pore formation or other membrane disruption mechanisms (164).

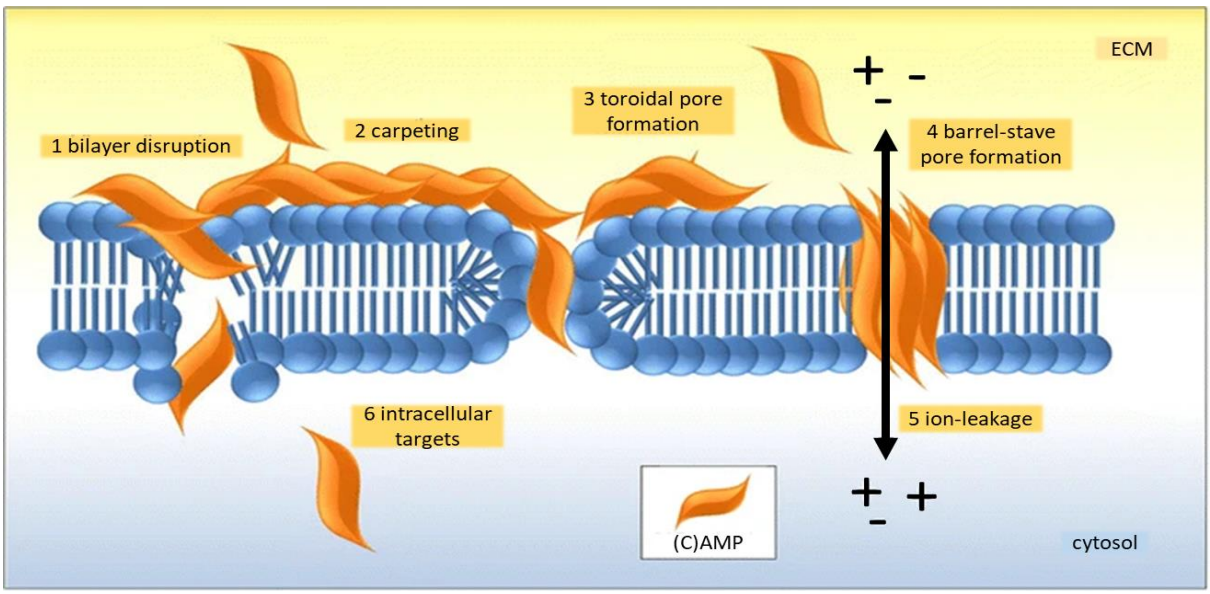

Figure 1.5: Mechanisms of action of peptide-membrane interaction leading to pore formation. Orange shapes represent cationic antimicrobial peptides (CAMP). Image adapted with permission from Springer International Publishing AG (150).

The thickness of the bilayer may be altered in a manner dependent on the size of an AMP. Longer peptides tend to induce thinning of membranes, but are unlikely to span across the membrane. Conversely, shorter peptides cause the membrane to thicken, but can also insert to span the entire membrane (**Figure 1.5** mechanisms 1 and 2) (165).

Toroidal pores are caused by β-barrel AMPs that interact with the phospholipid polar heads and as a result insert into bacterial membranes, resulting in protein and lipid lined pores. Disordered toroidal pores form and consist of less peptides and thus the pore is lined with a larger proportion of lipids than ordered toroidal pores (164, 166). The barrel stave model is similar to the toroidal pore, but with only peptides lining the pore (**Figure 1.5** mechanism 3) (98).

Infected or inflamed phospholipid bilayers are potential AMP targets. Infection and inflammation leads to oxidation of phosphatidylcholine lipids, making it easier for some AMPs to insert and cross the cell membranes (167). Membrane permeabilization can also occur with the help of anion carriers. Hydrophilic, anionic molecules complex with positively charged AMPs resulting in transport of the AMPs across the cellular membrane (168). AMPs may also use an electroporation approach to induce pore formation. Cationic AMPs (CAMPs) associate with the membrane until the electrical potential across the membrane causes spontaneous pore formation (169). AMPs with a large number of positive charges may induce the clustering of anionic membrane lipids, which in turn attracts more positively charged AMPs. As the local

concentration of AMPs increase, a pore may form, or AMPs may transcend the membrane resulting in cytoplasmic leakage (170). Non-bilayer intermediates may form within the membrane due to associations of AMPs with the cell membrane (171). An increase in efflux pump activity may release too many ions e.g. potassium from the cell causing disruption of the cell membrane potential without mechanical damage (**Figure 1.5** mechanisms 4 and 5) (172).

1.3.3. Other targets of antimicrobial peptides

Many other modes of action have been identified in AMPs, including: disruption of cell-wall biosynthesis, disruption of ribosomal protein synthesis, and interruption of DNA repair, transcription, and/or translation mechanism (**Figure 1.5** mechanism 6) (82, 173, 174).

AMPs like ramoplanin and enduracidin interfere with the transglycosylation step during peptidoglycan polymerisation. Whereas vancomycin and other glycopeptides bind to the D-Ala-D-Ala portion of NAG whether incorporated into the cell wall or not, AMPs bind mainly to the final dimer formed just before transglycosylation. Lower AMP concentrations might be needed to achieve the same effect as with vancomycin as less molecules are required to bind all the target sites (175-177).

Prokaryotic and eukaryotic ribosomes differ to some extent. These differences are sufficient to make bacterial ribosomes an attractive target. Ribosomes carry out protein synthesis in a multitude of precise steps, any of which may be targeted by AMPs. The most common mechanism of action is the binding of antimicrobial peptides to the aminoacyl entry site, the peptidyl catalyst site, or the exit site of the ribosome, actively blocking protein synthesis (178-180).

Finally, bacterial gyrase (topoisomerase type II) and topoisomerase IV are also attractive AMP targets. AMPs bind to the topoisomerase-DNA complex and prevent ligation of cleaved DNA strands. The accumulated double stranded breaks activate the bacterial SOS DNA repair system, resulting in cell death (181, 182).

1.3.4. Antimicrobial peptides as attractive antimicrobial agents against *S. epidermidis*

The rapid evolution of antibiotic resistance continues at an alarming rate, placing more focus on AMPs as therapeutic antibiotics. Yearly new AMPs of biological or synthetic origin are described with potential use as antibiotics (98, 147, 183).

Hepcidin, a cysteine-rich AMP produced within vertebrate livers, exhibits antimicrobial activity against *S. epidermidis*, *Escherichia coli* and *S. aureus* as well as antifungal activity against *C. albicans* and some species of the genus *Aspergillus*. Furthermore, a derivative of hepcidin called hepcidin-20 has biofilm inhibition activity against both PIA positive and negative strains of *S. epidermidis* (184, 185).

Magainin peptides extracted from the skin of *Xenopus laevis* (African clawed frog) exhibits antifungal activity against *C. albicans* as well as antimicrobial activity against several Gram-positive and -negative bacteria, including *S. epidermidis* (186). Pexiganan, a synthetic derivative of magainin 2, also exhibited similar antibiotic effects and was developed for use as a topical cream antimicrobial agent. However, the cream was never approved for clinical use as it offered no observable advantage over the standard treatment (187). Human β-defensin 3 (hBD-3) was found to exhibit biofilm inhibition activity against specifically *S. epidermidis* (ATCC 35984) biofilms developed on titanium (188). AMPs, including defensins, from a variety of sources exhibit antimicrobial and biofilm inhibition against *S. epidermidis*.

1.3.5. Antimicrobial resistance against antimicrobial peptides

AMPs targeting bacterial cell membranes are fast acting which makes development of AMP resistance difficult, but not impossible. Albeit to a lesser extent, AMPs remain susceptible to resistance mechanisms employed by bacterial cells (182, 189).

In order to efficiently detect AMPs, bacteria require antimicrobial peptide-sensing (*aps*) mechanism. The first Gram-positive bacterial *aps* mechanism was discovered in *S. epidermidis* in 2007 and is considered a common mechanism in Gram-positive bacteria (190, 191). Cationic AMPs activate the *aps* system which upregulate established AMP resistance genes including *dlt*, *mprF*, and an ABC transporter analog gene (191).

The *dlt* operon is responsible for D-alanylation of cell membrane teichoic acids, the most abundant anionic components of the cell membrane. Teichoic acid D-alanylation masks the teichoic acid negative charges and attract Ca^{2+}, Mg^{2+}, and Na^{+} (192, 193). The *mprF* gene is responsible for lysyl-phosphatidylglycerol biosynthesis and its upregulation results in increased positive charge of the cell wall. The combined effects of teichoic acid D-alanylation and increased lysyl-phosphatidylglycerol production confers resistance to CAMPs and other positively charged antimicrobial agents via electrostatic repulsion (192-194). The ABC transporter analog removes antimicrobial agents including CAMPs from the cytoplasm or membrane and releases it back into the environment (195).

D-alanylation also affects autolysin activity although the exact effects are still under investigation with varied reports on whether autolysin activity is increased to facilitate cell wall expansion and division during proliferation, or whether it is down-regulated to prevent cell lysis and subsequent death (11, 196).

In addition, cations such as Ca^{2+}, Mg^{2+}, and Na^{+} commonly found in physiological environments such as blood plasma can either prevent binding or displace bound AMPs limiting the further development of candidate peptides for therapeutic applications (197-199). Although AMPs can replace the Ca^{2+}, Mg^{2+}, and Na^{+} ions, this ability is restricted to low cation concentrations (200). To limit this effect AMPs can be combined with other AMPs or antimicrobial agents (201), or modified to resist or overcome inactivation in saline environments. Modifications include addition of more positively charged residues (202, 203), substituting histidine and/or tryptophan residues with modified alanine residues (204), including tryptophan motifs (205), or by designing novel sequences with repeated motifs and strategic placements of hydrophobic residues and GG or pG (*D*-Pro-Gly) fragments (204). Overall, peptides require higher positive charges, symmetry, and strategic placement of hydrophobic residues to retain activity in physiological environments.

1.3.6. Antimicrobial peptides used in combination therapies

More studies are warning against monotherapy and suggesting the use of combination therapies as this will potentially reduce antimicrobial resistance as well as decrease required effective doses (94, 95, 100). Due to the often low antimicrobial activity of AMPs *in vivo*, and the high toxicity of some antibiotics multiple investigations into combinatorial therapies are underway (**Table 1.1**) (122).

AMPs may act as carriers for conventional antibiotics, allowing for increased uptake, especially (but not limited to) Gram-negative bacteria (206) and this results in lower dosages of antibiotics that are required as more antibiotic molecules reach their intracellular targets (207).

Some AMPs have also been found to interfere with biofilm signalling molecules, increasing the efficacy of currently available anti-biofilm agents (208, 209). To this end, AMPs are able to accentuate biofilm inhibition or eradication of existing drugs, reducing considerably the dosage of antibiotic required for effective treatment (209, 210). In biofilms, the ECM is known to reduce the bioavailability of many AMPs and therefore to increase bioavailability, AMPs may be combined with compounds that disrupt the ECM or inhibit extracellular polymeric substances (EPS) synthesis (211). Another biofilm related target for AMP-antibiotic combinatory treatment is the quorum sensing pathway through which biofilm development occurs (212). This pathway is dependent on a variety of cell-to-cell communication molecules including *N*-acyl homoserine lactones (AHLs) and auto-inducers (AI) (106).

Finally, AMPs may be combined with other AMPs or peptide compounds, mimicking the natural synergistic activity of AMP-based defence systems (213). AMPs may be used in complex, or as separate molecules with differential targets in order to increase AMP antimicrobial activity (214, 215).

Table 1.1: Examples of antimicrobial agent - AMP combinations investigated for synergy, their target organisms, and proposed synergistic effects.

Antimicrobial agent	Antimicrobial peptide	Target organism(s)	Synergy effect	Reference
Vancomycin	Cathelicidin-related AMP (CRAMP)	Gram-negative	Increased intracellular uptake. CRAMP acts as trans-membrane carrier.	(216)
Tobramycin	G10KHc	*Pseudomonas aeruginosa*	Increased intracellular uptake; exact mechanism unknown but involves damage to cell membrane.	(217)
Vancomycin	BMAP-28	Gram-positive cocci	Increased intracellular uptake; exact mechanism unknown but involves damage to cell membrane.	(218, 219)
Carbapenems	DJK-6	*Klebsiella pneumoniae*	n/d; suspected interruption of biofilm development.	(220)
L-cysteine and other sulfhydryl compounds	Temporin (1Tb)	*S. epidermidis*	Downregulation of PIA synthesis.	(122, 221)
DHBA and other iron chelators	Nisin	*S. aureus*	Downregulation of PIA synthesis.	(222, 223)
DNAse I	hBD-3	*Haemophilus influenzae*	Prevention of biofilm development and killing biofilm associated cells.	(224)
EDTA	1Tb	*S. epidermidis*	Destabilisation of ECM.	(122)
Peptides	DD_{13} and RIP	*S. aureus* and *S. epidermidis*	Combination of membrane disruption and inhibition of quorum sensing.	(225, 226)

1.4. Molecular dynamics simulations in antimicrobial research

Peptide folding and structures are sensitive to the environment and interactions with surrounding molecules (227). As such, AMP structures are linked to their antimicrobial activity e.g. changes in secondary structural arrangements can enhance or limit peptide to peptide and peptide to membrane interactions.

To characterise such interactions, multiple nuclear magnetic resonance investigations would normally be needed. However, in recent years, MDSims have improved to the point where it can determine whether nuclear magnetic resonance (NMR) is necessary, or be used in combination with NMR to produce a wealth of data on AMP structure (228-232). Molecular dynamics simulations are advantageous for multiple reasons. In most cases MDSims is cheaper if the equipment is available; supercomputers used in MDSims can be accessed online from most modern computer terminals world-wide; MDSims require no physical reagents, including costly peptide; multiple facets of molecular interactions can be obtained from a single simulation; constraints related to cyclic, flexible, or large molecular structures are relaxed; and MDSims drastically increases efficiency by reducing input and analysis time and man-hours needed (233, 234). More studies are also suggesting the use of MDSims to replace

NMR and other experimental techniques due to the consistently increasingly similar accuracy of MDS outputs when compared to traditional methods. In some cases, MDSims might be more accurate than NMR or circular dichroism (CD) results due to differences in solutions used for each technique. For example, the NMR structures of cyclic peptides in solution are difficult to resolve due to inherent flexibility and multiple stable conformations. Some linear peptides exhibit flexible conformations without cyclic structures and can thus also be difficult to resolve using NMR. Side chains in larger molecules also cause overlapping signals which can be difficult to resolve. The principle of NMR is built on calculating the averages of conformational position. As such, resolving structures with multiple stable conformations result in inaccurate average conformational data (28, 166, 233-238).

Currently MDSims are limited by available processing power and high costs. However, availability of processing units are rapidly increasing while prices are decreasing. In most cases, MDSims can be used as a screening agent to determine which compounds are worth the effort and cost of NMR, or can be used on its own to describe molecular dynamics of AMPs.

Software applied in MDSims calculate potential energies of atoms and residues to determine residue interactions and conformations. Molecular bonds are simulated as springs while Van Der Waals interactions are calculated using the Lennard-Jones potential and Coulomb's Law (239, 240). Many software options, each with multiple simulated bonding force constants, are available to suit the needs of individual simulations as some approximations or calculations may not be as accurate as others (240-242). Simulations also require boundary restrictions to limit computational loads within the capability of current processors available. This is usually achieved using the particle mesh Ewald (PME) method, or adaptations thereof which counterbalances all positive and negative charges with anions or cations and fulfil the PME requirement of net neutral charge. The PME method also uses one of three constraint systems in which three system variables (molar amounts, volume, energy, pressure, or temperature) constrained (239, 240, 243, 244). Overall MDSims is dependent on a careful balance between limited computational capacity and required accuracy.

Applications of MDSims is diverse and potential applications are expanding as computational constraints are systematically lifted by new technologies. To date, MDSims was used to demonstrate: the steps peptides follow to insert and potentially traverse cellular membranes (245); peptide-inorganic substance interactions, including absorption into amorphous silica which is used to assist in tissue repair (246, 247), and interactions with nanoparticle surfaces

(248, 249); and peptide-membrane interactions (250, 251). In future, MDSims may very well replace *in vitro* techniques due to low costs, high data outputs, and increased efficiency.

1.5. Background information

Ticks have become a source of novel peptides with a wide variety of uses (252, 253).However, AMPs are expensive to produce, with the cost increasing per amino acid, and thus truncated peptides with similar antimicrobial activity are developed for in depth investigations.

Anti-haemostatic, anti-inflammatory, antimicrobial peptides have been identified from the eggs, haemolymph, saliva, and salivary glands of many tick species including *O. savignyi* (254-256). *Ornithodoros savignyi* is classified as a livestock parasite commonly found in arid and semi-arid African regions (257, 258). Two defensins AMPs, OsDef1 and OsDef2, were previously identified in the midguts of *O. savignyi* ticks, and synthetic forms of the peptides were found to have antibacterial activity against Gram-positive bacteria (252). As OsDef2 antimicrobial activity was marginally greater than that of OsDef1, if was used as a template to produce shorter derivatives such as, peptide Os, representative of the carboxyl terminus. Electron microscopy, cell permeabilization assays, and peptide localisation studies were used to elucidate the mode of action. Os targets the outer membrane of *E. coli*, causes membrane permeabilization, and enters cells by crossing the second membrane (252, 253, 259).

Os was further modified to Os-C in which the cysteine residues were deleted, as truncation reduces the cost of synthesis and prevents nonspecific disulphide linkage formation. However, these shorter peptides lost activity in salt environments limiting the further development of these peptides for systemic purposes. Tryptophan tagging has been identified as a method to overcome the limitations of peptides like Os-C. Tryptophan tagging is a proven method to improve antimicrobial activity against Gram-positive and Gram-negative bacteria by increasing membrane and liposome permeabilization, with little increase in eukaryotic cell cytotoxicity as the tagged peptides are similar in structure to lipopeptides already present in bacterial membranes (32-34).

The MSc study of Ramafoko (260) revealed that W_5(Os-C), a synthetic derivative of Os-C with a 5-residue tryptophan residue tag on the N terminus, when screened with either the radial diffusion (RD) or colony forming unit assays (CFU), had increased antibacterial activity against Gram-negative *E. coli* (ATCC 25922) compared to Os-C. The antibacterial activity in 30% human serum was lost for Os-C using both the RD and CFU assays, while the Trp-tagged

peptide retained activity evaluated with the RD assay. However, when evaluated with the CFU assay, W_5(Os-C) was inactive in both 30% HS and a salt mix containing 0.15 M NaCl, 0.001 M $MgCl_2$ and 0.002 M $CaCl_2$, the equivalent salt concentration in 30% HS. No cytotoxicity was observed for Os-C and W_5(Os-C) against L929 mouse fibroblast cells.

Sequences and properties of OsDef1, OsDef2, and derivatives leading to W_5(Os-C) are shown in **Table 1.2.**

Table 1.2: Properties of defensins from *O savignyi*, OsDef1 and OsDef2, and derived AMPs.

Peptide	Sequence	AA*	Q	MW [g/mol]
OsDef1	GYGCPFNQYQCHSHCSGIRGYRGGYCKGAFKQTCKCY	37	+5	4172.8
OsDef2	GYGCPFNQYQCHSHCKGIRGYKGGYCKGAFKQTCKCY	37	+6	4185.9
Os	KGIRGYKGGYCKGAFKQTCKCY	22	+6	2459.9
Os-C	KGIRGYKGGY_KGAFKQT_K_Y	19	+6	2150.5
W_5(Os-C)	WWWWWKGIRGYKGGY_KGAFKQT_K_Y	24	+6	3081.55
(Os-C)W_5	KGIRGYKGGY_KGAFKQT_K_YWWWWW	24	+6	3081.55

*Number of amino acids

1.6. Aim of the study

The aim of this study was to determine for W_5(Os-C), the antimicrobial and anti-biofilm activity against Gram positive *S. epidermidis* ATCC 35984, potential synergism with vancomycin, cytotoxicity and lastly to evaluate the interaction of W_5(Os-C) with a model Gram-positive membrane.

1.7. Objectives of the study

The objectives of the study were to:

- Characterise and optimise *S. epidermidis* (ATCC 35984) planktonic and biofilm cultures.
- Determine whether peptide W_5(Os-C) exhibited anti-planktonic or biofilm inhibitory activity against *S. epidermidis* (ATCC 35984).
- Determine whether combining peptide W_5(Os-C) with vancomycin will enhance the anti-planktonic and/or biofilm inhibitory activity of either antimicrobial agent against *S. epidermidis* (ATCC 35984).
- Determine whether W_5(Os-C) and/or vancomycin exhibited cytotoxic effects against human epithelial cells.
- Characterize the structure of W_5(Os-C), peptide-peptide, and peptide-membrane interactions in a simulated salt environment.

CHAPTER 2: MATERIALS AND METHODS

2.1. MATERIALS

2.1.1. *Staphylococcus epidermidis* (ATCC 35984) cultures

Frozen stock (-80°C) inoculums of *S. epidermidis* (Winslow and Winslow, Evans (ATCC® 35984), strain designation RP52A, BSL1, obtained from Industrial Analytical (Pty) Ltd (Kyalami, South Africa) were grown overnight under aerobic conditions at 37°C in tryptic soy broth (TSB) (casein 1.7% (w/v), soya peptone 0.3% (w/v), sodium chloride 0.5% (w/v), dipotassium phosphate 0.25% (w/v), and dextrose 2.5% (w/v) obtained from Sigma-Aldrich/Merck, Johannesburg, South Africa). Tryptic soy broth agar plates (TSB with added 1.25% (w/v) bacteriological agar) were prepared and then were streaked, sealed, and incubated at 37°C in an inverted position for 24 h. The plates were stored at 4°C and served as a source of colonies for inoculations. New streak plates were prepared every two weeks from frozen stocks to avoid variation in culture densities and genetic composition.

2.1.2. HaCat cell cultures

HaCat cells (Cellonex, Roodepoort, South Africa) were maintained in Dulbecco's Modified Eagle's Medium supplemented with foetal bovine serum 10% (w/v) and antibiotics 1% (w/v) (100 U/mL penicillin; 0.1 mg/mL streptomycin; 0.25 µg/mL amphotericin B; obtained from PAN Biotech, Aidenbach, Germany; DMEM/FCS). Incubation occurred in a 5% CO_2, 90% humidity environment until 75 ± 5% confluency (2 to 5 x 10^4) was achieved. Cell splitting occurred every 3-4 days as necessary.

2.1.3. Biofilm promoting media (BPM)

Many organisms including *S. epidermidis* develop biofilms in response to environmental stresses. Biofilm promoting media (BPM) was used to induce biofilm development in *S. epidermidis* (ATCC 35984) (122, 261). This media was prepared by diluting TSB in a 1:1 ratio with 0.01 M phosphate buffer (pH 6.6; Sigma-Aldrich/Merck, Johannesburg, South Africa) containing 0.25% D-α-glucose (Sigma-Aldrich, Johannesburg, South Africa).

2.1.4. Bacterial cell culture medium

For growth of general *S. epidermidis* (ATCC 35984) stock and experimental cultures, TSB was prepared by dissolving tryptic soy broth powder into double distilled, sterilized, filtered water (ddsH_2O) to prepare a 3% (w/v) solution. The solution was autoclaved, kept at 4°C for

maximum 4 weeks, and weekly spread plate sterility tests were performed to avoid contamination.

2.1.5. Antimicrobial agents

The sequence or structure and physicochemical properties of the different antimicrobial agents used in this study is summarised in **Table 2.1**.

Table 2.1: Properties of antimicrobial agents used in this study

Antimicrobial	Sequence	AA	Q	MW (g/mol)	pI	Hydro-phobicity (%)
Vancomycin	See Figure 1.1	7	+0.67	1449.2	8.30	N/A
Melittin	GIGAVLKVLTTGLPALSISWIK RKRQQ-NH_2	26	+6	2846.5	4.69	46.43
W_5(Os-C)	WWWWWKGIRGYKGGYKGA FKQTKY	24	+6	3081.55	10.67	33.33

AA = number of amino acids; Q = Charge at neutral pH ; MW =.Molar mass in $g.mol^{-1}$.: pI = isoelectric pH;

2.1.5.1. W_5(Os-C) and melittin

Peptides W_5(Os-C) and melittin, shown in **Table 2.1** were obtained from GenScript (Piscataway, NJ, USA). Melittin is a bee venom derived AMP used in this study as an antimicrobial and cytotoxicity positive control (262, 263). The purity (>95%) and molecular mass of the peptides were determined using reverse-phase high performance liquid chromatography and mass spectrometry, respectively. Vials each containing ± 1 mg were stored at -20°C until used. The content of one vial was suspended in 300 µL ddsH_2O. Once fully dissolved, a 20 µL sample was further diluted in 180 µL ddsH_2O and its absorbance measured at 280 nm using ddsH_2O as a blank. Absorbance values were used to determine the concentration using **Equation 2.1 c** derived from the Beer-Lambert Law (**Equation 2.1 a**).

2.1 a $$c_{mg/ml} = \frac{A_{280\ nm} \times df \times MW_{peptide}}{n(\varepsilon Tyr)\ n(\varepsilon Trp)}$$ (Beer-Lambert Law)

2.1 b $$c_M = \frac{c_{mg/ml}}{MW_{peptide}}$$

2.1 c $$c_M = \frac{A_{280\ nm} \times df}{n(\varepsilon Tyr) + n(\varepsilon Trp)}$$

In **Equations 2.1 a-c**, $c_{mg/ml}$ is the peptide concentration in mg/ml, c_M is the peptide concentration in mol/L, $A_{280\ nm}$ is the absorbance of the peptide at 280 nm, *df* is the dilution factor used to prepare sample used in absorbance measurement, *n* is the number of tryptophan

or tyrosine residues, and (εTrp) (5560 AU/mmol/mL) and (εTyr) (1200 AU/mmol/mL) are the extinction coefficients of tryptophan and tyrosine, respectively (264). Using the c_M data obtained, the suspension was further diluted using ddsH_2O to stock a concentration of 400 µM for W_5(Os-C) and 500 µM for melittin, aliquoted, and stored at -20°C.

2.1.5.2. Vancomycin

Vancomycin hydrochloride, dissolved in DMSO, was obtained from Sigma-Aldrich (Johannesburg, South Africa). The solution was diluted in ddsH_2O to a stock concentration of 400 µM, aliquoted, and stored at -20°C. The final concentration of dimethyl sulfoxide (DMSO) in the stock solutions was calculated as 0.58% (v/v), and thus 0.058% in all assays, at which the DMSO had no observable effect on the growth of *S. epidermidis* cultures (results not shown).

2.2 Methods

2.2.1 Growth curves of *S. epidermidis* (ATCC 35984) in different media

The growth curves of *S. epidermidis* under various conditions were determined to identify the optimal culture incubation period for further studies. *Staphylococcus epidermidis* cultures were prepared and incubated overnight. The culture was used to prepare a 1/200 dilution in either TSB or BPM. These dilutions, as well as that of a new culture from -80°C glycerol stocks were incubated over 32 h at 37°C with shaking. Hourly optical density at 600 nm (OD_{600}) measurements using the SpectraMax® Paradigm® Multi-Mode Microplate Reader (Molecular Devices, Sunnyvale, CA, USA) were recorded and plotted against time.

2.2.2 Anti-planktonic activity

2.2.2.1 Growth inhibition assays

The anti-planktonic activity of antimicrobial agents was determined using the microbroth dilution assay as described by Maisetta *et al.* (122) with the following optimized condition: *S. epidermidis* cultures were prepared by transferring 3-5 colonies from a single agar plate into TSB and incubated overnight. The inoculum was diluted to an OD_{600} of 0.650 (0.9 to 1.1 x10^7 CFU.mL^{-1}) and was then diluted 1/200 into BPM.

Sodium phosphate buffer (0.01 M, pH= 6.6) was prepared by dissolving sodium phosphate monobasic monohydrate and sodium phosphate dibasic heptahydrate (both obtained from Sigma-Aldrich/Merck, Johannesburg, South Africa) in a ratio of 1:1.3 (w:w) in ddsH_2O. The pH

was adjusted to pH 6.6 followed by autoclaving. The buffer was stored for a maximum of 4 weeks and weekly spread plate sterility tests were performed to avoid contamination.

Stock vials of vancomycin (antibiotic control), melittin (AMP control) and W_5(Os-C) were defrosted at room temperature and serially diluted two-fold in ddsH_2O to concentrations ranging from 3.13 µM to 400 µM for vancomycin and W_5(Os-C), and 0.78 µM to 500 µM for melittin. Aliquots of 10 µL of the antimicrobials, at the various concentrations, were added in triplicate to wells of flat bottom 96 well polypropylene plates (Merck, Modderfontein, South Africa). Wells with 10 µL ddsH_2O instead of antimicrobial agent served as the growth control and culture free BPM as the blank. Well volumes were made up to 100 µL by adding 90 µL inoculated BPM, diluting the antimicrobials ten-fold (final concentration range of 0.31 µM to 40 µM for vancomycin and W_5(Os-C), and 0.08 µM to 50 µM) . All empty wells were filled with ddsH_2O to prevent evaporation. The microplates were incubated for 16 h at 37°C with shaking, whereafter the OD_{600} was measured. Dose-response curves were generated by calculating the percentage growth inhibition using **Equation 2.2 a** and plotting it against the logarithm of the concentration of each antimicrobial:

Equation 2.2 a: $$Growth\ inhibition\ (\%) = 100 - \frac{Abs_{sample\ concentration} \times 100}{Abs_{growth\ control}}$$

The MIC_{50} values were defined as the concentration at which 50% inhibition was observed when compared to the growth control and calculated using GraphPad Prism (Dotmatics, San Diego, California). The MIC_{max} values were calculated as described by Rautenbach *et al.* (265) where the intercept of the slope and plateau tangents on the dose-response curves represents the concentration at which maximum inhibition was observed.

2.2.2.2 Vancomycin and peptide combination anti-planktonic assay

The antibacterial activity of W_5(Os-C) in combination with vancomycin at fixed ratios of 3:1 (3V:1W), 1:1 (2V:2W) and 1:3 (1V:3W) was evaluated as described by Shang *et al*. (266) with minor modifications (266). As this was a pilot study, testing fewer concentration ratios significantly reduced peptide usage. This study provided a preliminary indication of any synergistic effects, whilst also reducing the cost of antimicrobial agent screening. This method was used to determine whether a more extensive checkerboard assay would be required. Concentrations of 10 µM, 20 µM, 30 µM for vancomycin and W_5(Os-C) were prepared and equal volumes were then mixed together (**Table 2.2**) resulting in solutions with a total

antimicrobial concentration of 20 µM. Serial two fold dilutions were then prepared so that the final antimicrobial agent concentration in the dilution plate for the anti-planktonic assay (described in section 2.1.2.1) ranged from 0.16 µM 15 µM in terms of vancomycin.

Table 2.2: Preparation of combinations of vancomycin and W_5(Os-C).

Ratio*	Vancomycin (µM)	W_5(Os-C) (µM)	Final ratio [Total antimicrobial concentration (µM)]
3V:1W	30	10	15:5 [20]
2V:2W	20	20	10:10 [20]
1V:3W	10	30	5:15 [20]

*V = vancomycin; W = W_5(Os-C)

The fractional inhibitory index (∑FIC) is the standard method for identifying synergistic, additive, indifferent, or antagonistic effects as described in the EUCAST Definitive Document E.Def 1.2 (267) using the formulas 2.2 b to d.

2.2 b $$FIC_A = \frac{MIC_{A\ in\ the\ presence\ of\ B}}{MIC_{A\ alone}}$$

2.2 c $$FIC_B = \frac{MIC_{b\ in\ the\ presence\ of\ A)}}{MIC_{B\ alone}}$$

2.2 d $$\sum FIC = FIC_A + FIC_B$$

Where $MIC_{A\ in\ the\ presence\ of\ B}$ represents the concentration of antimicrobial A in the presence of antimicrobial B at which maximum inhibition (>95%) was observed and vice versa for $MIC_{B\ in\ the\ presence\ of\ A}$; $MIC_{A\ alone}$ represents the minimum inhibitory concentration of antimicrobial A in the absence of antimicrobial B and vice versa for $MIC_{B\ alone}$; FIC_A is the fractional inhibitory concentration of antimicrobial A in the presence of antimicrobial B and vice versa for FIC_B; and ∑FIC is the fractional inhibitory index of the combination of antimicrobials A and B.

However, due to incomplete or non-standard dose-response curves, no ∑FIC values for the effect of W_5(Os-C) on vancomycin were calculated.

2.2.3 Anti-biofilm activity

2.2.3.1 Optimisation of biofilm growth conditions

The biofilm inhibition assay as described by Maisetta *et al.* (122) produced biofilms too thick to visualise with an inverted microscope and thus the assay required optimisation. The cell dilution and incubation time required to develop stable mature biofilms, were optimised. To determine the required dilution, aliquots of 90 µL overnight *S. epidermidis* (OD_{600} = 0.6) broth

cultures were diluted to concentrations ranging from 1/100 to 1/800 in BPM and plated in polystyrene 96 well plates from Merck (Modderfontein, South Africa) for 24 h. Subsequently, at a dilution 1/200, the biofilm density development was evaluated at different time intervals ranging from 2 to 24 h.

Upon completion of both experiments, un-adhered cells were removed by washing the biofilm twice with sodium phosphate buffer (0.01 M, pH= 6.6), fixed with 10% formalin (100 µL) with 5 min incubation, washed again with sodium phosphate buffer, and stained with crystal violet (CV) to visualise biofilms and quantify the amount of biomass developed (**Figure 2.1**). The CV solution was prepared by dissolving CV powder from Sigma-Aldrich (Johannesburg, South Africa) into ethanol (EtOH) to form a 4% (w/v) solution. This solution was diluted to 0.1% (w/v) in ddsH_2O and stored at room temperature. Excess dye was removed by washing the fixed biofilms with 99.8% EtOH. Images of the developing and established biofilms were taken with an inverted microscope (Optika inverted light microscope and camera, Ponteranica, Italy).

Crystal Violet is a cationic dye that binds electrostatically to the negatively charged DNA (cellular) and eDNA (ECM) backbone phosphate groups, anionic cellular proteins within cells, and anionic teichoic and teichuronic acids within the ECM (268-270).

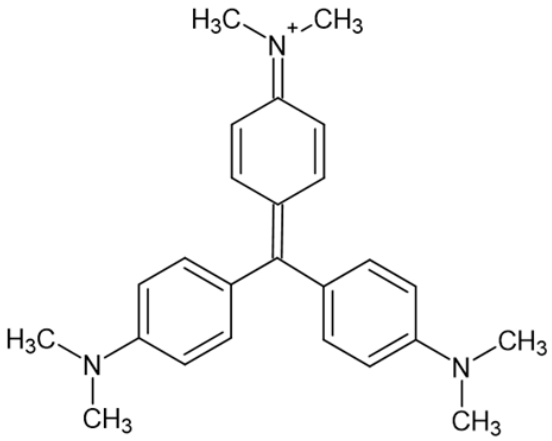

crystal violet

Figure 2.1: Chemical structure of crystal violet. CV is a positively charged (basic), purple dye binding to negative charges on cell components (DNA, RNA, proteins, and phosphate groups) and is commonly used in biomass quantification. Structure drawn using ChemSketch (ACD/Labs).

2.2.3.2 Biofilm inhibition assays

The biofilm inhibition assay was conducted as described by Maisetta *et al.* with a few adjustments following optimisation (122). Overnight *S. epidermidis* broth cultures were diluted 1/200 with BPM and incubated with vancomycin, melittin, or W_5(Os-C) in concentrations ranging from 0.31 µM to 40 µM for vancomycin, 0.78 µM to 50 µM for melittin, and 0.31 µM to 20 µM for W_5(Os-C) in polystyrene 96 well plates at 37°C, non-shaking, for 24 h to produce mature biofilms. The BPM provided a biofilm promoting environment while the polystyrene plates provided a surface suitable for cellular adherence. Biofilms developed in the absence of peptides served as the growth control and culture free BPM as the blank.

For the determination of biofilm cell viability, the CellTitre Blue (CTB) assay was used. In this reaction the weakly fluorescent blue-purple redox indicator resazurin is reduced by NADH in metabolically active cells to pink, fluorescent resorufin (**Figure 2.2**). Liquid alamarBlue Cell viability Reagent from Thermo Fisher Scientific (Johannesburg, South Africa), was kept at -20°C and diluted to 10% (v/v) using the sodium phosphate buffer (0.01 M, pH= 6.6) when needed. The solution was handled under low light intensity conditions and vials were covered in foil to avoid degradation of resazurin, the active dye in alamarBlue, as well as resorufin, the product of the CellTiter Blue® assay. Exposure of these chemicals to light causes increased background fluorescence during assay measurements. Only metabolically active cells produce enough NADH to reduce detectable amounts of resazurin to resorufin. The method is preferential to direct measurement of fluorescence of NADH as metabolically active cells rapidly recycle NADH into NAD^+. The quantity of resorufin formed is directly proportional to the metabolic activity of the cells (271).

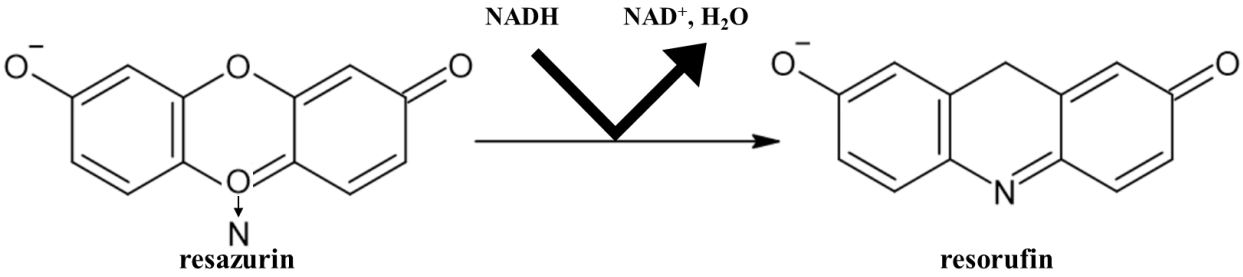

Figure 2.2: Chemical reaction of resazurin and NADH. Cell titre blue (resazurin) is reduced by NADH, a product of metabolically active cells, to pink resorufin. This redox reaction is often used to test for cell viability after exposure to a potential antimicrobial agent. Structures drawn using ChemSketch (ACD/Labs).

For biofilm cell viability determination, un-adhered cells were flushed out from the 24 h old biofilms by washing the biofilm twice with sodium phosphate buffer (0.01 M, pH = 6.6), 100 µL

1% CTB was then added, and the CTB filled wells were incubated for 1 h with mild shaking at 37°C. Fluorescence with excitation at 535 nm and emission at 590 nm was measured to quantify cell viability using the SpectraMax® Paradigm® Multi-Mode Microplate Reader (Molecular Devices, Sunnyvale, CA, USA).

From fluorescence measurements, dose-response curves were generated using **Equation 2.2a.** The $^{v}BIC_{50}$ values were defined as the concentration at which 50% inhibition of biofilm cell viability was observed when compared to a growth control and calculated using GraphPad Prism (Dotmatics, San Diego, California). The $^{v}BIC_{max}$ values were calculated as described by Rautenbach *et al.* (265) where the intercept of the slope and plateau tangents on the dose-response curves represents the concentration at which maximum inhibition of biofilm cell viability was observed.

For biofilm biomass determination, the biofilms were washed twice with sodium phosphate buffer (0.01 M, pH = 6.6), fixed with 100 µL 10% formalin with 5 min incubation as described by Yuwen *et al.* (272). The biofilms were washed again with sodium phosphate buffer, and stained with 0.1% (w/v) CV (see section 2.2.3.1). Following two more washing steps with sodium phosphate buffer, 100 µL 0.1% CV was added to each well and incubated at room temperature for 1 h. Excess CV was discarded, and wells washed with 99.8% EtOH to remove any unbound stain. Bound stain was extracted by incubating stained biofilms in 100 µL acetic acid for 15 min and then transferring the CV-acetic acid solution to a new 96 well plate.

From OD_{600} measurements, dose-response curves were generated using **Equation 2.2a**. The $^{bm}BIC_{50}$ values were defined as the concentration at which 50% inhibition of biofilm biomass was observed when compared to a growth control and calculated using GraphPad Prism (Dotmatics, San Diego, California). The $^{bm}BIC_{max}$ values were calculated as described by Rautenbach *et al.* (265) where the intercept of the slope and plateau tangents on the dose-response curves represents the concentration at which maximum inhibition of biofilm biomass was observed.

2.2.3.3 Vancomycin and W_5(Os-C) combination anti-biofilm assay

The anti-biofilm activity of W_5(Os-C) in combination with vancomycin at fixed ratios of 3:1 (3V:1W), 1:1 (2V:2W) and 1:3 (1V:3W) was evaluated as described by Mishra *et al.* (216) with slight modifications. The antimicrobial agents vancomycin and W_5(Os-C) were first prepared to concentrations ranging from 10 µM to 30 µM and mixed in equal volumes to prepare

combination concentrations as described for the anti-planktonic combination studies (**Table 2.2**). The biofilm inhibition CTB and CV assays were performed as described in sections 2.1.3.1 and 2.1.3.2. The FIC values were calculated if possible using **Equations 2.2 b-d (section 2.1.2.2)**.

2.2.4 HaCat cytotoxicity

A (3-(4,5-dimethylthiazol-2-yl)-2,5-diphenyltetrazolium bromide (MTT) solution was prepared by first preparing a 0.1 M phosphate buffered solution (PBS). The PBS was prepared by weighing and dissolving Na_2HPO_4, $NaH_2PO_4 \cdot H_2O$, and NaCl (3:1:25 w:w:w) from Merck (Modderfontein, South Africa) into ddsH_2O. Once the salts had dissolved, the solution pH was adjusted to 7.4 using 1 M HCl or 1 M NaOH solution and autoclaved to sterilize. Once the solution had cooled, MTT powder from Merck (Modderfontein, South Africa) was weighed and dissolved into the PBS to produce an MTT solution of 1 mg/mL.

The HaCat cells are primary spontaneously immortalized human keratinocytes obtained from a 62 year old male (273). As *S. epidermidis* is a skin-associated pathogen it was necessary to determine the cytotoxicity of the antimicrobials used in this study in a relevant cell type. Cytotoxicity was determined with the MTT cell viability assay. Metabolically active cells use NADH to reduce yellow MTT to insoluble purple formazan crystals as shown in **Figure 2.3**. Damaged or metabolically inactive cells do not produce NADH in sufficient amounts to reduce MTT (274).

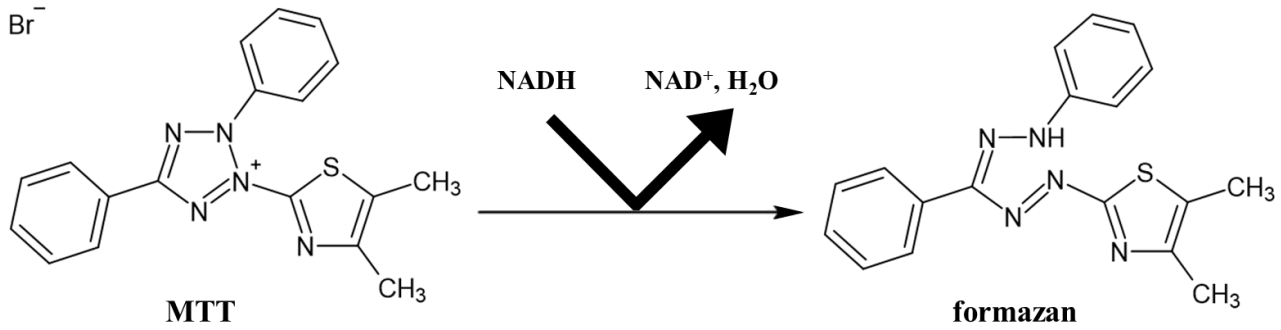

Figure 2.3: The reaction of MMT with NADH. Yellow MTT is reduced by NADH, a product of metabolically active cells, to purple, insoluble formazan. Structures drawn using ChemSketch (ACD/Labs).

Mature cell layers were grown by seeding 90 µL of cells at 75 ± 5% confluency into 96 well cell culture treated plates from Merck (Modderfontein, South Africa) and incubated for 24 h at 37°C to allow even attachment to the well surface. Subsequently, either 10 µL of vancomycin (5 µM

and 25 µM final concentrations), melittin (12.5 µM; AMP control) or W_5(Os-C) (5 µM and 25 µM final concentrations) were added in triplicate. The antimicrobial exposed mature cells were incubated for a further 24 h. Cell viability was then determined by adding 10 µL MTT (0.1 mg/mL) to each well. The plate was returned to the incubator and after 3 h the medium was discarded and the plates blotted until dry. All formazan crystals were dissolved in 100 µL of 25% DMSO in EtOH. The OD_{570} was measured using the UV/Vis spectrophotometer (KLAB, Yuseong-gu, Daejeon, Republic of Korea). The percentage cell viability was calculated relative to the control (100% viability) where no antimicrobial agents were added.

2.2.5 *In silico* peptide characterisation

In silico characterisation of AMPs can provide important information on the structure of peptides and their interaction with bacterial membranes, each other or with other molecules. The primary peptide sequence is submitted to an online algorithm, in this case PEP-FOLD. Predictions are determined from the average folding observed in known protein structures (275). This predictive model builds the peptide one amino acid at a time and runs 100-200 simulations as it constructs the full peptide sequence in order to predict folding. The limitations of this approach are that PEP-FOLD cannot predict disulphide bond formation, and the use of coarse-grained force fields in which molecules or side chains are simplified to single, large, round entities to circumvent high degrees of freedom (276, 277), and only determines the peptide structure at a neutral pH (278). Running a PEP-FOLD algorithm prediction produces a file which can be used to simulate a specific environment called a simulation box. The simulation box is usually a cubic simulated environment containing water molecules as well as the peptide of interest. Additional simulation components including ions, other proteins, membranes etc. may be added to the water box. The size of the box may be varied to accommodate specific factors included as well as computational limitations (279, 280). The box and environment is further restricted by one of three ensembles i.e. microcanonical (constant molar amount, volume, and energy; NVE), canonical (constant molar amount, volume, and pressure; NVP), or isothermal-isobaric (constant molar amount, pressure, and temperature; NPT) to increase simulation accuracy (240, 244). Ions are also added to obtain neutral electrical charge (240). The output simulation box is submitted to a supercomputer with sufficient processing ability.

The computer applies Chemistry at Harvard Macromolecular Mechanics (CHARMM) simulations using model molecules with experimentally determined properties as well as mathematical modelling to predict the interactions and lowest energy states of specific

simulation box components (281, 282). By applying CHARMM to run a simulation, multiple data parameters including atom to atom distances, hydrogen bonding, three-dimensional position within a simulation box, phi and psi angles etc. are measured. The data is finally processed by applying uniquely coded scripts specific to the aims of an investigation to extract and represent data in an easily interpretable format including data tables, graphs, and heatmaps using data science graphical user or command line interfaces and notebooks to accommodate and process the code in a user-friendly manner (283, 284).

Peptide characterisation was performed in three phases. The first phase was to predict the secondary and tertiary structure of W_5(Os-C) from the primary sequence. This was completed by entering the sequence of W_5(Os-C) into PEP-FOLD Peptide Structure Prediction server on the RPBS Mobyle Portal (278, 285-287). The PEP-FOLD algorithm utilizes a hidden Markov model to predict the folding of four sequential amino residues, then repeated with the first residue removed and the fifth added. This process is continued until the end of the sequence is reached (278). The algorithm also applies a greedy approach which allows forward (N to C terminal) as well as reverse (C to N terminal) building of the peptide while each consecutive fragment is overlapped with the previous fragment to align the α-carbons that are present in both fragments. The 1000 lowest energy conformations are selected, and 2000 random remaining low energy conformations are saved for further refinement procedures. Once the complete peptide is obtained, the saved energy conformations are used to rerun the algorithm on the entire protein sequence to produce a final structure. The first run results in limited conformational information due to consideration of only immediately neighbouring residues. The second run is applied to elucidate additional interactions among distant residues (288). This method can be improved by an additional run of fragments starting from random or predetermined internal portions of the peptide sequence and working outwards to the N- and C termini to predict folding influenced by internal residues without terminal residue interactions interfering (289). The limitation of not considering disulphide bridges did not affect the simulation of W_5(Os-C) as the peptide lacks cysteine residues. The most common structure predicted during the simulations was chosen and converted into a PyMOL file for visualisation and processing (290-292). The hydrophobicity of W_5(Os-C) was predicted using the color_h script in PyMOL which employs the Eisenberg hydrophobicity scale to calculate the hydrophobic dipole moment (293, 294).

For the second phase, the PyMOL file generated in the first phase was first submitted to CHARMM-GUI solution builder. A single W_5(Os-C) molecule was added to a water box

consisting of transferable intermolecular potential 3P water (TIP3P) (295, 296). The Nose-Hoover thermostat was then applied for using the steepest descent algorithm to determine the minimum energy at 303.15 K using the NVT ensemble for a 1000 ns production run. This method assumes constant number of particles, volume, and temperature of the system while allowing the energy of the system to vary. The thermostat also applies modified Newtonian dynamics with Lagrangian equations of motion. (297, 298). Salt concentrations were adjusted by adding Na^+ and Cl^- ions to a concentration of 0.15 M representing physiological conditions, or a concentration 0.30 M representing a high salt environment using the Monte-Carlo ion placing method.

The minimized and equilibrated W_5(Os-C) tertiary structure obtained from the H_2O simulation was then submitted for MDSims to begin the third phase. The MDSims were applied to predict the interaction between W_5(Os-C) and a simulated Gram-positive bacterial cell membrane. Simulations were performed using the Gromacs approach on a DELL Precision quad core T3400 or T3500 workstation, each with two NVIDA PNY GeForce GTX570 or GTX580 graphics cards powered by a 1kW power supply (299, 300). A pre-assembled bilayer of 1-palmitoyl-2-oleoyl-sn-glycero-3-phospho-(1'-rac-glycerol) (POPG), constructed using the CHARMM-GUI system, was used to simulate a Gram-positive cell membrane. Solvation of the system was performed using TIP3P (295, 296) and neutralized with Na^+ ions.

Four W_5(Os-C) peptides were inserted at least 100 Å above the POPG bilayer and at least 20 Å apart (301, 302). The Nose-Hoover thermostat was then applied using the steepest descent algorithm to determine the minimum energy at 303.15 K using the NVT ensemble. Once the maximum force was limited to <1000.00 kJ/ml/nm, equilibration was achieved by constraining the peptide positions, the NPT ensemble was run for 1000 ps. This ensemble keeps pressure and temperature constant while applying the Lincs algorithm to constrain hydrogen bond angles. Parameters for the NPT ensemble were to run simulations for 2 fs intervals with measurements recorded every 2 ps (301, 302). The simulations were run for a total of 1000 ns to investigate the dynamics of interactions between W_5(Os-C) and the Gram-positive membrane.

Output files from the simulations were processed with scripts in the Anaconda data science platform using the Jupyter notebook application to present data in graph and heatmap formats (283, 284).

2.2.6 Statistical analysis

All sigmoidal dose-response curves were generated with non-linear regression analysis using GraphPad Prism 7 software (GraphPad Software, San Diego, CA, UAS). Dose-response was calculated using **equation 2.2 e**:

$$Dose - response = \frac{response_{max} - response_{min}}{1 + 10^{\log(IC_{50}) - \log[peptide]) \times Hill\ slope}} \qquad \text{Equation 2.2 e}$$

Where $response_{max}$ is the maximum dose-response and $response_{min}$ the minimum dose-response, IC_{50} refers to the average of the maximum and minimum dose-response values determined using GraphPad Prism (Dotmatics, San Diego, California)., and Hill slope is the best-fit value as calculated by GraphPad software. Results are presented as mean ± standard error of the mean (SEM) with all experiments encompassing 3 biological repeats with 3 technical repeats each, unless otherwise stated.

CHAPTER 3: RESULTS

3.1 Growth curve determination of *S. epidermidis* (ATCC 35894)

In order to evaluate the antimicrobial activity of vancomycin, melittin, and W_5(Os-C) against *S. epidermidis*, growth conditions needed to be optimised. Using the methods described by Maisetta *et al.* (122) specifically required optimisation of BPM as the growth medium. Biofilm promoting media induces biofilm development through nutrient depletion stress which could affect growth of planktonic cultures. The first optimisation step was to determine the growth curve of *S. epidermidis* cultures under the various conditions to compare planktonic growth from overnight cultures in BPM and TSB, and glycerol stock cultures in TSB (**Figure 3.1**).

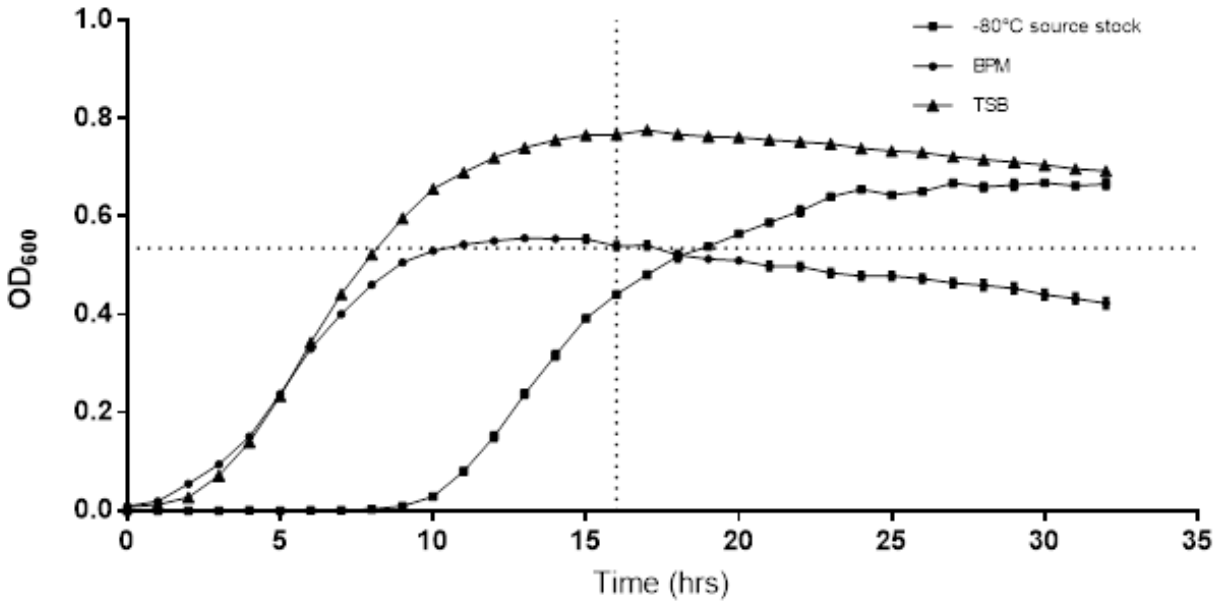

Figure 3.1: The growth curves of *S. epidermidis* under various conditions. A -80˚C stock culture inoculum was incubated in TSB (▪). Two overnight (16h) 1/200 inoculums were prepared from this initial culture and incubated in BPM (●) or TSB (▲). Results are from two independent experiments each with three technical repeats.

The growth curves indicated that when the bacteria is inoculated into TSB directly from source stocks kept at -80°C, there was a long lag phase of 9 h (**Figure 3.1**). In contrast, inoculations from overnight cultures in TSB or BPM resulted in a less than 2 h lag phase. The gradients of the logarithmic phase of growth under all three conditions were similar (**Table 3.1**).

Table 3.1: Analysis of the growth curves of *S. epidermidis* under various conditions used in this study.

	-80°C in TSB	Overnight in TSB	Overnight in BPM
Lag phase (hours)	9	2	2
Gradient of log phase	0.077	0.096	0.083
R^2 *	0.998	0.988	0.933

*Calculated for the linear log phase of growth

Source stock inoculations in TSB reached the stationary phase after 24 h while the overnight cultures in TSB reached the stationary phase after 15 h. After 10 h in BPM cultures reached a lower OD_{600} for the stationary phase when compared with cultures grown in TBS. This reduction in growth is possibly due to nutrient depletion after 16 h. The selected growth conditions for subsequent studies were 16-18 h in TSB for overnight cultures and 16 h for BPM cultures.

3.2 Antimicrobial activity

3.2.1 Anti-planktonic activity of W_5(Os-C)

The effect of the controls vancomycin and melittin, as well as W_5(Os-C) against planktonic *S. epidermidis*, was determined using the microbroth dilution method. Dose-response curves were generated in order to determine MIC_{50} and MIC_{max}. MIC_{50} values were calculated as the concentration at which 50% inhibition was observed. MIC_{max} values were obtained from the concentration at which the tangents to the slope and maximum of the dose-response curve intersect.

Vancomycin (**Figure 3.2A**) and W_5(Os-C) (**Figure 3.2B**) exhibited activity against planktonic cultures at similar concentrations and were more potent than melittin (**Figure 3.2C**). All antimicrobials were active in the low micro-molar range (**Table 3.2**).

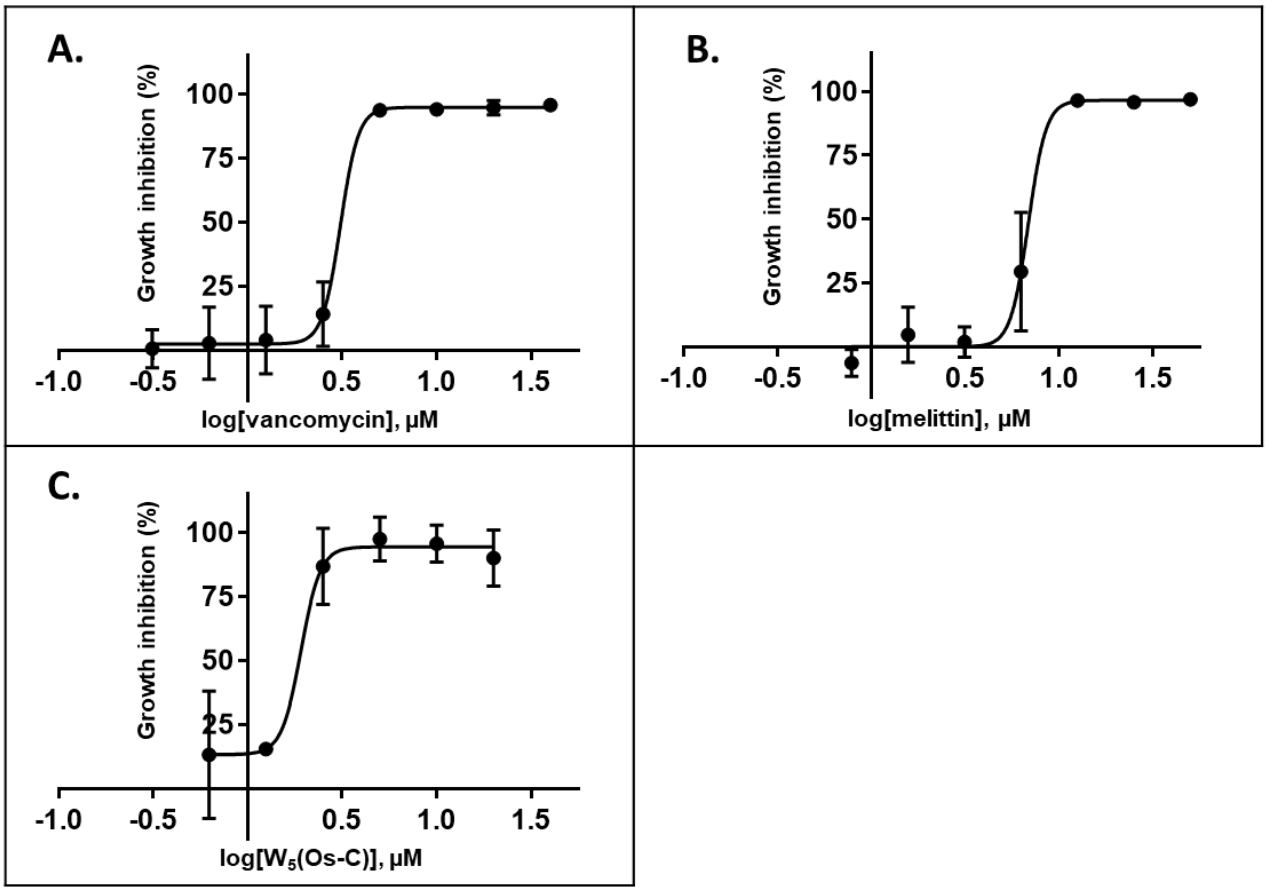

Figure 3.2: Inhibitory effect of (A) vancomycin, (B) melittin, and (C) W_5(Os-C) against planktonic *S. epidermidis* (ATCC 35984) cultures. The final concentration range for vancomycin, melittin and W_5(Os-C) were 0.31 µM to 40 µM for vancomycin, 0.78 µM to 50 µM for melittin, and 0.63 µM to 20 µM for W_5(Os-C) respectively. Error bars indicate mean ± SEM. Results are from three independent experiments each with three technical repeats.

When comparing the MIC_{50} values of all three antimicrobial agents, vancomycin and W_5(Os-C) had values significantly lower than that of melittin ($p<0.001$ and $p<0.0001$ respectively) with no significant difference between the MIC_{50} values of W_5(Os-C) when compared to vancomycin. However, the MIC_{max} of W_5(Os-C) was found to be significantly lower than that of vancomycin ($p<0.05$), with both vancomycin and W_5(Os-C) MIC_{max} values significantly lower than that of melittin ($p<0.0001$).

Table 3.2: MIC_{50} and MIC_{max} values of vancomycin, melittin, and W_5(Os-C).

Antimicrobial	MIC_{50} (µM)[a]	MIC_{max} (µM)[b]
Vancomycin	3.09 ± 0.09***	3.83 ± 0.17**** (>95%)
Melittin	6.84 ± 0.43	8.67 ± 0.30 (>95%)
W_5(Os-C)	1.91 ± 0.29****	2.44 ± 0.29**** † (>90%)

Each reported value represents the mean ± standard error of the mean (SEM). Results are from three independent experiments each with triplicate sampling. [a]MIC_{50} values were calculated as the concentration at which 50% inhibition was observed. [b]MIC_{max} values were obtained from the concentration at which the tangents to the slope and maximum of the dose-response curve intersect. Maximum percentage inhibition indicated in brackets next to MIC_{max} values.*** and **** Statistically significant difference to melittin ($p<0.001$ and $p<0.0001$); one way ANOVA with Tukey correction. *MIC_{max} statistically different from MIC_{50} of same compound ($p<<0.05$); unpaired, one tailed student's t-test (shown next to antimicrobial agent name). †Statistically significant difference to vancomycin ($p<0.05$); one way ANOVA with Tukey correction.

3.2.2 Synergism studies of W_5(Os-C) and vancomycin against planktonic cells

The antibacterial activity of W_5(Os-C) in combination with vancomycin at fixed ratios of 3V:1W, 2V:2W and 1V:3W was evaluated against planktonic *S. epidermidis.* The dose-response curves of vancomycin and W_5(Os-C) were included in **Figure 3.3A and B** for comparative purposes. A complete dose-response curve could be obtained for the 3V:1W and 2V:2W combinations but not for the 1V:3W combination (**Figure 3.3C to E**).

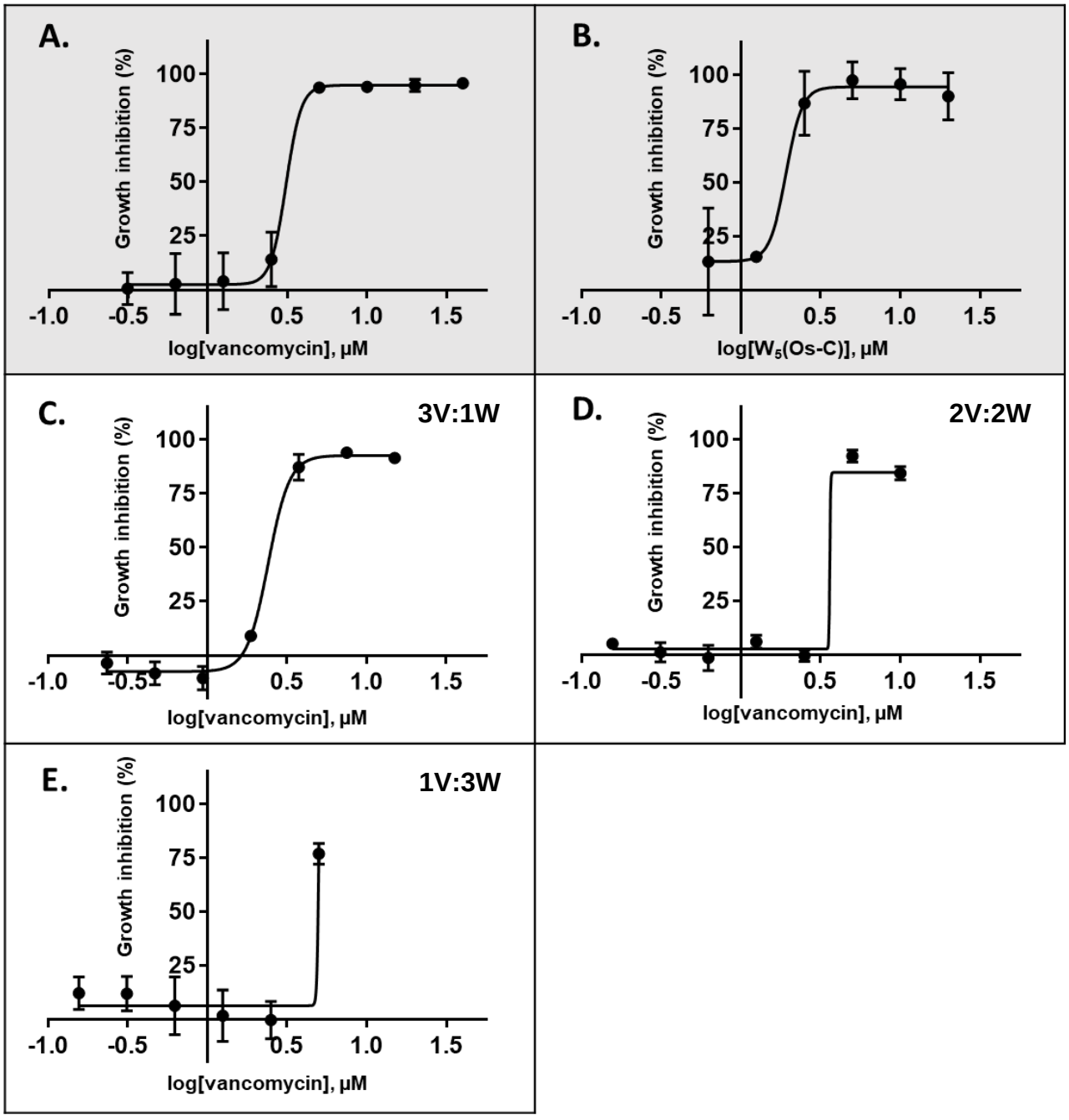

Figure 3.3: Growth inhibitory activity of (A) vancomycin, (B) W_5(Os-C), and vancomycin and W_5(Os-C) in combination ratios (C) 3V:1W, (D) 2V:2W, and (E) 1V:3W against planktonic *S. epidermidis* (ATCC 35984). Serial doubling dilutions of the combinations were prepared so that the final antimicrobial agent concentration ranged from 0.31 µM - 20 µM and plotted in terms of the concentration of vancomycin (0.16 µM - 15 µM). Error bars indicate mean ± SEM. Results are from three independent experiments each with three technical repeats.

Both MIC_{50} and MIC_{max} values were calculated for the 3V:1W and 2V:2W ratios but not the 1V:3W ratio due to the poor fit of the generated curve. None of the ratios could reach the >95% inhibition cut-off (**Table 3.3**).

Table 3.3: MIC_{50} and MIC_{max} values of vancomycin, W_5(Os-C), and vancomycin and W_5(Os-C) in combination ratios 3V:1W, 2V:2W and 1V:3W.

Antimicrobial agent	MIC_{50} (µM)[a]	MIC_{max} (µM)[b]
Vancomycin alone	3.09 ± 0.09	3.83 ± 0.17 (>95%)
W_5(Os-C) alone	1.91 ± 0.29	2.44 ± 0.29 (>90%)
Ratio 3V:1W	2.01 ± 0.15¥	3.31 ± 0.43¥ (>90%)
Ratio 2V:2W	3.61†	3.63 (84%)
Ratio 1V:3W	5.00†	ND (76%)

Each reported value represents the mean ± standard error of the mean (SEM). Results are from three independent experiments each with triplicate sampling. [a]MIC_{50} values were calculated as the concentration at which 50% inhibition was observed. [b]MIC_{max} values were obtained from the concentration at which the tangents to the slope and maximum of the dose-response curve intersect. Maximum percentage inhibition indicated in brackets next to MIC_{max} values. ¥ Value and statistics not considered accurate due to complete but insufficient dose-response curve fit.† No statistical analysis due to an incomplete dose-response curve. ND- not determined due to an incomplete dose-response curve.

Initial observations indicated significantly increased activity for a 3V:1W ratio at the respective concentrations of 2.50 µM: 0.83 µM ($p<0.005$). As such, the MIC_{50}, and MIC_{max} values for this ratio were calculated as 2.01 ± 0.15 µM and 3.31 ± 0.43 µM, respectively. At 5.00 µM with respect to vancomycin, the antimicrobial concentration ratios 3V:1W, 2V:2V, and 1V:3W inhibited planktonic cell growth 91.57%, 92.1%, and 76.77% respectively. At concentrations lower than 5 µM with respect to vancomycin, very little activity was observed for all other combinations. Addition of W_5(Os-C) to vancomycin had no significant effect on the activity of either antimicrobial agent. Larger variation in sample readings was obtained at lower antimicrobial concentrations due to the inherent variability of biological systems. However, no significant difference was observed at $p=0.05$. No ∑FIC values could be calculated as no combination was able to inhibit 95% or more planktonic cell growth.

3.3 Anti-biofilm activity

3.3.1 Biofilm growth optimisation and characterisation

The optimum starting cell density was determined at 1/200 dilution (**Figure 3.4B**) from a late log-phase overnight culture (OD_{600} = 0.650 ± 0.025; 10^6 CFU). Higher cell densities resulted in ultra-dense biofilms not suitable for microscopic imaging (**Figure 3.4A**) while lower cell densities (**Figure 3.4C and D**) produced fragmented, unstable biofilms that easily dislodged during staining and washing in preparation for imaging.

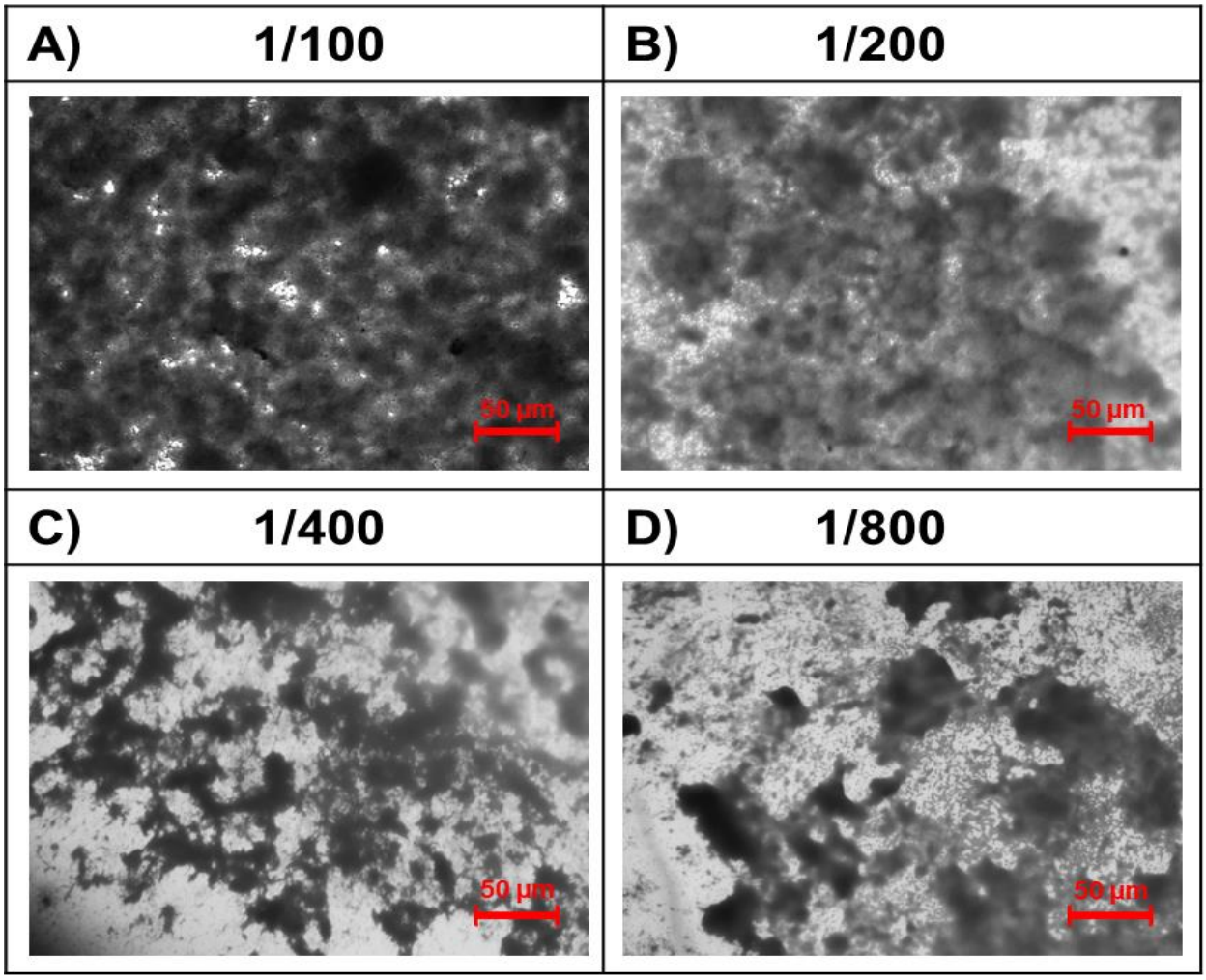

Figure 3.4: Mature, crystal violet stained 24 hr old biofilms prepared from (A) 1/100, (B) 1/200, (C) 1/400, and 1/800 cell dilutions cultured in BPM. Magnification 20x evaluated with inverted microscopy.

Using the 1/200 dilution, a time-based study was undertaken to investigate the rate of biofilm formation and the optimal incubation time required for a well-established biofilm to form. Inoculated BPM was incubated in flat bottom polystyrene plates for 2, 4, 6, 12, 18, and 24 h (**Figure 3.5**). After 2 h, cells had adhered. Extracellular matrix was only visible after 6 h, and after 24 h, dense, consistent biofilms could be observed.

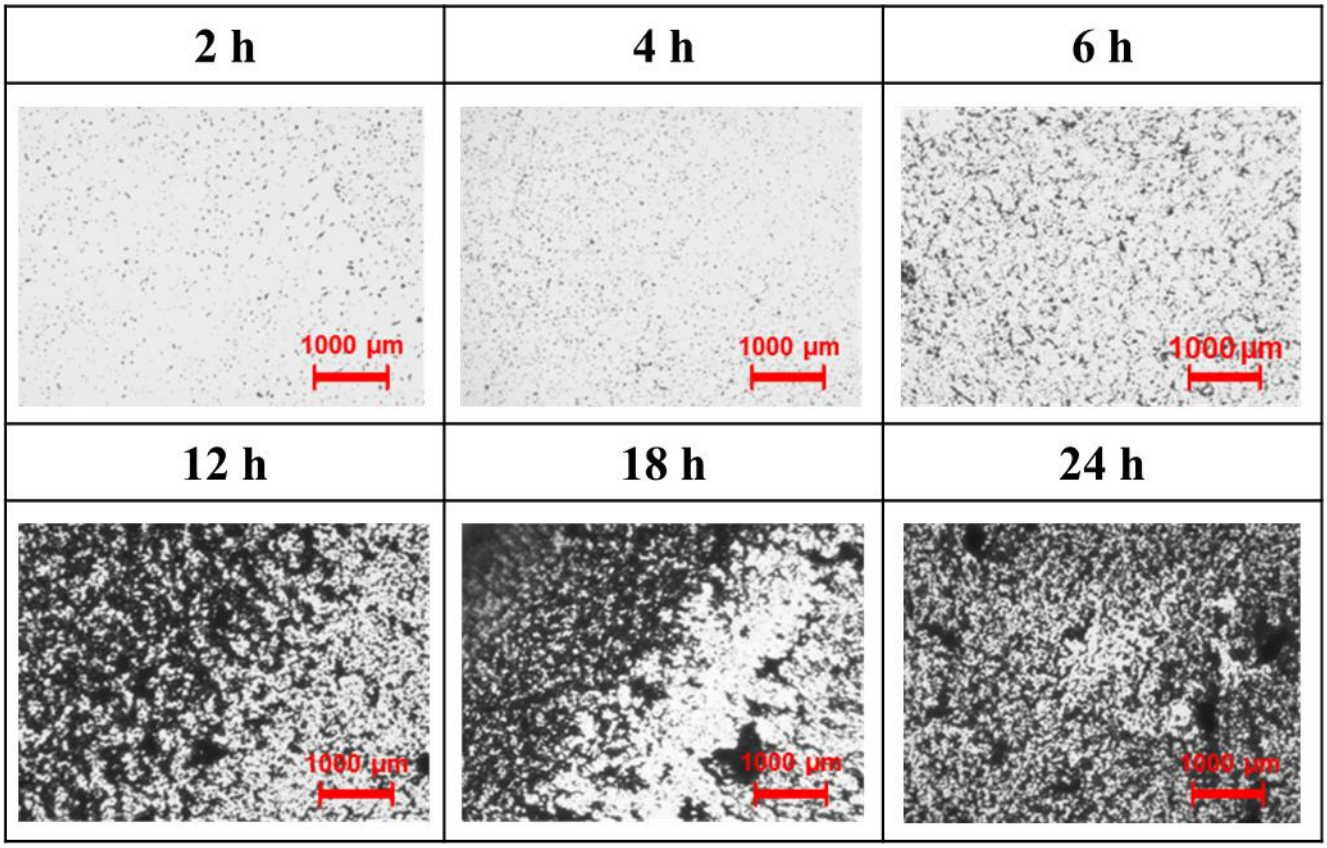

Figure 3.5: Time based study of biomass development of *S. epidermidis* (ATCC 35984) incubated in BPM at a cell dilution 1/200. Magnification 10x under inverted microscopy with crystal violet staining.

3.3.2 Biofilm inhibitory activity of W_5(Os-C)

The biofilm formation inhibiting activity of vancomycin, melittin and W_5(Os-C) after 24 h exposure was determined. The biofilms were assessed for cell viability with CTB and biomass with CV. Vancomycin (**Figure 3.6A**), melittin (**Figure 3.6B**), and W_5(Os-C) (**Figure 3.6C**), inhibited biofilm formation in a dose-dependent manner at low micromolar concentrations.

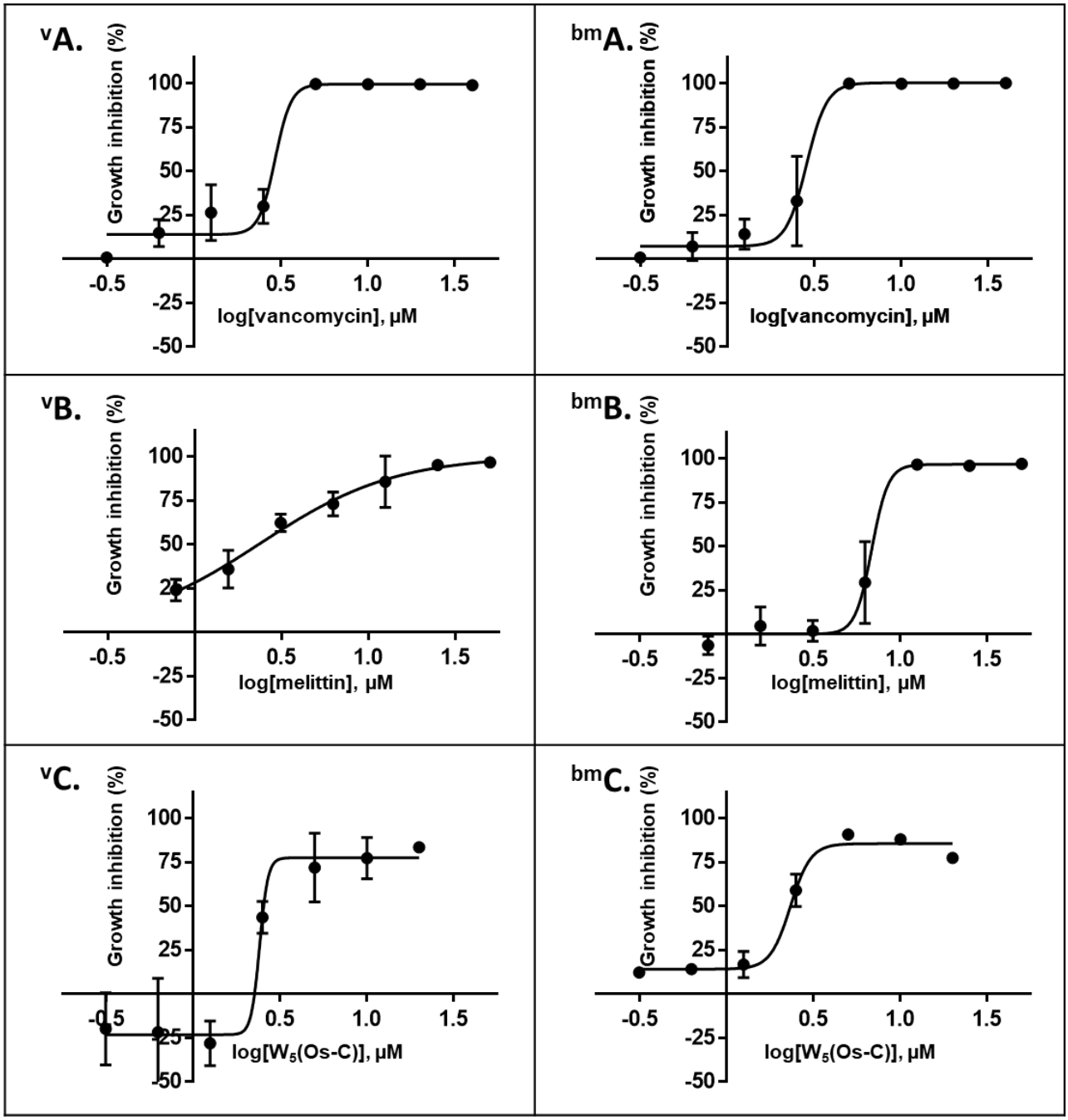

Figure 3.6: Percentage inhibition of *S. epidermidis* (ATCC 35984) cell viability (^{v}) and biomass accumulation (^{bm}) from 24 h old biofilms developed in the presence of (A) vancomycin, (B) melittin, and (C) W_5(Os-C). Final concentrations are 0.31 µM to 40 µM for vancomycin and W_5(Os-C) and 0.78 µM to 50 µM for melittin from three independent experiments each with three technical repeats. Error bars indicate mean ± SEM.

The dose-response curves were used to determine the BIC_{50} and BIC_{max} values (**Table 3.4**). Vancomycin inhibited biofilms from a cell viability perspective with $^{v}BIC_{50}$ and $^{v}BIC_{max}$ values of 2.84 µM and 3.81 µM respectively. Its biofilm biomass inhibition activity followed a similar trend with $^{bm}BIC_{50}$ and $^{bm}BIC_{max}$ values of 2.92 µM and 3.76 µM respectively.

Melittin exhibited inhibition with a $^{v}BIC_{50}$ value of 7.18 µM and a $^{bm}BIC_{max}$ of 9.04 µM, concentrations significantly higher than that of vancomycin or W_5(Os-C) ($p<0.0001$). The effect of melittin on biofilm cell viability resulted in a non-sigmoidal dose-response curve which prevented the calculation of a $^{v}BIC_{max}$ value although the $^{v}BIC_{50}$ value was determined as 3.77 µM. Melittin was used to optimise the biofilm CV assay and inverted microscopy images were obtained (data not shown). The presence of melittin during biofilm biomass development at any concentration interfered with biomass accumulation patterns when compared to the growth control and resulted in clusters of ECM covered cells between patches of little to no biomass. Higher concentrations still resulted in cell adherence without any visible ECM.

Melittin was unable to completely inhibit biomass development at concentrations ranging from 0.039 µM to 1.56 µM. At 3.13 µM, only a few clusters of biomass could be seen. Melittin was able to inhibit biomass clusters development for higher concentrations (6.25 µM to 50 µM) with a BIC_{50} of 3.77 µM but could not completely inhibit biomass development or cell adherence.

The peptide W_5(Os-C) inhibited cell viability at higher concentrations with $^{v}BIC_{50}$ and $^{v}BIC_{max}$ of 2.14 µM and 3.06 µM, respectively. However, at concentrations of 1.25 µM and lower, it induced cell proliferation. Although >80% biomass inhibition was not achieved, peptide W_5(Os-C) inhibited biofilm biomass development with $^{bm}BIC_{50}$ and $^{bm}BIC_{max}$ values of 2.32 µM and 3.07 µM respectively.

Table 3.4: BIC_{50} and BIC_{max} values of vancomycin, melittin, and W_5(Os-C) in terms of cell viability inhibition (CTB) and biomass development inhibition (CV).

	Cell viability inhibition (CTB)		Biomass development inhibition (CV)	
	$^{v}BIC_{50}$ (µM)	$^{v}BIC_{max}$ (µM)	$^{bm}BIC_{50}$ (µM)	$^{bm}BIC_{max}$ (µM)
Vancomycin	2.84 ± 0.22	3.81 ± 0.16 (100%)	2.92 ± 0.17	3.76 ± 0.95 (>95%)
Melittin	7.18 ± 0.50****	N/A (>95%)	3.77 ± 0.36	9.04**** ± 0.31 (>95%)
W_5(Os-C)	2.14 ± 0.07	3.06 ± 0.41 (>75%)	2.32 ± 0.39*	3.07 ± 1.18 (>80%)

BIC_{50} values were calculated as the concentration at which 50% inhibition was observed. BIC_{max} values were obtained from the concentration at which the tangents to the slope and maximum of the dose-response curve intersect. Results are from three independent experiments each with triplicate sampling. Each reported value represents the mean ± standard error of the mean (SEM). *Statistically significant difference to melittin ($p<0.05$); one way ANOVA with Tukey correction. ****Statistically significant difference to vancomycin and W_5(Os-C) ($p<0.0001$); one way ANOVA with Tukey correction.

3.3.3 Synergism studies: W_5(Os-C) and vancomycin – biofilm inhibition

Increasingly the anti-biofilm activity of combined antimicrobials are being investigated as a strategy to mitigate risk of antimicrobial resistance as well as lower cytotoxicity (303-307). Some combinations of antimicrobial agents exhibit synergism against biofilm cultures even

when little to no synergy is observed against planktonic cultures (226). As such, the effect of W_5(Os-C) on the biofilm inhibitory activity of vancomycin was investigated. W5(Os-C) and vancomycin combinations in the ratios 3V:1W, 2V:2W or 1V:3W were added to inoculated BPM and incubated for 24 hours. The biofilms were assessed for cell viability with CTB and biomass with CV. Vancomycin (**Figure 3.7A and Figure 3.8A**) and W_5(Os-C) (**Figure 3.7B and Figure 3.8B**) dose-response curves were included for comparison. Concentration ratios 3V:1W (**Figure 3.7C and Figure 3.8C)** and 2V:2W (**Figure 3.7D and Figure 3.8D)** inhibited biofilm development in a dose-dependent manner at micromolar concentrations. Concentration ratio 1V:3W (**Figure 3.7E and Figure 3.8E**) inhibited *S. epidermidis* ATCC 35984 biofilm formation in a dose-dependent trend, however, limited solubility of W_5(Os-C) prevented exposure to higher concentrations to complete the dose-response curve (suspected precipitation due to clear peptide solution turning opaque when mixed with BPM at concentrations of 20 µM or higher).

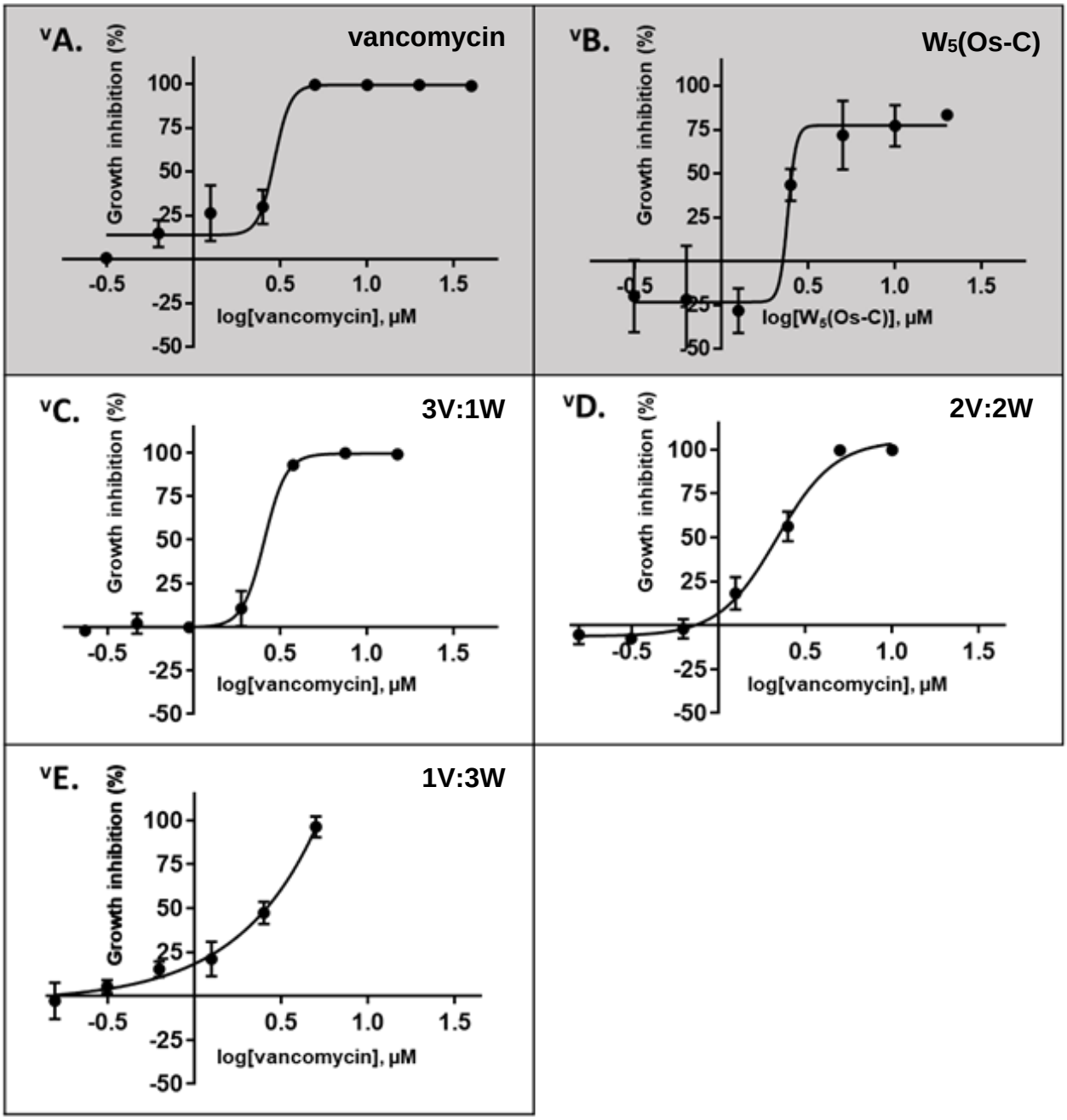

Figure 3.7: Percentage inhibition of *S. epidermidis* ATCC 35984 cell viability (ᵛ) from 24 hour old biofilms developed in the presence of (A) vancomycin, (B) W_5(Os-C), and vancomycin and W_5(Os-C) in combination ratios (C) 3V:1W, (D) 2V:2W, and € 1V:3W. Serial doubling dilutions of the combinations were prepared so that the final antimicrobial agent concentration ranged from 0.31 –M - 20 µM and plotted in terms of the concentration of vancomycin (0.16 –M - 15 µM). Results are from three independent experiments each with three technical repeats. Error bars indicate mean ± SEM.

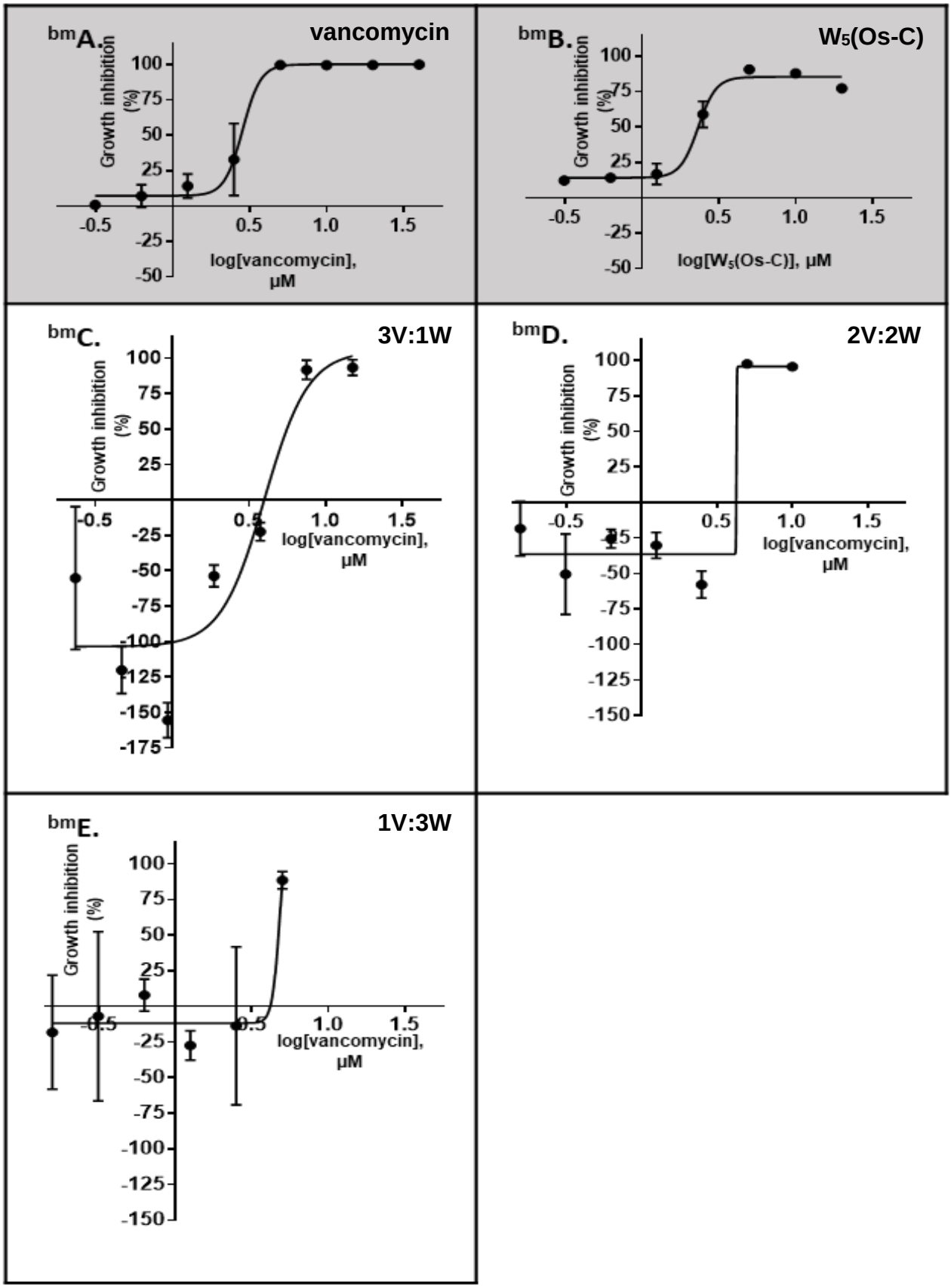

Figure 3.8: Percentage inhibition of *S. epidermidis* ATCC 35984 biomass development (^{bm}) from 24 hour old biofilms developed in the presence of (A) vancomycin, (B) W_5(Os-C), and vancomycin and W_5(Os-C) in combination ratios (C) 3V:1W, (D) 2V:2W, a€(E) 1V:3W. Serial doubling dilutions of the combinations were prepared so that the final antimicrobial agent concentration ranged from 0.–1 µM - 20 µM and plotted in terms of the concentration of vancomycin (0.–6 µM - 15 µM).Results are from three independent experiments each with three technical repeats. Error bars indicate mean ± SEM.

The dose-response curves from **Figure 3.7** and **Figure 3.8** were used to determine $^{v}BIC_{50}$, $^{v}BIC_{max}$, $^{bm}BIC_{50}$, and $^{bm}BIC_{max}$ values (**Table 3.5**).

Table 3.5: BIC_{50} and BIC_{max} values of vancomycin, W_5(Os-C), and vancomycin and W_5(Os-C) in combination ratios 3V:1W, 2V:2W; and 1V:3W in terms of cell viability inhibition (CTB) and biomass development inhibition (CV).

	Cell viability inhibition (CTB)		Biomass development inhibition (CV)	
Antimicrobial	**$^{v}BIC_{50}$ (µM)**	**$^{v}BIC_{max}$(µM)**	**$^{bm}BIC_{50}$ (µM)**	**$^{bm}BIC_{max}$(µM)**
Vancomycin alone	2.84 ± 0.22	3.81 ± 0.16 (100%)	2.92 ± 0.17	3.76 ± 0.95 (>95%)
Ratio 3V:1W	2.56 ± 0.16	3.48 ± 0.07 (>95%)	4.71 ± 0.21	6.68 ± 1.43 (>90%)
Ratio 2V:2W	2.16 ± 0.10	4.51 ± 0.56 (>95%)	4.25 ± 0.09	4.40 ± 0.10 (>95%)
Ratio 1V:3W	N/A	N/A (>95%)	N/A	N/A (>85%)
W_5(Os-C) alone	2.14 ± 0.07	3.06 ± 0.41 (>75%)	2.32 ± 0.39*	3.07 ± 1.18 (>80%)

BIC_{50} values were calculated as the concentration at which 50% inhibition was observed. BIC_{max} values were obtained from the concentration at which the tangents to the slope and maximum of the dose-response curve intersect. Each reported value represents the mean ± standard error of the mean (SEM). Results are from three independent experiments each with triplicate sampling.

In the 3V:1W ratio, biofilms were inhibited from a cell viability perspective with $^{v}BIC_{50}$ and $^{v}BIC_{max}$ values of 2.56 µM and 3.48 µM, respectively, relative to vancomycin. Its biofilm biomass inhibition activity was less effective, with $^{bm}BIC_{50}$ and $^{bm}BIC_{max}$ values of 4.71 µM and 6.68 µM, respectively, relative to vancomycin.

In the 2V:2W ratio, biofilms were inhibited from a cell viability perspective with $^{v}BIC_{50}$ and $^{v}BIC_{max}$ values of 2.16 µM and 34.51 µM, respectively, relative to vancomycin. Its biofilm biomass inhibition activity was less effective, with $^{bm}BIC_{50}$ and $^{bm}BIC_{max}$ values of 4.25 µM and 4.40 µM, respectively, relative to vancomycin.

Due to incomplete dose-response curves, no $^{v}BIC_{50}$, $^{v}BIC_{max}$, $^{bm}BIC_{50}$, or $^{bm}BIC_{max}$ values could be determined.

Concentration ratio 3V:1W (**Table 3.5A**), 2V:2W (**Table 3.5B**), and 1V:3W (**Table 3.5C**) inhibited biofilm biomass development at concentrations equal to or higher than the BIC of vancomycin alone. However, at mid to low concentrations, the combination antimicrobials induced biomass development by 125% to 250% when compared to growth controls (**Figure 3.9**).

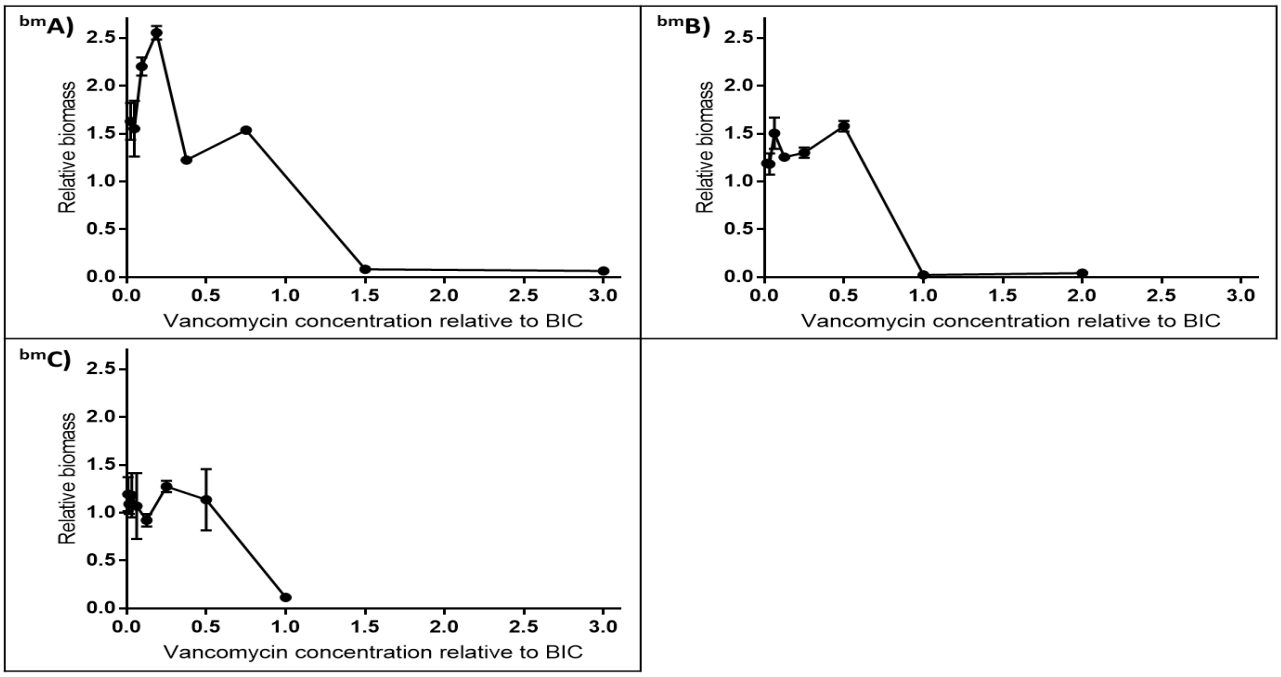

Figure 3.9: Relative biofilm formation of *S. epidermidis* ATCC 35984 from 24 hour old biofilms developed in the presence of and vancomycin and W_5(Os-C) in combination ratios (A) 3V:1W, (B) 2V:2W, and (C) 1V:3W. Horizontal axis indicates final vancomycin concentration in the antibiotic combination relative the BIC. Results are from three independent experiments each with three technical repeats. Error bars indicate mean ± SEM.

To better visualise the increase in biomass development in the presence of the combination ratios, **Figure 3.9** was produced. The figure expresses biomass development as a fraction of the total biomass produced in the absence of antimicrobial agents at the different vancomycin concentrations which are expressed as the fraction of the $^{bm}BIC_{max}$.

3.4 Keratinocyte (HaCat) Cytotoxicity

Previous studies showed that Os, Os-C, and some of their derivatives were not cytotoxic to human erythrocytes, Caco-2, and SC-1 cells (252, 308). Human erythrocytes also showed no haemolysis when exposed to Os derivatives. Since the activity of W_5(Os-C) was tested against a bacterial strain commonly found in skin wounds, its cytotoxic effects on keratinocytes (HaCat cells) were determined (**Figure 3.10**).

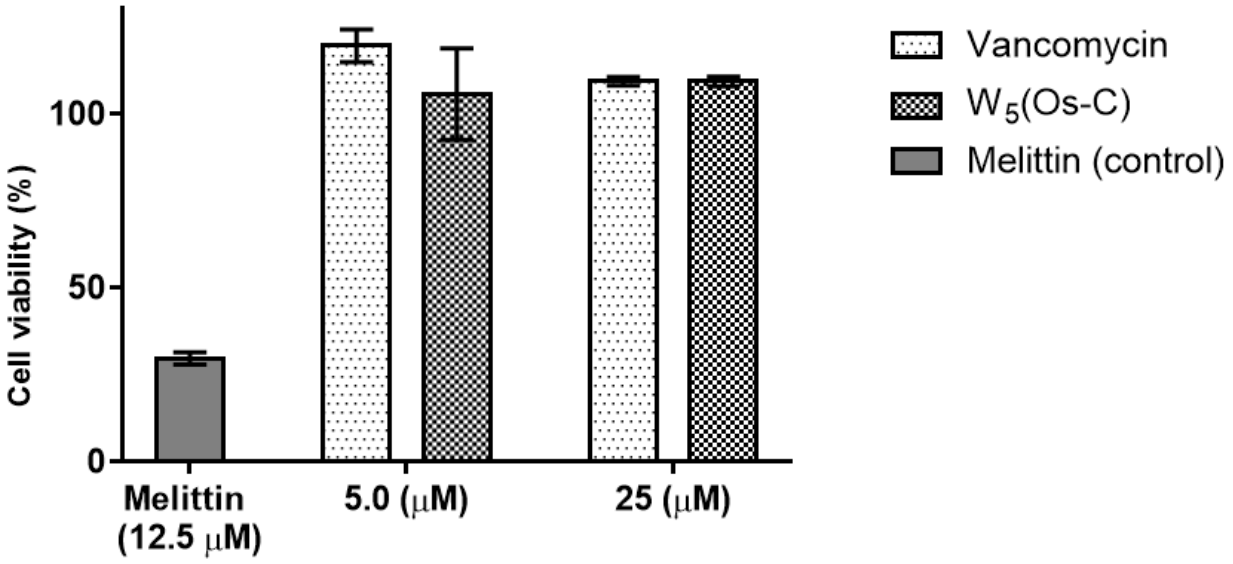

Figure 3.10 Effects of melittin, vancomycin and W_5(Os-C), on cell viability in HaCat keratinocytes. Error bars indicate mean ± SEM. Results are from three independent experiments each with three technical repeats.

Vancomycin had no cytotoxic effects on HaCat cells at 5 µM or 25 µM after 24 h exposure. Under the same conditions, melittin at 12.5 µM caused a decrease in cell viability by >70%. Similar to vancomycin, W_5(Os-C) did not significantly decrease cell viability compared to untreated cells. At 5 µM, cell viability in the presence of vancomycin was increased by <10% when compared with the untreated cell control, however, this increase was not statistically significant at p=0.05.

3.5 Peptide characterisation

3.5.1 Peptide structure and folding

In order to predict the secondary and tertiary structure of peptide W_5(Os-C) in the presence of a Gram-positive membrane, the peptide sequence was submitted to PEP-FOLD to produce an initial structure. Multiple possible structures were produced and one of the structures that resembles predicted structures for OsDef2 was selected for submission to MDSims (252). The structure was further analysed to indicate hydrophobicity in red and hydrophilicity in white according to the Eisenberg hydrophobicity scale and the positions of the side chains investigated (**Figure 3.11A**). The PEP-FOLD analysis produced a structure with two α-helices folded for which the hydrophilic regions are orientated towards each other and the hydrophobic regions pointing outwards.

Peptide W_5(Os-C) was submitted to CHARMM-GUI to simulate folding in an aqueous solution. The simulation dynamically determined the minimized energy state over 1000 ns. An extended peptide conformation was produced (**Figure 3.11B**). As with the PEP-FOLD structure, the

peptide was folded double with the loop along residues Typ11 and Lys12, however, no α-helices were formed. Folding was accommodated by the glycine rich sequence surrounding these residues labelled yellow (**Figure 3.11B**). The peptide background was also turned to allow residues Trp1, Trp2, Trp5, Phe19, and Tyr24 to form a hydrophobic pocket.

The output structure of the energy minimization simulation in water was submitted for MDSims to predict the interaction between W_5(Os-C) and a POPG bacterial cell membrane in physiological salt concentration (0.15 M) (**Figure 3.11C**) or high salt concentration (0.30 M) (**Figure 3.11**). This was done to determine whether loss of activity at higher concentrations of peptides were due to high salt environments which would need to be overcome if it were to be used under physiological conditions. In the presence of a POPG (Gram-positive) membrane, two α-helices of different residue lengths were formed when in physiological salt concentration, but only the N-terminal helix formed in a high salt environment. The helices allowed more hydrophobic residues to turn towards the centre of the peptide with Trp1, Trp2, Trp5, Tyr11 Phy19, and Tyr24 all turned inward under physiological conditions. When exposed to high salt conditions, Trp1 turned outward while Tyr15 turned inward. The disordered loop was in a more extended position in the presence of physiological and high salt concentrations than when exposed to water alone.

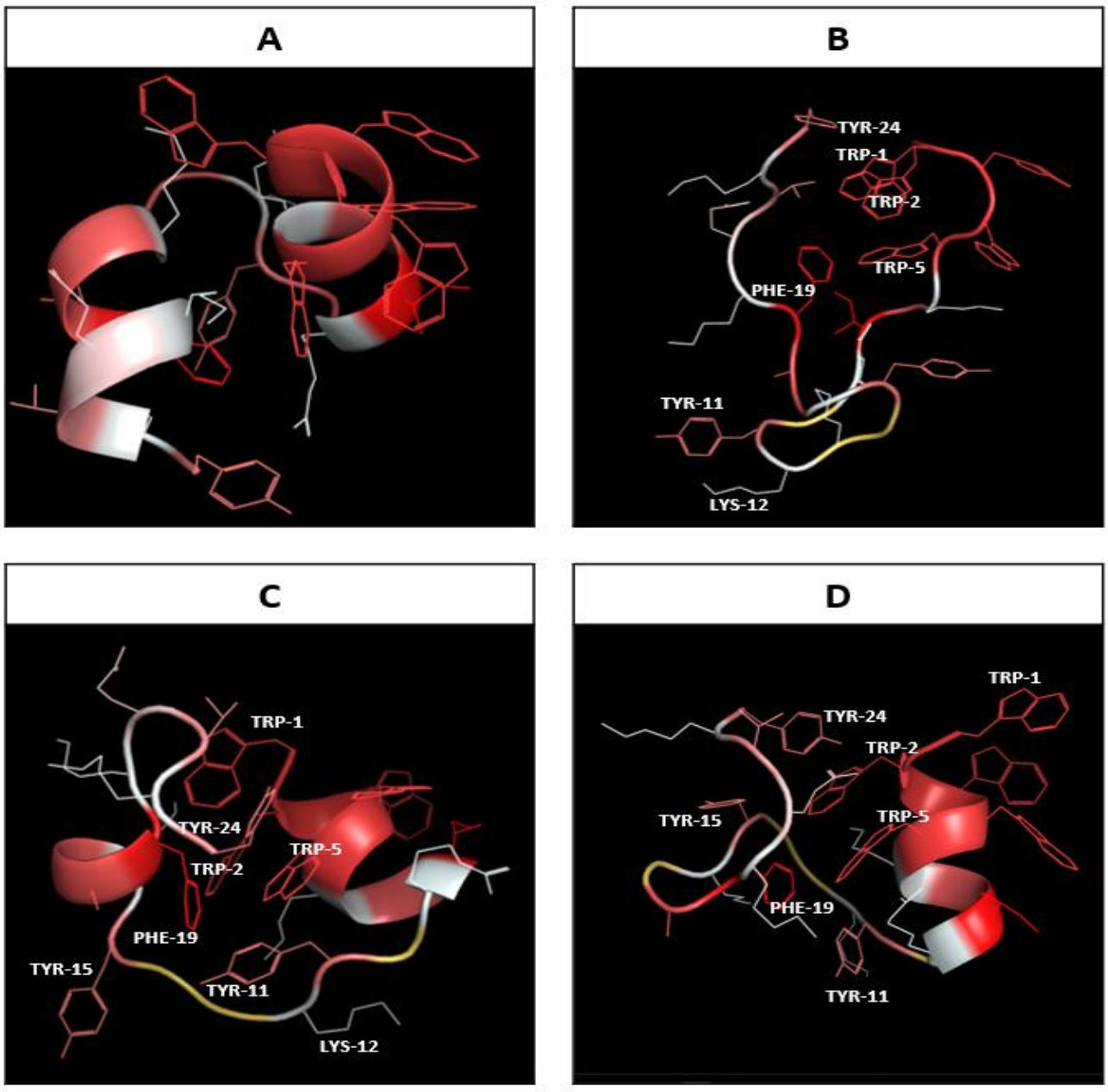

Figure 3.11: Structure of a single W_5(Os-C) molecule showing the backbone cartoon with side chain stick representations following simulations: in (A) PEP-FOLD to be submitted for molecular dynamic simulations, (B) pure TIP3P water, (C) water box containing a POPG membrane and physiological salt concentration (0.15 M), and (D) water box containing a POPG membrane and high salt concentration (0.30 M). Red indicates hydrophobicity and white indicates hydrophilicity. Glycine residues shaded yellow are hydrophobic. Images were processed in PyMOL.

3.5.2 Peptide to peptide interactions in the presence of a Gram-positive membrane

To determine the peptide folding and peptide to peptide interactions in the presence of a Gram-positive membrane, four W_5(Os-C) peptides were placed in a water box containing a pre-assembled POPG membrane and salt ions at physiological concentration (0.15 M) (**Figure 3.12A to C**) or at high salt concentration (0.30 M) (**Figure 3.12D to F**). Peptide positions were randomly assigned with each peptide being at least 20 Å apart.

Under physiological salt conditions in the presence of a POPG membrane, the peptide alternated between apparent dimer and trimer states of association (**Figure 3.12B and C**). The association was mediated by hydrophobic interactions of the N-terminal tryptophan tags as well as residues Ile8 on both peptides and Tyr11 of one peptide at a time to facilitate dimerization. Additional hydrophilic interactions were observed between Arg9, Lys12, Thr22 and the C-terminal of Tyr24 which allowed for trimerization. The lack of a side chain would suggest that short Cα-Cα distances between glycine and these residues were due to interactions between residues flanking these glycine residues.

When exposed to high salt conditions in the presence of a POPG membrane, the peptide again alternated between dimer and trimer states of association, but was more prone to combine into a trimer, or to dissociate completely (**Figure 3.12E and F**). Hydrophobic associations between the N-terminal tryptophan tags were notably absent, although the Cα-Cα distances between Tyr15 and Phe19 were small enough to suggest the presence of hydrophobic interactions.

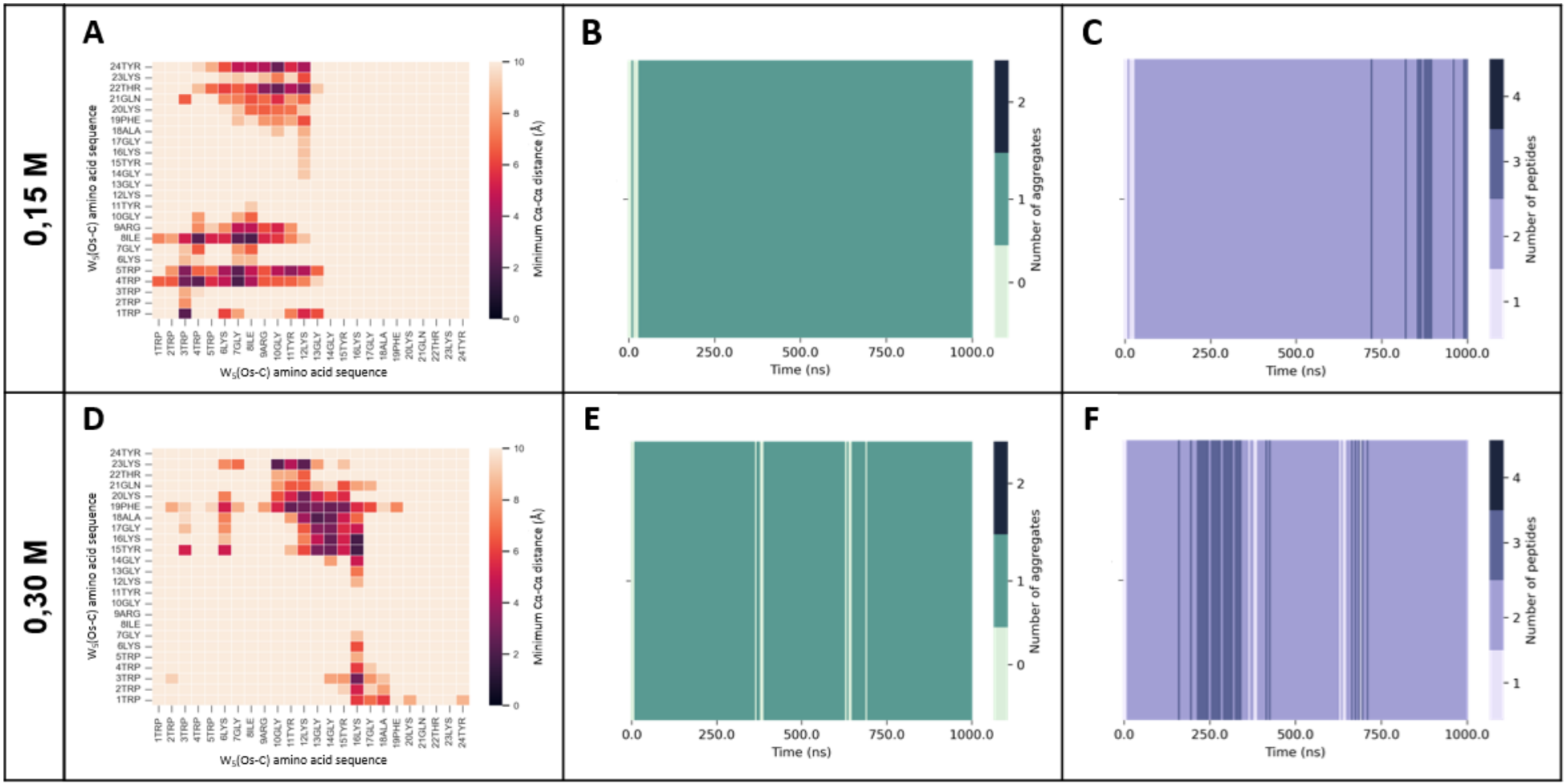

Figure 3.12: Peptide-peptide interactions from *in silico* simulation in POPG membrane (A-C) with physiological salt concentration (0.15 M), and (D-F) high salt concentration (0.30 M). Average Cα-Cα between residues of two W_5(Os-C) molecules in (A) physiological, and (D) high salt concentration presented as a heatmap. Number of aggregates formed, and number of peptides involved in each aggregate over 1000 ns in (B and C) physiological, and (E and F) high salt concentration.

3.5.3 Peptide interactions with the Gram-positive membrane

In order to investigate interactions between W_5(Os-C) and a Gram-positive cell membrane, the resulting water boxes with four W_5(Os-C) peptides and a POPG membrane each were analysed. The average psi and phi angles of each peptide bond of the four POPG exposed peptides were determined over the 1000 ns simulation for both the physiological (**Figure 3.13A and C**), and high salt concentration (**Figure 3.13A and C**) environments. The conformational stability of the peptide bonds were also determined by calculating the variation in psi and phi angles expressed as circular variance for both physiological salt concentration (**Figure 3.13B and D**), and high salt concentration (**Figure 3.13B and D**).

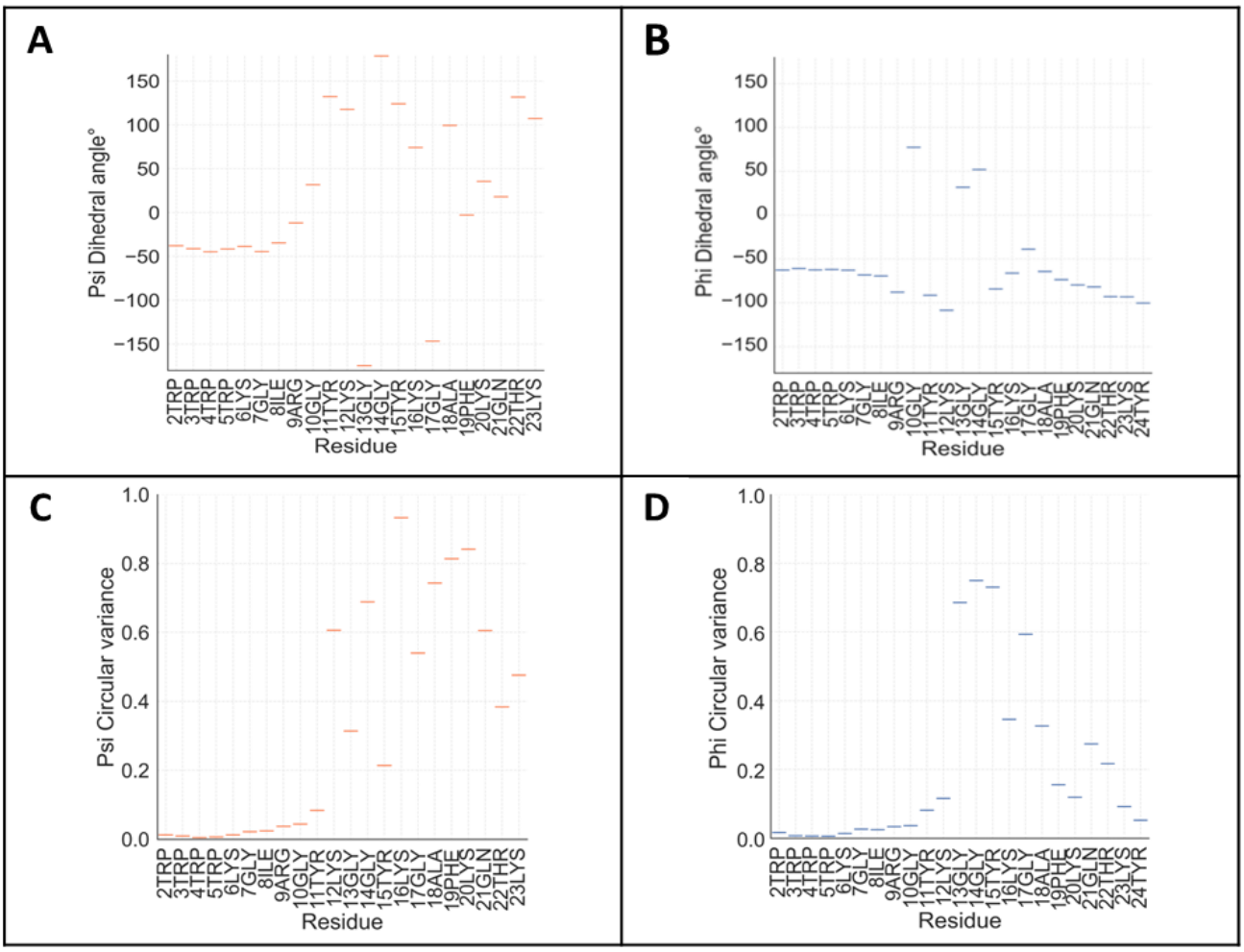

Figure 3.13: Analysis of W_5(Os-C) secondary structure obtained from *in silico* molecular dynamic simulations in physiological salt concentration. The (A) average psi angle, (B) average phi angle, and circular variance for (C) psi angle, and (D) phi angle indicating dynamic changes in conformation of residues during interaction with POPG membrane.

Under physiological salt conditions, the hydrophobic N-terminal tryptophan tags were fixed in a right handed α-helix based on the psi (**Figure 3.13A**) and phi angles (**Figure 3.13C**) with circular variances of almost 0.0 indicating effectively no conformational flexibility, while the rest

of the peptide sequence continued to move freely in extended conformation as indicated by the circular variance of both the psi (**Figure 3.13B**) and phi (**Figure 3.13D**) angles.

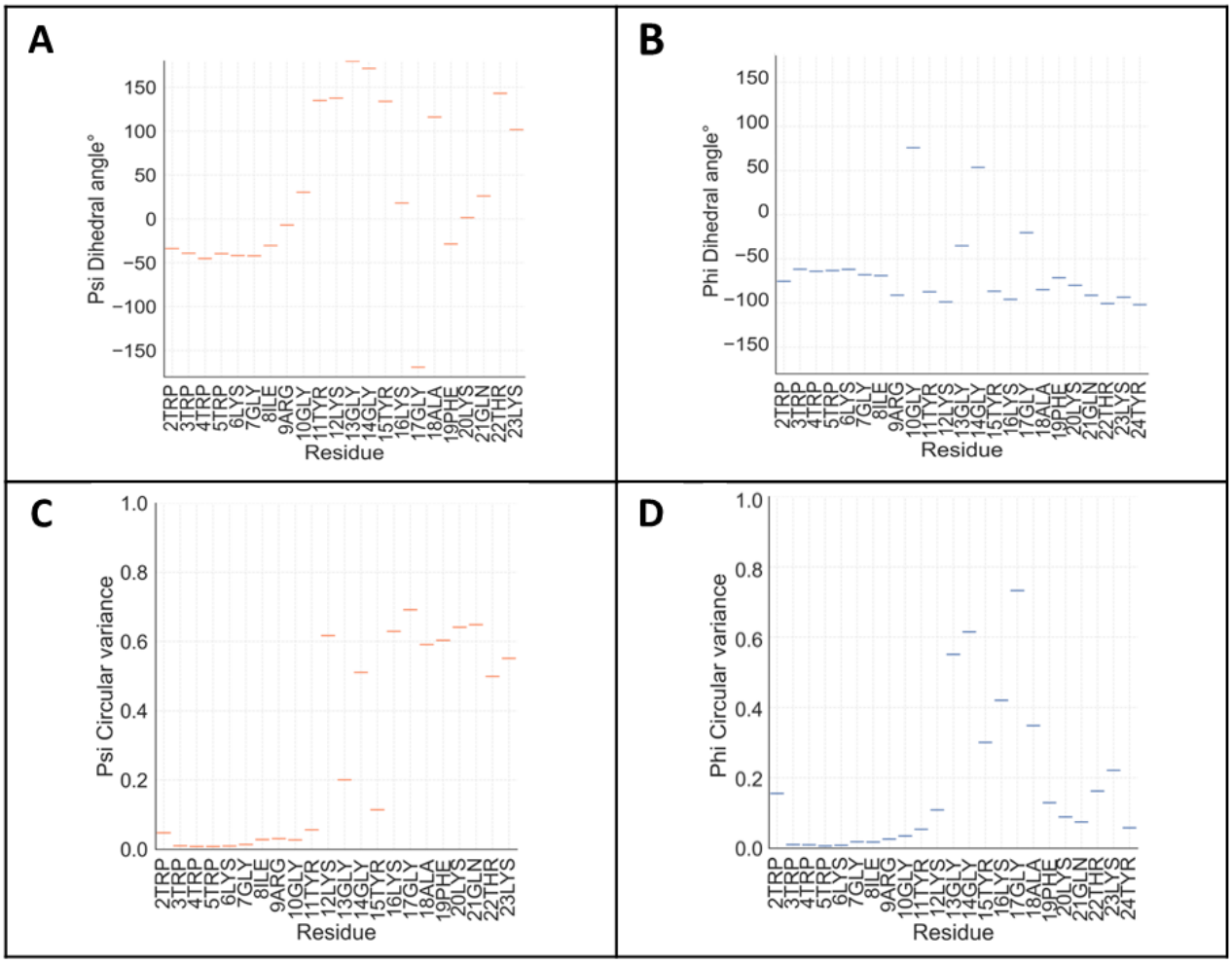

Figure 3.14: Analysis of W_5(Os-C) secondary structure obtained from *in silico* molecular dynamic simulations in high salt concentration. The (A) average psi angle, (B) average phi angle, and circular variance for (C) psi angle, and (D) phi angle indicating dynamic changes in conformation of residues during interaction with POPG membrane.

When exposing the peptide to a high salt environment, the hydrophobic N-terminal remained in a fixed right handed α-helix with the rest of the peptide chain in extended form as indicated by the psi (**Figure 3.14A**) and phi (**Figure 3.14C**) angles. The circular variance in terms of the psi (**Figure 3.14B**) and phi (**Figure 3.14D**) angles indicated a slight conformational variation in the N-terminal portion of the peptide. The rest of the hydrophobic N-terminal was highly stable in conformation while the extended tail exhibited high conformational flexibility.

3.5.4 Peptide dynamics in presence of a Gram-positive membrane

The dynamic interactions of the peptide with a Gram-positive membrane in physiological and high salt environments were investigated by determining the average number of hydrogen

bonds each residue of the four peptides made during the 1000 ns simulation (**Figure 3.15A and C**) as well as the average Z-position of each residue of the four peptides relative to the plane of the POPG membrane phosphate groups (**Figure 3.15B and D**). The final steps in the 1000 ns simulations were also visualized to observe the peptide to peptide and peptide to Gram-positive membrane interactions (**Figure 3.16**).

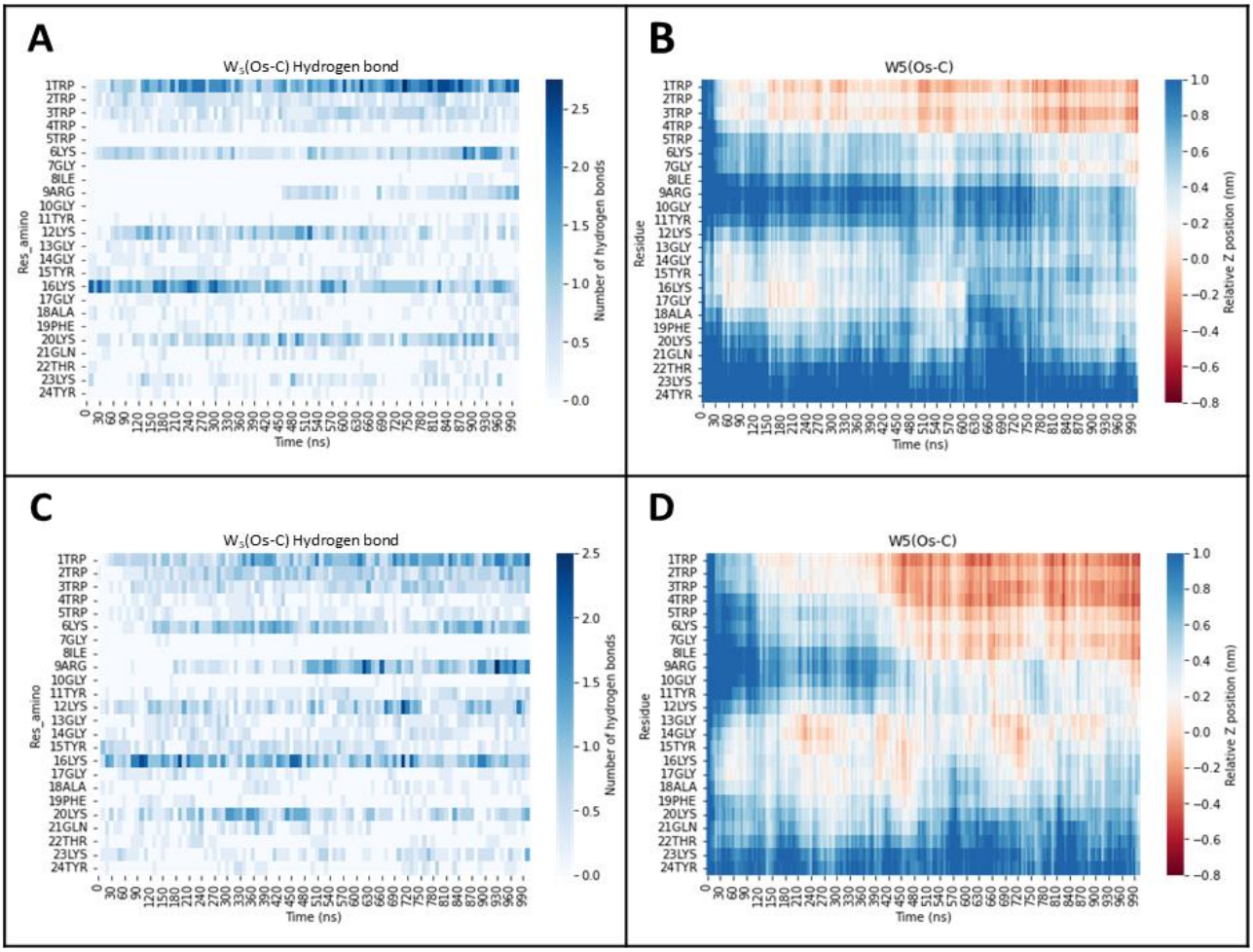

Figure 3.15: Analysis of W_5(Os-C) interaction with a POPG membrane obtained from *in silico* molecular dynamic simulations. In physiological salt concentration (A) number of hydrogen bonds with the membrane per residue, (B) average Z position indicating insertion into membrane, and in high salt concentration (C) number of hydrogen bonds with the membrane per residue, (D) average Z position indicating insertion into membrane.

In a physiological salt environment, residue Lys-16 is the first to interact with the phosphate portion of the POPG lipid layer, followed by the amine group of residue Trp-1 (**Figure 3.15A**). Although the Lys-16 seems to initiate attachment and subsequent insertion into the cell membrane, only the hydrophobic N-terminal inserts in a stable manner (**Figure 3.15B**). During the simulation, positively charged residues Lys-6, Lys-12, and Lys-20 intermittently interacted with the negative phosphate groups of POGP via hydrogen bonding (**Figure 3.15A**) but did not insert into the membrane (**Figure 3.15B**).

In a high salt environment, a similar pattern of hydrogen bonding of residues with the POPG membrane was observed, with the exception of additional strong hydrogen bonding of the residue Arg-9 (**Figure 3.15C**). The high salt environment induced a deeper insertion of the N-terminal hydrophobic residues (**Figure 3.15D**). In contrast to the physiological salt environment, residues Lys-6 to Ile-8 neighbouring the N-terminal tryptophan tag also inserted in a stable manner while residues Gly-13 to Phe-19 inserted intermittently into the POPG membrane.

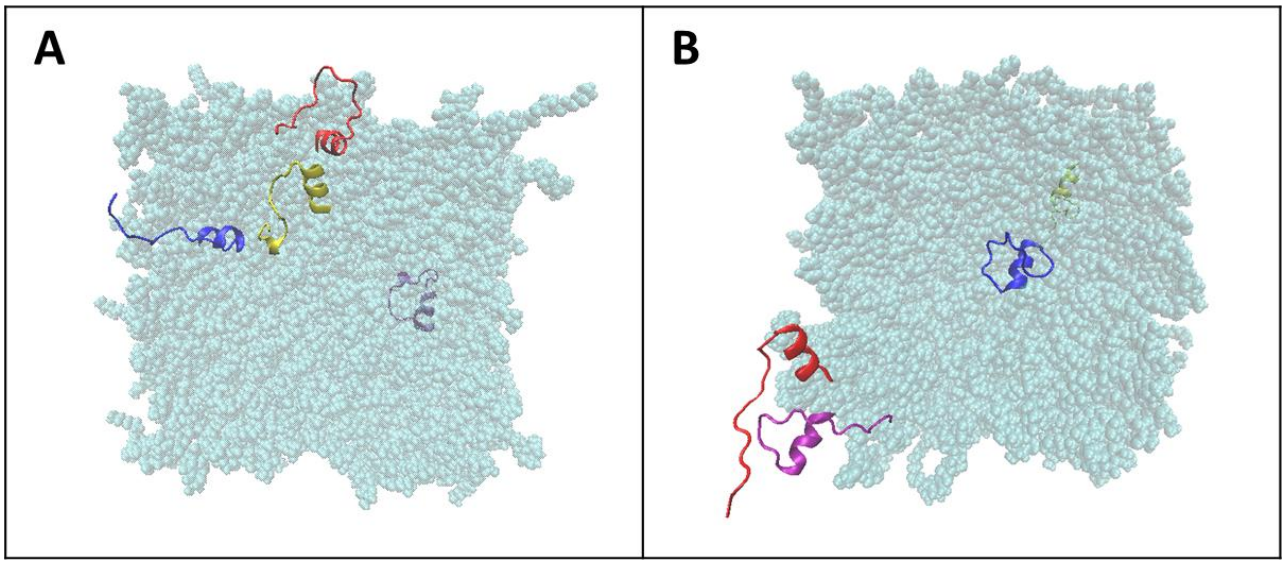

Figure 3.16: Top view snapshot after 1000 ns showing peptide-POPG membrane where (A) W_5(Os-C) trimer formed in physiological salt concentration, and (B) dimer formed in high salt concentration.

In physiological salt and high salt conditions, all four peptides inserted into the membrane within 1000 ns (**Figure 3.16**). In physiological salt conditions, three peptides were observed as a trimer in the 1000th ns while the fourth peptide inserted into the POPG membrane from the other side of the water box (**Figure 3.16A**). Peptide to peptide interactions within the trimer were observed to occur via both the hydrophobic N-terminal α-helix and the extended hydrophilic portions. Insertion into the membrane was strictly observed via the α-helix.

In high salt conditions, two peptides were observed as a dimer in the 1000th ns while the other two peptides each inserted into the membrane from opposite sides of the water box (**Figure 3.16B**). Peptide to peptide interactions within the dimer were observed to occur mainly between the extended hydrophilic portions, with the α-helices in proximity of each other, although the simulation did not report interactions. All peptides were observed to insert with the α-helix portions of the peptides.

CHAPTER 4: DISCUSSION

4.1 Antimicrobial activity of W_5(Os-C)

Biofilm development of microorganisms in a clinical setting is of growing concern due to its contribution to antibiotic resistance (108). These biofilms are formed on artificial surfaces e.g. urinary or venous catheters, prosthetic implants, and at operative incision sites by opportunistic microorganisms like *S. epidermidis* and *C. albicans* but can also be formed by multi-drug resistant organisms like methicillin resistant *S. aureus* (MRSA) (67, 68, 121, 309, 310). Both the development of biofilm, and the resulting increased antibiotic resistance often leads to longer hospitalisation, more expensive and toxic therapies, and an increased mortality rate, especially among immunocompromised individuals (67, 68, 93). Besides mechanical protection of the underlying cells against antibiotics, biofilms also often contain persister cells, proteases and efflux pump that render some antibiotics ineffective in treating the infection by disposing or expelling antimicrobial agents (105, 132, 134, 136, 137).

The development and characterisation of novel antibiotics as well as investigating combination therapies are critical in preventing emergence and outbreak of multi-drug resistant microorganisms. Antimicrobial peptides, especially in combination with other antimicrobial agents (**Table 1.1**) could provide an alternative treatment for severe, drug resistant infections as they often have multiple membrane associated and intracellular targets (82, 311). Target diversity prevents the development of antibiotic resistance. These peptides are usually amphipathic, short, and cationic amino acid sequences with antibiotic activity (49, 146). Many AMPs are modified amino acid sequences derived from biological peptides and are usually shorter analogues, that are altered to be active in a high salt environment and resistant to proteases.

This study investigated the anti-planktonic and anti-biofilm activity of W_5(Os-C), a synthetic analogue of OsDef2, a defensin previously identified in the midgut of the soft tick *O. savignyi*. Derivatives of OsDef2, including Os-C, revealed activity against Gram-positive and -negative bacteria (253-256). However, in a high salt environment activity was lost. In previous studies, the addition of a tryptophan tag at either the C or N terminal increased activity in physiological salt environments. Using the radial diffusion assay, the peptides W_5(Os-C) and (Os-C)W_5 were active against *E. coli*, with MIC values of 0.80 µM and 1.50 µM respectively in a physiological salt environment when compared to MIC values of 1.0 µM and 11.9 µM respectively in the presence of 30% human serum an sodium buffered environment (lower salinity) (260).

The aim of this study was to focus on W_5(Os-C) and to determine the antimicrobial and anti-biofilm activity against Gram-positive *S. epidermidis* (ATCC 35984), potential synergism with vancomycin, cytotoxicity and lastly to evaluate the interaction of W_5(Os-C) with a model Gram-positive membrane. Investigation of AMPs like W_5(Os-C) are crucial to provide a next line of defence against antimicrobial resistance development of *S. epidermidis* infections. Additional predictions of peptide-peptide and peptide-membrane interactions will allow for potential modifications to W_5(Os-C) to enhance membrane permeabilization and avoid unwanted peptide clustering.

The growth of *Staphylococcus epidermidis* ATCC 35984 in BPM, a non-standard planktonic medium was optimised. Overnight *S. epidermidis* cells reached the stationary phase within 12-14 h whether grown in TSB or BPM (**Figure 3.1**). However, BPM cultures reached a lower cell density (OD_{600} of ± 0.550) stationary phase and entered the death phase after an incubation period of 16 h as opposed to the standard 24 h incubation period. The -80°C inoculum remained in the lag phase for 8-10 h before active growth could be observed, then increased in cell density at a rate lower than that of the BPM or TSB inoculums to an OD_{600} of 0.650 after 24 h. This confirmed that 24 h incubation was required for any work with inoculums from the frozen stock.

The individual anti-planktonic activity of W_5(Os-C) was determined via a standard microdilution assay using vancomycin as the antibiotic and melittin as the AMP control (**Figure 3.2; Table 3.2**). Vancomycin, a clinically relevant control was highly active against planktonic *S. epidermidis* cells with an MIC_{50} of 3.09 µM and MIC_{max} of 3.83 µM with less than 0.20 µM variation between replicates. All values were higher than that reported in literature (MIC of 1.35 µM to 1.37 µM) (312, 313) due to differences in types of broth used, supplementation with nutrients, and starting cell concentrations (314, 315). Although the MIC value for melittin against *Staphylococcus spp* has been determined (207, 263), no MIC value for melittin against *S. epidermidis* ATCC 35984 cultured in BPM as used in this study could be found. Melittin was the least active of the three antimicrobial agents with an MIC_{50} value of 6.84 µM and an MIC_{max} value of 8.67 µM. These values are higher than what is reported in literature for the melittin MIC against *S. aureus* methicillin sensitive and resistant strains ($MIC_{S.\ aureus}$ of 0.18 µM to 2.20 µM) in various broth media (207, 316) and within range of MIC values found for *S. epidermidis* in broths different to the TSB composition used in this study ($MIC_{S.\ epidermidis}$ of 0.79 µM to 17.57 µM) (313, 317). These differences could be explained by the use of different media with

different compositions and/or with different salt concentrations. The difference in MIC ranges for *S. aureus* and *S. epidermidis* should be further explored under the same conditions.

The MIC_{50} and MIC_{max} for W_5(Os-C) were determined as 1.91 µM and 2.44 µM, concentrations lower than that of melittin and vancomycin, indicating more potent anti-planktonic activity of W_5(Os-C). Although different conditions and a different bacterium were used, it is worthy to note the MBC value of parent peptide Os-C against *S. aureus* was reported as 6.98 µM in sodium phosphate buffer (252), higher than the MIC observed with W_5(Os-C). Whether W_5(Os-C) is bacteriostatic or bactericidal is unknown, however, other studies have reported tryptophan tagged peptides exhibiting bactericidal activity due to increased interaction with the bacterial membrane especially in high salt environments (32, 34, 318).

In order to investigate the effect of W_5(Os-C) on the anti-planktonic activity of vancomycin, the two antimicrobial agents were mixed in three different ratios. The maximum concentration of W_5(Os-C) in each ratio, and overall concentrations were limited by the concentration of W_5(Os-C) stock solutions. A microdilution assay was used to determine the activity of the ratios (**Figure 3.3; Table 3.3)**. Due to incomplete dose-response curves, the calculated MIC_{50} and MIC_{max} values cannot serve as indicators of antimicrobial activity. None of the combinations were able to inhibit planktonic cell cultures >95%, and subsequently no fractional inhibitory concentrations could be calculated. However, at 2.50 µM relative to vancomycin, the combination ratio 3V:1W inhibited 87.12% planktonic cell growth of *S. epidermidis* when compared to a growth control This was significantly higher activity than that of vancomycin alone, but not significantly different to that of W_5(Os-C). At 5.00 µM relative to vancomycin, the combination 1V:3W showed significantly decreased planktonic cell inhibition when compared to vancomycin alone, indicating that increasing the concentration of W_5(Os-C) relative to vancomycin in combination ratios may decrease the activity of vancomycin. Although not commonly found in literature, examples of vancomycin antagonists do exist (319, 320).

Biofilm inhibition assays were based on the protocol of Maisetta *et al.* (2016) but required optimisation for effective investigation (122). The optimal inoculum concentration of 1/200 from an overnight culture was selected and produced consistently stable, mature biofilms with an acceptable biomass density to allow for microscopic visualisation. The process of biofilm formation was evaluated and cell adherence alone was observed for up to 4 h; biofilm development was observed after 6 h, and biomass continually increased after 12 and 18 h. At

24 h incubation, a mature and stable biofilm was produced, and these conditions were used throughout this study.

To determine the potential of W_5(Os-C) to inhibit biofilms, CellTitre Blue® cell viability and CV assays that measure cell viability and biomass respectively were used (**Figure 3.6; Table 3.4**). This would determine feasibility of using W_5(Os-C) as a biofilm inhibition substance on catheters, prosthetic implants, or at the site of surgical incisions. For vancomycin, a drug used to treat biofilms, the $^{v}BIC_{50} \approx {}^{bm}BIC_{50}$ (2.84 µM and 2.92 µM respectively), and $^{v}BIC_{max} \approx {}^{bm}BIC_{max}$ (3.81 µM and 3.76 µM respectively) suggesting bactericidal or bacteriostatic activity as the biofilm inhibition mechanism.

Melittin was included as a peptide control and inhibited biofilm associated cell viability with a $^{v}BIC_{50}$ and $^{v}BIC_{max}$ values of 7.18 µM and 9.04 µM respectively (**Figure 3.4**) which were similar to the MIC_{50} and MIC_{max} of melittin. This indicates a possible mechanism of biofilm inhibition by inhibiting cell growth. Melittin inhibited biomass development with a $^{bm}BIC_{50}$ of 3.77 µM, but the $^{bm}BIC_{max}$ could not be calculated due to the shape of the dose-response curve and biomass inhibition peaked at 83.47%. The literature ^{bm}BIC values reported for melittin against *S. epidermidis* ATCC 35984 were reported as 1.76 µM and differences in biofilm inhibition may be related to the growth media used (314, 315).

Vancomycin and W_5(Os-C) inhibited biofilm associated cells as well as biofilm biomass development with similar BIC_{50} and BIC_{max} values, with the exception of the $^{v}BIC_{max}$ of W_5(Os-C) which could not be obtained as no more than 90% inhibition of biomass development was observed. The highest biomass development inhibitory effect was achieved at 5 µM, with a decrease in inhibition at higher concentrations, as observed with the MIC determination assay. In contrast with the MIC assay, W_5(Os-C) exhibited comparable activity to vancomycin. Albeit under different conditions, tryptophan containing AMPs LL-37 and C9 have been identified with MIC values ranging between 3.12 µM and 12.5 µM with a notable decrease in MIC as the number of tryptophan residues increased (266, 321). Peptide LL-37 is well studied and unique as it is the only cathelicidin-like AMP identified in the human body (322-324) while peptide C9 is derived from AMP Cec4 from amphibian (frog) origin with reported antimicrobial activity against *S. epidermidis*) (321, 325).

Higher cell viability was observed at W_5(Os-C) concentrations below 1.25 µM when compared to the positive growth control. Although antibiotics act as stress inducers at higher

concentrations, they have often been identified to activate antimicrobial resistance or tolerance mechanisms at sub-inhibitory concentrations (326-328). These mechanisms include SOS responses, release of eDNA, and upregulated quorum sensing pathways (326, 328-330). How these mechanisms result in increased cell viability is yet to be determined, but is suspected to be due to altered genome expression induced via quorum sensing and subsequent accelerated cell growth.

Successful synergistic inhibition of planktonic and biofilm states of *S. epidermidis* by vancomycin in combination with melittin, rifampin, or cis-2-decenoic acid (C2DA) were reported (262, 331, 332). Yet, combining vancomycin and W_5(Os-C) failed to produce sufficient evidence of synergism against planktonic cells (**Figure 3.3**). Anti-biofilm investigations were completed despite inadequate anti-planktonic activity to determine whether vancomycin and W_5(Os-C) individually or combined could target biofilm specific pathways as a method to inhibit biomass development.

The CellTitre Blue® Cell Viability and Crystal Violet assays were used to determine the combined biofilm inhibitory activity of vancomycin and W_5(Os-C) against *S. epidermidis* biofilms. Using the MIC and/or the BIC values as reference, the same concentration ratios and ranges were used as in the combination anti-planktonic assay. Both combination ratios 3V:1W and 2V:2W inhibited biofilm biomass development in a dose-dependent manner at micromolar concentrations, and produced complete sigmoidal dose-response curves. The dose-response curve of ratio 1V:3W was incomplete due to the concentration limit of W_5(Os-C) and could thus not be used to determine accurate BIC_{50} or BIC_{max} values. Combination ratio 2V:2W inhibited biofilm associated cells with a $^{v}BIC_{50}$ of 2.16 µM (**Figure 3.7; Table 3.5**) relative to vancomycin which was lower than that of the 3V:1W ratio ($^{v}BIC_{50}$ = 2.65 µM; **Figure 3.7; Table 3.5**), as well as that of vancomycin (2.84 µM; **Figure 3.7; Table 3.5**). Combination ratio 1V:3W was unable to completely inhibit biofilm associated cell growth and an estimated $^{v}BIC_{50}$ of 2.50 µM relative to vancomycin.

Combination ratio 2V:2W had the highest biofilm biomass inhibition activity compared to the other combination ratios, with $^{bm}BIC_{50}$ and $^{bm}BIC_{max}$ values of 4.25 µM and 4.40 µM respectively **Figure 3.8; Table 3.5**) as well as complete biomass inhibition (>95% compared to 98.88%) for vancomycin at concentrations above 5.00 µM combination ratio 3V:1W inhibited biomass development at concentrations above 7.50 µM with respect to vancomycin, but only to a maximum of 93.38% inhibition (**Figure 3.8; Table 3.5**). No $^{bm}BIC_{50}$, $^{bm}BIC_{max}$, ^{bm}BIC values

were determined for combination ratio 1V:3W as the dose-response curve did not represent a sigmoidal curve and the combination was unable to inhibit biomass development >95%.

For all three combinations, concentrations lower than 3.75 µM resulted in more biomass than the growth control (**Figure 3.9**). This is consistent with the increased biomass observed for W_5(Os-C) alone (**Figure 3.6**). The amount of biomass increased when compared to the growth control as the proportion of W_5(Os-C) decreased in the combination ratio with over 250% more biomass produced in the 3V:1W ratio, over 150% more biomass produced in the 2V:2W ratio, and over 125% in the 1V:3W ratio. Multiple studies show that this phenomenon is explained by poly-*N*AG production upregulation on the DNA level (113, 118, 333).

4.2 Cytotoxicity of W_5(Os-C) against human keratinocytes

All antimicrobial agents considered for human use require extensive cytotoxicity testing. The peptide Os, and some derivatives have been screened for cytotoxicity against human colon epithelium (CaCo-2) or mouse embryo fibroblast (SC-1) cells (252). Additionally, Os and Os-C were shown not to induce inflammation in macrophage or monocyte like cells (RAW 264.7 (254). However, W_5(Os-C) needed to be tested for cytotoxicity against human keratinocytes as topical treatments are considered one of the viable uses of peptide based antimicrobial agents (334-336). Fully mature, 75% confluent keratinocyte cultures were incubated in the presence of vancomycin, melittin, or W_5(Os-C) for 24 h to assess cytotoxicity. Neither vancomycin nor W_5(Os-C) exhibited any cytotoxic effects against HaCat keratinocytes at MIC or 5xMIC concentrations (**Figure 3.10**). Further literature studies of other tryptophan tagged AMPs indicated cytotoxicity against HaCat cells is uncommon (337, 338). Melittin was used as the control and reduced cell viability by 70% which is consistent with literature values of between 60% and 80% cell inhibition (252, 254, 339). The MTT assay thus indicates that both vancomycin and W_5(Os-C) are viable topical antimicrobial agents from a clinical safety perspective.

4.3 Molecular dynamics of W_5(Os-C)

The purpose of tryptophan tagging is to increase the stability and activity of AMPs in high salt or physiological salt environments. No studies have been undertaken to investigate the interaction between W_5(Os-C) and a model membrane thus far. Tryptophan tagging has been shown to increase activity in a physiological salt (*in vitro*) environment. The ionic strength of plasma and serum is 0.15 M and thus the concentrations of physiological conditions (0.15 M)

and high salt conditions (0.30 M) were used to understand the interaction of the W_5(Os-C) with a model membrane.

Simulations on molecular dynamics are rapidly becoming a valuable tool in characterising and investigating AMPs (340). Molecular dynamics simulations provide structural data of AMPs individually; the dynamic structural changes as AMPs interact with each other or with cell components; and facilitate faster AMP screening (237, 341). Application of MDSims technology provided an opportunity to elucidate a possible mechanism for these observations.

Structures obtained from PEP-FOLD (**Figure 3.11A**) are not considered accurate and are only used as a starting structure due to the inherent PEP-FOLD assumptions of pH and simplification of side chains (237, 278, 285-287). The structure obtained from CHARMM-GUI (**Figure 3.11B**) was considered a more accurate representation of the stable conformational structure in an aqueous solution as the structure is determined via much more complex algorithms that account for more parameters than PEP-FOLD. Peptide folding in an aqueous solution resulted in a peptide folded double, facilitated by the low steric hinderance of glycine residues, as well as hydrophobic and hydrophilic interactions (342, 343).

The parent compound OsDef2 was predicted to include α-helices (252), yet W_5(Os-C) remained extended in pure water environments. The differences between the two structures can be explained by the lack of cysteine residues in W_5(Os-C) as well as truncation and other modifications of OsDef2 from 37 residues to 19 residues to form Os-C before addition of the N-terminal tryptophan tag. Tryptophan is considered overall hydrophobic due to the large aromatic side chain but can interact with water molecules via H-bonding via the amine and carboxyl groups of the backbone. Furthermore, the indole N-H group from the side chain can also interact with water molecules via hydrogen bonding as well as cation-π interactions (344-346).

Once peptide W_5(Os-C) was exposed to the Gram-positive simulating POPG membrane under physiological (**Figure 3.11C**), or high (**Figure 3.11D**) salt concentrations, α-helices were formed at the N-terminal, and in physiological salt conditions also near the C-terminal. The helices formed mainly in portions of the peptide that inserted or strongly interacted with the POPG membrane. Similar changes in peptide secondary structure were observed when introduced to a bacterial membrane as interactions and even the degree of membrane curving can affect peptide stability (166).

Compared to folding in aqueous solution, the peptides were more globular and included more hydrophobic residues within the inner hydrophobic pocket although the exact hydrophobic residues folding inwards varied. The differences between the structures of the peptide in aqueous solution, in physiological, or in high salt conditions may be due to the different ionic concentrations leading to different stable conformations of the tryptophan tag as the salt concentrations increased (346-348). However, this may only be confirmed by repeating simulations to obtain statistical validation for each residue interaction from peptide to peptide, peptide to solvent, and a peptide to POPG membrane viewpoints (349).

Variation in the specific residues involved in the hydrophobic pocket and α-helical structures of W_5(Os-C) in physiological and high salt concentrations can be contributing factors of differences in peptide to peptide interaction in the presence of a POPG membrane (**Figure 3.12A and D**). Both hydrophobic and hydrophilic interactions were present in physiological conditions, providing two points of interaction. The large hydrophobic interaction domain present in the physiological salt environment but absent in the high salt environment diversified the types of interactions between peptides. This in turn increased the stability of aggregates, allowing a single aggregate of two peptides to form for the majority of the simulation time (**Figure 3.12B and Figure 3.12A**). However, less peptide to peptide interactions as is seen in the high salt environment did not definitively indicate decreased stability of aggregates but did indicate that peptide interactions occur in a different manner (**Figure 3.12E and Figure 3.12B**). Overall, peptides in a higher salt concentration showed slight difficulty in maintaining aggregate status, and increased variability in the number of peptides involved in an aggregate (**Figure 3.12**). It should be noted that although data on Cα-Cα distance is a valuable measure of peptide to peptide interaction, investigators should be careful to assume short Cα-Cα distances are due to interactions or aggregations as the distances can indicate association of neighbouring residue side chains, or interactions between other peptide residues resulting in back-to-back proximity of the alpha carbons.

Although W_5(Os-C) exhibited variation in secondary structure and aggregation status when compared in physiological and high salt concentrations, the peptide maintained its hydrophobic N-terminal α-helix which inserted into the membrane in both environments (**Figure 3.13A and C; Figure 3.14A and C**). In both physiological and high salt environments, the remaining residues exhibited high flexibility (**Figure 3.13B and D; 3.14B and D**), extending into the exterior of the membrane and with charged residues interacting with the charged heads of the

POPG membrane phospholipid heads (**Figure 3.15**). When considering hydrogen bonding of the peptide with the POPG membrane, both environments initiated contact with the membrane through Lys-16 closely followed by other charged residues. This led to insertion into the membrane within 90 ns in both environments. However, in a higher salt concentration, W_5(Os-C) exhibited more hydrogen bonding, most notably additional multiple hydrogen bonds of Arg-9 with the POPG membrane (**Figure 3.15C**). The increased hydrogen bonding also resulted in deeper and more stable insertion into the cellular membrane (**Figure 3.15D**). Despite definitive and stable insertion into the membrane, no pore formation activity was observed in physiological or high salt concentrations. Current limitations in computational hours available on MDSims super computers restricted simulations for this investigation to 1000 ns, while pore formation is usually observed on a millisecond scale in *in silico* investigations (350). Furthermore, pore formation might require more than four peptides as was used in this study (351). The number of peptide molecules needed for membrane pores to form vary among AMPs e.g. melittin is reported to require between three and five molecules to form a membrane pore (352).

CHAPTER 5:

CONCLUSION AND FUTURE PERSPECTIVES

The aim of this study was to focus on the antimicrobial activity of W_5(Os-C) against Gram-positive *S. epidermidis* (ATCC 35984), potential synergism with vancomycin and lastly to evaluate its cytotoxicity and interaction with a model Gram-positive membrane.

A microdilution assay indicated that W_5(Os-C) is a more potent antibacterial agent than melittin ($p<0.0001$) and comparable to vancomycin. Peptide W_5(Os-C) also exhibited more potent activity against biofilm associated cells and inhibited biomass development at lower micromolar concentrations than vancomycin and melittin from the perspective of BIC_{50} values. However, the use of W_5(Os-C) as an antimicrobial agent is limited by its loss of activity at higher concentrations with an average decrease of 10% at 20 µM. This study can be expanded by investigating the effect of peptide and salt concentration on W_5(Os-C) structure, peptide-peptide interactions, and peptide-model membrane interactions with a focus on higher concentrations using MDSims and confirmation of results with NMR and CD spectroscopy (302). The activity of W_5(Os-C) on methicillin and multidrug resistant strains of *S. epidermidis* should also be investigated under physiological and high salt environments using the same parameters used in this study. Furthermore, risk of resistance development should be determined for various MRSE, methicillin sensitive *S. epidermidis* (MSSE), biofilm producing and non-biofilm producing strains by initially incubating strains in subinhibitory concentrations of W_5(Os-C), and exposing subsequent subcultures to increasing W_5(Os-C) concentrations until no inhibitory activity is observed (353). Additionally the activity and wound healing capacity of W_5(Os-C) alone or in combination with vancomycin may be investigated against *S. epidermidis* in a mouse open wound model (266).

The high potency of W_5(Os-C) makes it an attractive target for clinical use based on planktonic activity, but the peptide does not reliably inhibit more than 90% biofilm formation and can in fact increase biomass production. Furthermore, combining W_5(Os-C) with vancomycin fails to overcome the incomplete biofilm inhibitory activity of W_5(Os-C) or reduce the inhibitory concentrations of vancomycin. This may be due to binding of W_5(Os-C) to the substrate binding site of vancomycin and interfering with the mode of action of vancomycin. Interactions between vancomycin and W_5(Os-C) and vancomycin may be characterised using MDSims hydrogen bond and interaction energy analyses (177). Simultaneous administration of vancomycin and W_5(Os-C) is not advised, but cycling or alternating treatments may offer an alternative solution.

In order to determine whether alternating treatments will produce the desired antimicrobial effect, the killing times of both vancomycin and W_5(Os-C) will need to be determined. Various planktonic or biofilm associated *S. epidermidis* strains including methicillin or vancomycin resistant strains should then be exposed to vancomycin and W_5(Os-C) in alternating fashion, introducing the next agent as the killing time of the other is reached. In this manner, any antagonistic interaction between the antimicrobial agents can be avoided and the risk of drug resistance development may be reduced (354). Alternatively, W_5(Os-C) may also be combined with other antimicrobial agents such as rifampin, penicillin, erythromycin, or modified vancomycin molecules which may result in synergism (177, 262, 266).

Peptides Os, and Os-C exhibited reduced antibacterial activity in higher salt conditions (252). As such, W_5(Os-C) was produced to attempt to increase the antimicrobial activity of the AMP in physiological salt conditions. The high salt environments were investigated by simulating the interactions of W_5(Os-C) molecules with each other as well as with a POPG model membrane. As tryptophan tagging was used to increase activity in a salt environment, the interaction of W_5(Os-C) with a model membrane was investigated at 0.15 mM physiological and 0.3 mM high salt concentrations.

Peptide-membrane interactions between cationic AMPs and a POPG membrane start with electrostatic attraction between the positive charges on the peptide and the negatively charged phospholipid heads. Once the peptide is close enough to the membrane surface, it may remain in a horizontal orientation on the surface and further bind to the membrane via hydrogen bonding of the phospholipid heads with the peptide N and C terminals. Alternatively, the peptide may interact with the membrane through cation-π bonding of peptide side chains with non-polar lipid portions of the membrane or sink into the membrane to allow hydrophobic interactions using the hydrogen bonding as a stabilisation force (355, 356). Final insertion of the peptide usually requires a threshold concentration which induces conformational changes allowing peptide molecules to change orientation and insert according to the membrane insertion model followed by each specific peptide (164, 357). Peptide W_5(Os-C) interacted with the membrane initially through hydrogen bonding and suspected electrostatic interaction of a key lysine residue side chain. This was immediately followed by N-terminal hydrogen bonding and potential cation-π bonding of the N-terminal tryptophan tag with the membrane constituents. Under higher salt concentrations, more widespread hydrogen bonding suggests stronger attraction forces between peptide molecules and the membrane. The peptides do not, however, appear to fully insert into the membrane which may be due to sub-insertion threshold

concentrations. This may be confirmed by increasing the number of peptides in MDSims. Overall, MDSims showed slightly enhanced membrane insertion at high salt concentrations. Peptide aggregation was eliminated as the cause of loss of activity as the four peptides did not combine to form a tetramer during the MDSims of 1000 ns and could not maintain a stable trimer.

To confirm high salt concentrations are not the cause of loss of W_5(Os-C), the microdilution may be repeated with lower percentages of TSB to determine the optimal TSB – phosphate buffer concentration ratio at which no precipitate is observed to form and the activity of the peptide is not affected. However, by decreasing the percentage of TSB and thus salt content of the nutrient medium, the study deviates more from physiological conditions under which the peptide will be used (358, 359). Alternatively, MDSims may be repeated with more peptides in each water box to determine whether larger polymers form and may result in hydrophobic exclusion zones. Alternatively, the secondary structure in the presence and absence of a high salt environment produced by MDSims may be confirmed using CD as described by Strömstedt *et al*. (27, 28, 34) followed by feedback driven modification of the peptide.

As the peptide was active at lower concentrations, and MDSims did not provide conclusive evidence for salts interfering with antimicrobial activity of W_5(Os-C), other potential explanations need to be investigated. One possible explanation is the formation of casein micelles, since casein in pancreatic digested form is a component of TSB. These micelles could also potentially seclude the hydrophobic peptide according to the Horne model, when combined with specific ions, e.g. the phosphate ion, although this would be reflected by a dosage effect where increased peptide concentrations are more active than lower concentrations (360-362). At high peptide concentrations, W_5(Os-C) may form micelles or vesicles even in the absence of casein due to its surfactant-like sequence of a hydrophobic N terminal and cationic, hydrophilic C-terminal (363, 364). Micelle, vesicle and aggregate formation may be investigated using conductivity measurements of various W_5(Os-C) concentrations in various salt concentrations to identify threshold concentrations at which micelles, vesicles, or aggregates form, using high performance liquid chromatography (HPLC) to determine size of peptide complexes, or by atomic force microscopy or transmission electron microscopy to visualise type of complexes formed (364).

Simulations investigating peptide-solvent, peptide-peptide, and peptide-membrane interactions should be repeated using a higher concentration of the peptide to better simulate

a clinical treatment environment. Additionally, further modifications may be made to W_5(Os-C) which include substitution of tryptophan residues with β-naphtylalanines to increase salt resistance as described by Yu *et al.* (204); or selective substitution of L-amino acids for D-amino acids or unnatural origin residues like L-ornithine or L-homoarginine for overall increased stability against proteases. However, this must be done with care as such substitutions may lead to loss of activity and D-amino acid containing peptides are costly to synthesize (205, 365-367).

In conclusion, peptide W_5(Os-C) shows promising antimicrobial activity against *S. epidermidis* ATCC 35984 but cannot be pursued as such in its current form due to loss of activity at higher concentrations and its ability to induce excess biofilm formation at low concentrations. The peptide is also not suitable for combination therapy with vancomycin. Alternative combination partner drugs should be investigated, mechanisms responsible for loss of activity at high peptide concentrations should be elucidated, and peptide structural modifications need to be made before W_5(Os-C) can be pursued as an antimicrobial agent.

Table 5.1: Summary of *in vitro* investigation results.

	Vancomycin	W_5(Os-C)	3V:1W	2V:2W	1V:3W	Melittin (control)
Anti-planktonic activity	Y	Y	Y	Y	Y	Y
Cytotoxicity against HaCat cells	N	N				Y
Biofilm cell inhibition	Y	Y	Y	Y	N	Y
Biofilm biomass inhibition	Y	Y	Y	Y	N	Y

Table 5.2: Summary of *in silico* investigation results.

	Physiological conditions (0.15 M salt)	High salt conditions (0.30 M salt)
Peptide structure in H_2O	Extended.	Extended.
Peptide structure in presence of POPG membrane	Folded with two helices.	Folded with one helix, remaining peptide is extended.
Peptide-Peptide interactions	N terminal interaction with C-terminal; Single aggregate of 2 peptides.	Middle and C-terminal interactions; Single aggregate alternating between 2 and 3 peptides.
Secondary structure and flexibility	Tryptophan tag fixed in helical formation; Rest of peptide highly variable.	Tryptophan tag fixed in helical formation; Rest of peptide highly variable.
Peptide-POPG membrane interactions	Specific residues involved in hydrogen bonding; tryptophan tag main insertion point into membrane.	More wide-spread hydrogen bonding; Deeper membrane insertion with more residues involved.

REFERENCES

1. Valaperta R, Tejada MR, Frigerio M*, et al. Staphylococcus aureus* nosocomial infections: The role of a rapid and low-cost characterization for the establishment of a surveillance system. New Microbiologica. 2010;33(3):223-232.
2. Kim YW, Mosteller MP, Meyer MT*, et al.*, editors. Microfluidic biofilm observation, analysis, and treatment (micro-boat) platform. Proc A Solid-State Sens, Actuators Microsyst Workshop (Hilton Head Workshop); 2012.
3. Savini V, Catavitello C, Astolfi D*, et al.* Bacterial contamination of platelets and septic transfusions: Review of the literature and discussion on recent patents about biofilm treatment. Recent patents on anti-infective drug discovery. 2010;5(2):168-176.
4. Chessa D, Ganau G, Spiga L*, et al. Staphylococcus aureus* and *Staphylococcus epidermidis* virulence strains as causative agents of persistent infections in breast implants. PLoS One. 2016;11(1):1-15.
5. Kresken M, Klare I, Wichelhaus TA*, et al.* Glycopeptide resistance in *Enterococcus spp* And coagulase-negative staphylococci from hospitalized patients in germany: Occurrence, characteristics, and susceptibility to dalbavancin. Journal of Global Antimicrobial Resistance. 2021;28(3):102-107.
6. Yu Y, Huang Q, Liu A. Analysis of pathogens, drug resistance, sensitive antibiotic treatment and risk factors of early-onset sepsis in very low birth weight infants. American Journal of Translational Research. 2021;13(11):12939-12948.
7. Campoccia D, Montanaro L, Baldassarri L*, et al.* Antibiotic resistance in *Staphylococcus aureus* and *Staphylococcus epidermidis* clinical isolates from implant orthopedic infections. The International Journal of Artificial Organs. 2005;28(11):1186-1191.
8. Bloemendaal AL, Brouwer EC, Fluit AC. Methicillin resistance transfer from staphylocccus epidermidis to methicillin-susceptible *Staphylococcus aureus* in a patient during antibiotic therapy. PloS one. 2010;5(7):1-5.
9. Otto M. Coagulase-negative staphylococci as reservoirs of genes facilitating mrsa infection: Staphylococcal commensal species such as *Staphylococcus epidermidis* are being recognized as important sources of genes promoting MRSA colonization and virulence. Bioessays. 2013;35(1):4-11.
10. Chiew YF, Charles M, Johnstone MC*, et al.* Detection of vancomycin heteroresistant *Staphylococcus haemolyticus* and vancomycin intermediate resistant *Staphylococcus epidermidis* by means of vancomycin screening agar. Pathology. 2007;39(3):375-377.
11. Peschel A, Vuong C, Otto M*, et al.* The d-alanine residues of *Staphylococcus aureus* teichoic acids alter the susceptibility to vancomycin and the activity of autolytic enzymes. Antimicrobial agents and chemotherapy. 2000;44(10):2845-2847.
12. Sieradzki K, Roberts RB, Serur D*, et al.* Heterogeneously vancomycin-resistant *Staphylococcus epidermidis* strain causing recurrent peritonitis in a dialysis patient during vancomycin therapy. Journal of Clinical Microbiology. 1999;37(1):39-44.
13. Jenssen H, Hamill P, Hancock RE. Peptide antimicrobial agents. Clinical Microbiology Reviews. 2006;19(3):491-511.
14. Moretta A, Scieuzo C, Petrone AM*, et al.* Antimicrobial peptides: A new hope in biomedical and pharmaceutical fields. Frontiers in Cellular and Infection Microbiology. 2021;11(6):1-26.
15. Bahar AA, Ren D. Antimicrobial peptides. Pharmaceuticals (Basel). 2013;6(12):1543-1575.
16. Amso Z, Hayouka Z. Antimicrobial random peptide cocktails: A new approach to fight pathogenic bacteria. Chemical Communications (Cambridge, England). 2019;55(14):2007-2014.
17. Mahlapuu M, Håkansson J, Ringstad L*, et al.* Antimicrobial peptides: An emerging category of therapeutic agents. Frontiers in Cellular Infection Microbiology. 2016;6(194):1-12.
18. Rathinakumar R, Walkenhorst WF, Wimley WC. Broad-spectrum antimicrobial peptides by rational combinatorial design and high-throughput screening: The importance of interfacial activity. Journal of the American Chemical Society. 2009;131(22):7609-7617.
19. Som A, Vemparala S, Ivanov I*, et al.* Synthetic mimics of antimicrobial peptides. Peptide Science. 2008;90(2):83-93.
20. Schweizer F. Cationic amphiphilic peptides with cancer-selective toxicity. European Journal of Pharmacology. 2009;625(1):190-194.
21. Wang K, Zhang B, Zhang W*, et al.* Antitumor effects, cell selectivity and structure-activity relationship of a novel antimicrobial peptide polybia-mpi. Peptides. 2008;29(6):963-968.
22. Starr CG, Wimley WC. Antimicrobial peptides are degraded by the cytosolic proteases of human erythrocytes. Biochimica et Biophysica Acta (BBA) - Biomembranes. 2017;1859(12):2319-2326.
23. Lai Z, Yuan X, Chen H*, et al.* Strategies employed in the design of antimicrobial peptides with enhanced proteolytic stability. Biotechnology Advances. 2022;59(4):1-20.
24. Bradshaw J. Cationic antimicrobial peptides : Issues for potential clinical use. BioDrugs : clinical immunotherapeutics, biopharmaceuticals and gene therapy. 2003;17(4):233-240.

25. Guo L, Lim KB, Poduje CM, *et al.* Lipid a acylation and bacterial resistance against vertebrate antimicrobial peptides. Cell. 1998;95(2):189-198.
26. Blake KL, Randall CP, O'Neill AJ. *in vitro* studies indicate a high resistance potential for the lantibiotic nisin in *Staphylococcus aureus* and define a genetic basis for nisin resistance. Antimicrobial Agents and Chemotherapy. 2011;55(5):2362-2368.
27. Hilpert K, Volkmer-Engert R, Walter T, *et al.* High-throughput generation of small antibacterial peptides with improved activity. Nature Biotechnology. 2005;23(8):1008-1012.
28. Rathinakumar R, Wimley WC. Biomolecular engineering by combinatorial design and high-throughput screening: Small, soluble peptides that permeabilize membranes. Journal of the American Chemical Society. 2008;130(30):9849-9858.
29. Slezina MP, Istomina EA, Kulakovskaya EV, *et al.* The γ-core motif peptides of amps from grasses display inhibitory activity against human and plant pathogens. International Journal of Molecular Sciences. 2022;23(15):1-21.
30. Koch P, Schmitt S, Heynisch A, *et al.* Optimization of the antimicrobial peptide bac7 by deep mutational scanning. BMC biology. 2022;20(1):1-21.
31. Oliva R, Campanile M, Del Vecchio P, *et al.* The c-terminus of the gky20 antimicrobial peptide, derived from human thrombin, plays a key role in its membrane perturbation capability. Physical Chemistry Chemical Physics. 2022;24(13):7994-8002.
32. Schmidtchen A, Pasupuleti M, Mörgelin M, *et al.* Boosting antimicrobial peptides by hydrophobic oligopeptide end tags. Journal of Biological Chemistry. 2009;284(26):17584-17594.
33. Straus SK, Hancock REW. Mode of action of the new antibiotic for gram-positive pathogens daptomycin: Comparison with cationic antimicrobial peptides and lipopeptides. Biochimica et Biophysica Acta (BBA) - Biomembranes. 2006;1758(9):1215-1223.
34. Strömstedt AA, Pasupuleti M, Schmidtchen A, *et al.* Oligotryptophan-tagged antimicrobial peptides and the role of the cationic sequence. Biochimica et Biophysica Acta (BBA) - Biomembranes. 2009;1788(9):1916-1923.
35. Koksharova O, Safronova N, Dunina-Barkovskaya A. New antimicrobial peptide with two crac motifs: Activity against *Escherichia coli* and bacillus subtilis. Microorganisms. 2022;10(8):1-14.
36. Chen X, Takai T, Xie Y, *et al.* Human antimicrobial peptide ll-37 modulates proinflammatory responses induced by cytokine milieus and double-stranded rna in human keratinocytes. Biochemical and Biophysical Research Communications. 2013;433(4):532-537.
37. Papo N, Oren Z, Pag U, *et al.* The consequence of sequence alteration of an amphipathic α-helical antimicrobial peptide and its diastereomers. Journal of Biological Chemistry. 2002;277(37):33913-33921.
38. Rao A, Chopra S, Ram G, *et al.* Application of the “codon-shuffling” method: Synthesis and selection of de novo proteins as antibacterials. Journal of Biological Chemistry. 2005;280(25):23605-23614.
39. Fjell CD, Hiss JA, Hancock RE, *et al.* Designing antimicrobial peptides: Form follows function. Nature Reviews Drug Discovery. 2012;11(1):37-51.
40. Rasheed A, Farhat R. Combinatorial chemistry: A review. International Journal of Pharmaceutical Sciences and Research. 2013;4(7):2502-2516.
41. Kennedy JP, Williams L, Bridges TM, *et al.* Application of combinatorial chemistry science on modern drug discovery. Journal of Combinatorial Chemistry. 2008;10(3):345-354.
42. Liu R, Li X, Lam KS. Combinatorial chemistry in drug discovery. Current Opinion in Chemical Biology. 2017;38(6):117-126.
43. Chen CH, Starr CG, Guha S, *et al.* Tuning of a membrane-perforating antimicrobial peptide to selectively target membranes of different lipid composition. The Journal of Membrane Biology. 2021;254(1):75-96.
44. Puentes PR, Henao MC, Torres CE, *et al.* Design, screening, and testing of non-rational peptide libraries with antimicrobial activity: *In silico* and experimental approaches. Antibiotics. 2020;9(12):854.
45. Ting DSJ, Li J, Verma CS, *et al.* Evaluation of host defense peptide (cad23)-antibiotic interaction and mechanism of action: Insights from experimental and molecular dynamics simulations studies. Frontiers in Pharmacology. 2021;12(10):1-13.
46. Lousa D, Pinto AR, Campos SR, *et al.* Effect of ph on the influenza fusion peptide properties unveiled by constant-ph molecular dynamics simulations combined with experiment. Scientific Reports. 2020;10(1):1-18.
47. Mohamed MF, Abdelkhalek A, Seleem MN. Evaluation of short synthetic antimicrobial peptides for treatment of drug-resistant and intracellular *Staphylococcus aureus*. Scientific reports. 2016;6(1):1-14.
48. Shurko JF, Galega RS, Li C, *et al.* Evaluation of ll-37 antimicrobial peptide derivatives alone and in combination with vancomycin against *S. aureus*. The Journal of Antibiotics. 2018;71(11):971-974.
49. Wang G, Mishra B, Lau K, *et al.* Antimicrobial peptides in 2014. Pharmaceuticals. 2015;8(1):123-150.
50. Yu G, Baeder DY, Regoes RR, *et al.* Combination effects of antimicrobial peptides. Antimicrobial Agents and Chemotherapy. 2016;60(3):1717-1724.
51. Keller LJ, Lentz CS, Chen YE, *et al.* Characterization of serine hydrolases across clinical isolates of commensal skin bacteria *Staphylococcus epidermidis* using activity-based protein profiling. ACS Infectious Diseases. 2020;6(5):930-938.

52. Kloos WE, Musselwhite MS. Distribution and persistence of *staphylococcus* and *micrococcus* species and other aerobic bacteria on human skin. Applied Microbiology. 1975;30(3):381-395.
53. Oh J, Byrd AL, Deming C*, et al.* Biogeography and individuality shape function in the human skin metagenome. Nature. 2014;514(7520):59-64.
54. Carey RM, Chen B, Adappa ND*, et al.*, editors. Human upper airway epithelium produces nitric oxide in response to *Staphylococcus epidermidis*. International Forum of Allergy & Rhinology; 2016: Wiley Online Library.
55. Jain B. Modulation of airway epithelial cell ciliary beat frequency by nitric oxide. Biochemical and Biophysical Research Communications. 1993;191(1):83.
56. Iwase T, Uehara Y, Shinji H*, et al. Staphylococcus epidermidis* esp inhibits *Staphylococcus aureus* biofilm formation and nasal colonization. Nature. 2010;465(7296):346-349.
57. Sugimoto S, Iwamoto T, Takada K*, et al. Staphylococcus epidermidis* esp degrades specific proteins associated with *Staphylococcus aureus* biofilm formation and host-pathogen interaction. Journal of Bacteriology. 2013;195(8):1645-1655.
58. Conlan S, Mijares LA, Becker J*, et al. Staphylococcus epidermidis* pan-genome sequence analysis reveals diversity of skin commensal and hospital infection-associated isolates. Genome Biology. 2012;13(7):1-13.
59. Claudel J-P, Auffret N, Leccia M-T*, et al. Staphylococcus epidermidis*: A potential new player in the physiopathology of acne? Dermatology. 2019;235(4):287-294.
60. Rogers KL, Fey PD, Rupp ME. Coagulase-negative staphylococcal infections. Infectious Disease Clinics of North America. 2009;23(1):73-98.
61. Masters EA, Ricciardi BF, Bentley KLdM*, et al.* Skeletal infections: Microbial pathogenesis, immunity and clinical management. Nature Reviews Microbiology. 2022;20(7):385-400.
62. Arciola CR, An YH, Campoccia D*, et al.* Etiology of implant orthopedic infections: A survey on 1027 clinical isolates. Int J Artif Organs. 2005;28(11):1091-1100.
63. Harris LG, El-Bouri K, Johnston S*, et al.* Rapid identification of staphylococci from prosthetic joint infections using maldi-tof mass-spectrometry. International Journal Artificial Organs. 2010;33(9):568-574.
64. Tande AJ, Osmon DR, Greenwood-Quaintance KE*, et al.* Clinical characteristics and outcomes of prosthetic joint infection caused by small colony variant staphylococci. mBio. 2014;5(5):1-9.
65. Crump JA, Collignon PJ. Intravascular catheter-associated infections. European journal of clinical microbiology & infectious diseases : European Society of Clinical Microbiology. 2000;19(1):1-8.
66. Gandelman G, Frishman WH, Wiese C*, et al.* Intravascular device infections: Epidemiology, diagnosis, and management. Cardiology in Review. 2007;15(1):13-23.
67. Hellmark B, Unemo M, Nilsdotter-Augustinsson Å*, et al.* Antibiotic susceptibility among *Staphylococcus epidermidis* isolated from prosthetic joint infections with special focus on rifampicin and variability of the rpob gene. Clinical Microbiology and Infection. 2009;15(3):238-244.
68. Wang A, Athan E, Pappas PA*, et al.* Contemporary clinical profile and outcome of prosthetic valve endocarditis. Journal of the American Medical Association. 2007;297(12):1354-1361.
69. Zetrenne E, McIntosh BC, McRae MH*, et al.* Prosthetic vascular graft infection: A multi-center review of surgical management. The Yale Journal of Biology and Medicine. 2007;80(3):113-121.
70. Dyke KGH, Jevons MP, Parker MT. Penicillinase production and intrinsic resistance to penicillins in *Staphylococcus aureus*. The Lancet. 1966;287(7442):835-838.
71. Namvar AE, Bastarahang S, Abbasi N*, et al.* Clinical characteristics of *Staphylococcus epidermidis*: A systematic review. German Medical Society Hyciene and Infection Control. 2014;9(3):1-10.
72. Utsui Y, Yokota T. Role of an altered penicillin-binding protein in methicillin- and cephem-resistant *Staphylococcus aureus*. Antimicrobial Agents and Chemotherapy. 1985;28(3):397-403.
73. Antoci V, Jr., Adams CS, Parvizi J*, et al.* The inhibition of *Staphylococcus epidermidis* biofilm formation by vancomycin-modified titanium alloy and implications for the treatment of periprosthetic infection. Biomaterials. 2008;29(35):4684-4690.
74. Peacock SJ, Paterson GK. Mechanisms of methicillin resistance in *Staphylococcus aureus*. Annual Review of Biochemistry. 2015;84:577-601.
75. Wong-Beringer A, Joo J, Tse E*, et al.* Vancomycin-associated nephrotoxicity: A critical appraisal of risk with high-dose therapy. International Journal of Antimicrobial Agents. 2011;37(2):95-101.
76. Dieterich C, Puey A, Lin S*, et al.* Gene expression analysis reveals new possible mechanisms of vancomycin-induced nephrotoxicity and identifies gene markers candidates. Toxicological Science. 2009;107(1):258-269.
77. Wang S, Cai C, Shen Y*, et al. In vitro* activity of contezolid against methicillin-resistant *Staphylococcus aureus*, vancomycin-resistant *enterococcus*, and strains with linezolid resistance genes from china. Frontiers in Microbiology. 2021;12(8):1-5.
78. Cusumano JA, Klinker KP, Huttner A*, et al.* Towards precision medicine: Therapeutic drug monitoring–guided dosing of vancomycin and β-lactam antibiotics to maximize effectiveness and minimize toxicity. American Journal of Health-System Pharmacy. 2020;77(14):1104-1112.
79. Ghuysen JM, Strominger JL. Structure of the cell wall of *Staphylococcus aureus*, strain copenhagen. I. Preparation of fragments by enzymatic hydrolysis. Biochemistry. 1963;2:1110-1119.

80. Gründling A, Schneewind O. Cross-linked peptidoglycan mediates lysostaphin binding to the cell wall envelope of *Staphylococcus aureus*. Journal of Bacteriology. 2006;188(7):2463-2472.
81. Höltje J-V. A hypothetical holoenzyme involved in the replication of the murein sacculus of *Escherichia coli*. Microbiology. 1996;142(8):1911-1918.
82. Walsh C. Molecular mechanisms that confer antibacterial drug resistance. Nature. 2000;406(6797):775-781.
83. Jacob GS, Schaefer J, Wilson Jr GE. Direct measurement of peptidoglycan cross-linking in bacteria by 15n nuclear magnetic resonance. Journal of Biological Chemistry. 1983;258(18):10824-10826.
84. Vollmer W, Blanot D, De Pedro MA. Peptidoglycan structure and architecture. FEMS Microbiology Reviews. 2008;32(2):149-167.
85. Barna JC, Williams DH. The structure and mode of action of glycopeptide antibiotics of the vancomycin group. Annual Review of Microbiology. 1984;38(10):339-357.
86. Bugg TD, Dutka-Malen S, Arthur M*, et al.* Identification of vancomycin resistance protein vana as a d-alanine:D-alanine ligase of altered substrate specificity. Biochemistry. 1991;30(8):2017-2021.
87. Cho H, Uehara T, Bernhardt TG. Beta-lactam antibiotics induce a lethal malfunctioning of the bacterial cell wall synthesis machinery. Cell. 2014;159(6):1300-1311.
88. Tipper DJ, Strominger JL. Mechanism of action of penicillins: A proposal based on their structural similarity to acyl-d-alanyl-d-alanine. Proceedings of the National Academy of Sciences of the United States of America. 1965;54(4):1133-1141.
89. Organization WH. Antimicrobial resistance. World Health Organization; 2021.
90. Abraham EP, Chain E. An enzyme from bacteria able to destroy penicillin. Nature. 1940;146(3713):837-837.
91. Bondi Jr A, Dietz CC. Penicillin resistant *Staphylococci*. Proceedings of the Society for Experimental Biology and Medicine. 1945;60(1):55-58.
92. York MK, Gibbs L, Chehab F*, et al.* Comparison of pcr detection of meca with standard susceptibility testing methods to determine methicillin resistance in coagulase-negative *Staphylococci*. Journal of Clinical Microbiology. 1996;34(2):249-253.
93. World Health Organization. Antimicrobial resistance: 2014 global report on surveillance: World Health Organization; 2014.
94. Zavasky DM, Sande MA. Reconsideration of rifampin: A unique drug for a unique infection. Journal of the American Medical Association. 1998;279(19):1575-1577.
95. Zimmerli W, Widmer AF, Blatter M*, et al.* Role of rifampin for treatment of orthopedic implant–related *Staphylococcal* infections a randomized controlled trial. Journal of the American Medical Association. 1998;279(19):1537-1541.
96. Mendes RE, Deshpande L, Rodriguez-Noriega E*, et al.* First report of *Staphylococcal* clinical isolates in mexico with linezolid resistance caused by cfr: Evidence of *in vivo* cfr mobilization. Journal of Clinical Microbiology. 2010;48(8):3041-3043.
97. Sung JML, Lindsay JA. *Staphylococcus aureus* strains that are hypersusceptible to resistance gene transfer from *Enterococci*. Antimicrobial Agents and Chemotherapy. 2007;51(6):2189-2191.
98. Brogden KA. Antimicrobial peptides: Pore formers or metabolic inhibitors in bacteria? Nature Reviews microbiology. 2005;3(3):238-250.
99. Gu B, Kelesidis T, Tsiodras S*, et al.* The emerging problem of linezolid-resistant *Staphylococcus*. Journal of Antimicrobial Chemotherapy. 2013;68(1):4-11.
100. O'Connor C, Powell J, Finnegan C*, et al.* Incidence, management and outcomes of the first cfr-mediated linezolid-resistant *Staphylococcus epidermidis* outbreak in a tertiary referral centre in the republic of Ireland. Journal of Hospital Infection. 2015;90(4):316-321.
101. Håkanson A, Fröding I, Ottosson C. Vancomycin resistant *Staphylococcus epidermidis* caused prosthesis infection. Linezolid and rifampicin healed the complicated infection. Lakartidningen. 2014;111(9-10):396-398.
102. Costerton JW, Stewart PS, Greenberg EP. Bacterial biofilms: A common cause of persistent infections. Science. 1999;284(5418):1318-1322.
103. Ziebuhr W, Heilmann C, Götz F*, et al.* Detection of the intercellular adhesion gene cluster (ica) and phase variation in *Staphylococcus epidermidis* blood culture strains and mucosal isolates. Infection and Immunity. 1997;65(3):890-896.
104. Nobile CJ, Mitchell AP. Regulation of cell-surface genes and biofilm formation by the *C. albicans* transcription factor bcr1p. Current Biology. 2005;15(12):1150-1155.
105. Grassi L, Maisetta G, Esin S*, et al.* Combination strategies to enhance the efficacy of antimicrobial peptides against bacterial biofilms. Frontiers in Microbiology. 2017;8(12):1-8.
106. Davies DG, Parsek MR, Pearson JP*, et al.* The involvement of cell-to-cell signals in the development of a bacterial biofilm. Science. 1998;280(5361):295-298.
107. Li Y-H, Tang N, Aspiras MB*, et al.* A quorum-sensing signaling system essential for genetic competence in *Streptococcus mutans* is involved in biofilm formation. Journal of Bacteriology. 2002;184(10):2699-2708.
108. O'Neill E, Pozzi C, Houston P*, et al.* A novel *Staphylococcus aureus* biofilm phenotype mediated by the fibronectin-binding proteins, fnbpa and fnbpb. Journal of Bacteriology. 2008;190(11):3835-3850.

109. Fey PD, Olson ME. Current concepts in biofilm formation of *Staphylococcus epidermidis*. Future Microbiology. 2010;5(6):917-933.
110. Yoshida A, Kuramitsu HK. Multiple streptococcus mutans genes are involved in biofilm formation. Applied and Environmental Microbiology. 2002;68(12):6283-6291.
111. Hall-Stoodley L, Costerton JW, Stoodley P. Bacterial biofilms: From the natural environment to infectious diseases. Nat Rev Microbiol. 2004;2(2):95-108.
112. Vuong C, Gerke C, Somerville GA*, et al.* Quorum-sensing control of biofilm factors in *Staphylococcus epidermidis*. The Journal of Infectious Diseases. 2003;188(5):706-718.
113. Vuong C, Kocianova S, Yao Y*, et al.* Increased colonization of indwelling medical devices by quorum-sensing mutants of *Staphylococcus epidermidis in vivo*. The Journal of Infectious Diseases. 2004;190(8):1498-1505.
114. Kahl BC, Belling G, Becker P*, et al.* Thymidine-dependent *Staphylococcus aureus* small-colony variants are associated with extensive alterations in regulator and virulence gene expression profiles. Infection and Immunity. 2005;73(7):4119-4126.
115. Mann EE, Rice KC, Boles BR*, et al.* Modulation of eDNA release and degradation affects *Staphylococcus aureus* biofilm maturation. Public Library of Science One. 2009;4(6):1-12.
116. Qin Z, Ou Y, Yang L*, et al.* Role of autolysin-mediated DNA release in biofilm formation of *Staphylococcus epidermidis*. Microbiology. 2007;153(7):2083-2092.
117. Begun J, Gaiani JM, Rohde H*, et al. Staphylococcal* biofilm exopolysaccharide protects against *Caenorhabditis elegans* immune defenses. Public Library of Science Pathology. 2007;3(4):526-540.
118. Vuong C, Voyich JM, Fischer ER*, et al.* Polysaccharide intercellular adhesin (pia) protects *Staphylococcus epidermidis* against major components of the human innate immune system. Cellular Microbiology. 2004;6(3):269-275.
119. Vuong C, Otto M. *Staphylococcus epidermidis* infections. Microbes and Infection. 2002;4(4):481-489.
120. Beenken KE, Dunman PM, McAleese F*, et al.* Global gene expression in *Staphylococcus aureus* biofilms. Journal of Bacteriology. 2004;186(14):4665-4684.
121. Cramton SE, Gerke C, Schnell NF*, et al.* The intercellular adhesion (ica) locus is present in *Staphylococcus aureus* and is required for biofilm formation. Infection and Immunity. 1999;67(10):5427-5433.
122. Maisetta G, Grassi L, Di Luca M*, et al.* Anti-biofilm properties of the antimicrobial peptide temporin 1tb and its ability, in combination with EDTA, to eradicate *Staphylococcus epidermidis* biofilms on silicone catheters. Biofouling. 2016;32(7):787-800.
123. Fox EP, Cowley ES, Nobile CJ*, et al.* Anaerobic bacteria grow within *Candida albicans* biofilms and induce biofilm formation in suspension cultures. Current Biology. 2014;24(20):2411-2416.
124. Adam B, Baillie GS, Douglas LJ. Mixed species biofilms of candida albicans and *Staphylococcus epidermidis*. Journal of Medical Microbiology. 2002;51(4):344-349.
125. Ji G, Beavis R, Novick RP. Bacterial interference caused by autoinducing peptide variants. Science. 1997;276(5321):2027-2030.
126. Otto M. *Staphylococcal* biofilms. Current Topics in Microbiology and Immunology. 2008;322(11):207-228.
127. Cho JS, Guo Y, Ramos RI*, et al.* Neutrophil-derived il-1β is sufficient for abscess formation in immunity against *Staphylococcus aureus* in mice. Public Library of Science Pathology. 2012;8(11):1-20.
128. Craven RR, Gao X, Allen IC*, et al. Staphylococcus aureus* α-hemolysin activates the nlrp3-inflammasome in human and mouse monocytic cells. Public Library of Science One. 2009;4(10):1-11.
129. Kebaier C, Chamberland RR, Allen IC*, et al. Staphylococcus aureus* α-hemolysin mediates virulence in a murine model of severe pneumonia through activation of the nlrp3 inflammasome. Journal of Infectious Diseases. 2012;205(5):807-817.
130. Götz F. *Staphylococcus* and biofilms. Molecular Microbiology. 2002;43(6):1367-1378.
131. Peters G, Locci R, Pulverer G. Microbial colonization of prosthetic devices. I. Scanning electron microscopy of naturally infected intravenous catheters. Zentralblatt fur Bakteriologie, Mikrobiologie und Hygiene 1 Abt Originale B, Hygiene. 1981;173(5):293-299.
132. Fraiha RO, Pereira APR, Brito EdCA*, et al.* Stress conditions in the host induce persister cells and influence biofilm formation by *Staphylococcus epidermidis* rp62a. Revista da Sociedade Brasileira de Medicina Tropical. 2019;52(7):1-6.
133. Kocianova S, Vuong C, Yao Y*, et al.* Key role of poly-γ-dl-glutamic acid in immune evasion and virulence of *Staphylococcus epidermidis*. The Journal of Clinical Investigation. 2005;115(3):688-694.
134. Yang S, Hay ID, Cameron DR*, et al.* Antibiotic regimen based on population analysis of residing persister cells eradicates *Staphylococcus epidermidis* biofilms. Scientific Reports. 2015;5(1):1-11.
135. Schommer NN, Christner M, Hentschke M*, et al. Staphylococcus epidermidis* uses distinct mechanisms of biofilm formation to interfere with phagocytosis and activation of mouse macrophage-like cells 774a. 1. Infection and Immunity. 2011;79(6):2267-2276.
136. Ribič U, Jakše J, Toplak N*, et al.* Transporters and efflux pumps are the main mechanisms involved in *Staphylococcus epidermidis* adaptation and tolerance to didecyldimethylammonium chloride. Microorganisms. 2020;8(3):1-18.

137. Sabatini S, Piccioni M, Felicetti T, *et al.* Investigation on the effect of known potent *S. aureus* nora efflux pump inhibitors on the *Staphylococcal* biofilm formation. Royal Society of Chemistry Advances. 2017;7(59):37007-37014.
138. Fosgerau K, Hoffmann T. Peptide therapeutics: Current status and future directions. Drug Discovery Today. 2015;20(1):122-128.
139. Seo M-D, Won H-S, Kim J-H, *et al.* Antimicrobial peptides for therapeutic applications: A review. Molecules. 2012;17(10):12276-12286.
140. Skarnes RC, Watson DW. Antimicrobial factors of normal tissues and fluids. Bacteriological reviews. 1957;21(4):273-294.
141. Bechinger B, Zasloff M, Opella SJ. Structure and orientation of the antibiotic peptide magainin in membranes by solid-state nuclear magnetic resonance spectroscopy. Protein Science. 1993;2(12):2077-2084.
142. Ganz T, Selsted ME, Szklarek D, *et al.* Defensins. Natural peptide antibiotics of human neutrophils. The Journal of Clinical Investigation. 1985;76(4):1427-1435.
143. Bahar AA, Ren D. Antimicrobial peptides. Pharmaceuticals. 2013;6(12):1543-1575.
144. Zasloff M. Antimicrobial peptides of multicellular organisms. Nature. 2002;415(6870):389-395.
145. Brzoza P, Godlewska U, Borek A, *et al.* Redox active antimicrobial peptides in controlling growth of microorganisms at body barriers. Antioxidants (Basel). 2021;10(3):1-16.
146. Wanders RJ, Duran M, Loupatty FJ. Enzymology of the branched-chain amino acid oxidation disorders: The valine pathway. Journal of Inherited Metabolic Disease. 2012;35(1):5-12.
147. Hancock RE, Sahl H-G. Antimicrobial and host-defense peptides as new anti-infective therapeutic strategies. Nature Biotechnology. 2006;24(12):1551-1557.
148. Hiemstra T, Van Riemsdijk WH. A surface structural approach to ion adsorption: The charge distribution (cd) model. Journal of Colloid and Interface Science. 1996;179(2):488-508.
149. Simpson A, Maxwell A, Govan J, *et al.* Elafin (elastase-specific inhibitor) has anti-microbial activity against gram-positive and gram-negative respiratory pathogens. Federation of European Biochemical Societies Letters. 1999;452(3):309-313.
150. Baxter AA, Lay FT, Poon IKH, *et al.* Tumor cell membrane-targeting cationic antimicrobial peptides: Novel insights into mechanisms of action and therapeutic prospects. Cellular and Molecular Life Sciences. 2017;74(20):3809-3825.
151. Huang J, Hao D, Chen Y, *et al.* Inhibitory effects and mechanisms of physiological conditions on the activity of enantiomeric forms of an α-helical antibacterial peptide against bacteria. Peptides. 2011;32(7):1488-1495.
152. Ramanathan B, Davis EG, Ross CR, *et al.* Cathelicidins: Microbicidal activity, mechanisms of action, and roles in innate immunity. Microbes and Infection. 2002;4(3):361-372.
153. Zanetti M. The role of cathelicidins in the innate host defenses of mammals. Current Issues in Molecular Biology. 2005;7(2):179-196.
154. Kavanagh K, Dowd S. Histatins: Antimicrobial peptides with therapeutic potential. Journal of Pharmacy and Pharmacology. 2004;56(3):285-289.
155. Troxler R, Offner G, Xu T, *et al.* Structural relationship between human salivary histatins. Journal of Dental Research. 1990;69(1):2-6.
156. Costley D, Nesbitt H, Ternan N, *et al.* Sonodynamic inactivation of gram-positive and gram-negative bacteria using a rose bengal–antimicrobial peptide conjugate. International Journal of Antimicrobial Agents. 2017;49(1):31-36.
157. Hobta A, Lisovskiy I, Mikhalap S, *et al.* Epidermoid carcinoma–derived antimicrobial peptide (ecap) inhibits phosphorylation by protein kinases *in vitro*. Cell Biochemistry and Function. 2001;19(4):291-298.
158. Lee JY, Suh JS, Kim JM, *et al.* Identification of a cell-penetrating peptide domain from human beta-defensin 3 and characterization of its anti-inflammatory activity. International Journal of Nanomedicine. 2015;10:5423-5434.
159. Lehrer RI, Ganz T, Szklarek D, *et al.* Modulation of the *in vitro* candidacidal activity of human neutrophil defensins by target cell metabolism and divalent cations. The Journal of Clinical Investigation. 1988;81(6):1829-1835.
160. Akkam Y. A review of antifungal peptides: Basis to new era of antifungal drugs. Jordan Journal of Pharmaceutical Sciences. 2016;9(1):51-75.
161. Bulet P, Dimarcq J-L, Hetru C, *et al.* A novel inducible antibacterial peptide of *Drosophila* carries an o-glycosylated substitution. Journal of Biological Chemistry. 1993;268(20):14893-14897.
162. Pasupuleti M, Schmidtchen A, Malmsten M. Antimicrobial peptides: Key components of the innate immune system. Critical Reviews in Biotechnology. 2012;32(2):143-171.
163. Simmaco M, Mignogna G, Barra D. Antimicrobial peptides from amphibian skin: What do they tell us? Peptide Science. 1998;47(6):435-450.
164. Nguyen LT, Haney EF, Vogel HJ. The expanding scope of antimicrobial peptide structures and their modes of action. Trends in Biotechnology. 2011;29(9):464-472.
165. Lohner K. New strategies for novel antibiotics: Peptides targeting bacterial cell membranes. General Physiology and Biophysics. 2009;28(2):105-116.

166. Chen R, Mark AE. The effect of membrane curvature on the conformation of antimicrobial peptides: Implications for binding and the mechanism of action. European Biophysics Journal. 2011;40(4):545-553.
167. Mattila J-P, Sabatini K, Kinnunen PK. Oxidized phospholipids as potential molecular targets for antimicrobial peptides. Biochimica et Biophysica Acta (BBA)-Biomembranes. 2008;1778(10):2041-2050.
168. Rokitskaya TI, Kolodkin NI, Kotova EA*, et al.* Indolicidin action on membrane permeability: Carrier mechanism versus pore formation. Biochimica et Biophysica Acta (BBA)-Biomembranes. 2011;1808(1):91-97.
169. Miteva M, Andersson M, Karshikoff A*, et al.* Molecular electroporation: A unifying concept for the description of membrane pore formation by antibacterial peptides, exemplified with nk-lysin. Federation of European Biochemical Societies Letters. 1999;462(1-2):155-158.
170. Epand RM, Epand RF. Bacterial membrane lipids in the action of antimicrobial agents. Journal of Peptide Science. 2011;17(5):298-305.
171. Haney EF, Nathoo S, Vogel HJ*, et al.* Induction of non-lamellar lipid phases by antimicrobial peptides: A potential link to mode of action. Chemistry and Physics of Lipids. 2010;163(1):82-93.
172. Jeu L, Fung HB. Daptomycin: A cyclic lipopeptide antimicrobial agent. Clinical Therapeutics. 2004;26(11):1728-1757.
173. Dangel A, Ackermann N, Abdel-Hadi O*, et al.* A de novo-designed antimicrobial peptide with activity against multiresistant *Staphylococcus aureus* acting on rsbw kinase. The Federation of American Societies of Experimental Biology Journal. 2013;27(11):4476-4488.
174. Xiong YQ, Bayer AS, Elazegui L*, et al.* A synthetic congener modeled on a microbicidal domain of thrombin-induced platelet microbicidal protein 1 recapitulates staphylocidal mechanisms of the native molecule. Antimicrobial Agents and Chemotherapy. 2006;50(11):3786-3792.
175. Fang X, Tiyanont K, Zhang Y*, et al.* The mechanism of action of ramoplanin and enduracidin. Molecular BioSystems. 2006;2(1):69-76.
176. Reynolds PE. Structure, biochemistry and mechanism of action of glycopeptide antibiotics. European Journal of Clinical Microbiology and Infectious Diseases. 1989;8(11):943-950.
177. Olademehin OP, Kim SJ, Shuford KL. Molecular dynamics simulation of atomic interactions in the vancomycin binding site. American Chemical Society Omega. 2020;6(1):775-785.
178. Krizsan A, Volke D, Weinert S*, et al.* Insect-derived proline-rich antimicrobial peptides kill bacteria by inhibiting bacterial protein translation at the 70 s ribosome. Angewandte Chemie International Edition. 2014;53(45):12236-12239.
179. Mardirossian M, Grzela R, Giglione C*, et al.* The host antimicrobial peptide bac71-35 binds to bacterial ribosomal proteins and inhibits protein synthesis. Chemistry and Biology. 2014;21(12):1639-1647.
180. Roy RN, Lomakin IB, Gagnon MG*, et al.* The mechanism of inhibition of protein synthesis by the proline-rich peptide oncocin. Nature Structural and Molecular Biology. 2015;22(6):466-469.
181. Shah AJ, Serafim V, Xu Z*, et al.* Determination of antimicrobial resistance using tandem mass spectrometry. 1st ed ed: Josh Wiley & Sons; 2017.
182. Ciumac D, Gong H, Hu X*, et al.* Membrane targeting cationic antimicrobial peptides. Journal of Colloid and Interface Science. 2019;537(11):163-185.
183. Finlay BB, Hancock RE. Can innate immunity be enhanced to treat microbial infections? Nature Reviews Microbiology. 2004;2(6):497-504.
184. Brancatisano FL, Maisetta G, Di Luca M*, et al.* Inhibitory effect of the human liver-derived antimicrobial peptide hepcidin 20 on biofilms of polysaccharide intercellular adhesin (pia)-positive and pia-negative strains of *Staphylococcus epidermidis*. Biofouling. 2014;30(4):435-446.
185. Park CH, Valore EV, Waring AJ*, et al.* Hepcidin, a urinary antimicrobial peptide synthesized in the liver. Journal of Biological Chemistry. 2001;276(11):7806-7810.
186. Zasloff M. Magainins, a class of antimicrobial peptides from xenopus skin: Isolation, characterization of two active forms, and partial cDNA sequence of a precursor. Proceedings of the National Academy of Sciences. 1987;84(15):5449-5453.
187. Lamb HM, Wiseman LR. Pexiganan acetate. Drugs. 1998;56(6):1047-1052.
188. Zhu CMDP, Tan HMDP, Cheng TMDP*, et al.* Human β-defensin 3 inhibits antibiotic-resistant *Staphylococcus* biofilm formation. Journal of Surgical Research. 2013;183(1):204-213.
189. Manniello JM, Heymann H, Adair FW. Resistance of spheroplasts and whole cells of *Pseudomonas cepacia* to polymyxin b. Antimicrobial Agents and Chemotherapy. 1978;14(3):500-504.
190. Joo H-S, Fu C-I, Otto M. Bacterial strategies of resistance to antimicrobial peptides. Philosophical Transactions of the Royal Society B: Biological Sciences. 2016;371(1695):1-11.
191. Li M, Lai Y, Villaruz AE*, et al.* Gram-positive three-component antimicrobial peptide-sensing system. Proceedings of the National Academy of Sciences. 2007;104(22):9469-9474.
192. Keith Rose R, Hogg SD. Competitive binding of calcium and magnesium to *Streptococcal* lipoteichoic acid. Biochimica et Biophysica Acta (BBA) - General Subjects. 1995;1245(1):94-98.
193. Lambert PA, Hancock IC, Baddiley J. Influence of alanyl ester residues on the binding of magnesium ions to teichoic acids. Biochemical Journal. 1975;151(3):671-676.

194. Yang S-J, Mishra NN, Rubio A*, et al.* Causal role of single nucleotide polymorphisms within the mprf gene of *Staphylococcus aureus* in daptomycin resistance. Antimicrobial Agents and Chemotherapy. 2013;57(11):5658-5664.
195. Otto M, Peschel A, Götz F. Producer self-protection against the lantibiotic epidermin by the abc transporter epifeg of *Staphylococcus epidermidis* tü3298. Federation of European Microbiological Societies Microbiology Letters. 1998;166(2):203-211.
196. Wecke J, Perego M, Fischer W. D-alanine deprivation of *Bacillus subtilis* teichoic acids is without effect on cell growth and morphology but affects the autolytic activity. Microbial Drug Resistance. 1996;2(1):123-129.
197. da Silva Jr A, Teschke O. Effects of the antimicrobial peptide pgla on live *Escherichia coli*. Biochimica et Biophysica Acta (BBA)-Molecular Cell Research. 2003;1643(3):95-103.
198. Hancock RE. Alterations in outer membrane permeability. Annual Review of Microbiology. 1984;38(1):237-264.
199. Huang LC, Redfern RL, Narayanan S*, et al. In vitro* activity of human beta-defensin 2 against *Pseudomonas aeruginosa* in the presence of tear fluid. Antimicrobial Agents and Chemotherapy. 2007;51(11):3853-3860.
200. Lei J, Sun L, Huang S*, et al.* The antimicrobial peptides and their potential clinical applications. Americal Journal of Translational Research. 2019;11(7):3919-3931.
201. Nagaoka I, Hirota S, Yomogida S*, et al.* Synergistic actions of antibacterial neutrophil defensins and cathelicidins. Inflammation Research. 2000;49(2):73-79.
202. Harder Jr, Bartels J, Christophers E*, et al.* Isolation and characterization of human μ-defensin-3, a novel human inducible peptide antibiotic. Journal of Biological Chemistry. 2001;276(8):5707-5713.
203. Bals R, Wang X, Wu Z*, et al.* Human beta-defensin 2 is a salt-sensitive peptide antibiotic expressed in human lung. The Journal of Clinical Investigation. 1998;102(5):874-880.
204. Yu H-Y, Tu C-H, Yip B-S*, et al.* Easy strategy to increase salt resistance of antimicrobial peptides. Antimicrobial Agents and Chemotherapy. 2011;55(10):4918-4921.
205. Zhong C, Zhang F, Yao J*, et al.* Antimicrobial peptides with symmetric structures against multidrug-resistant bacteria while alleviating antimicrobial resistance. Biochemical Pharmacology. 2021;186(2):1-25.
206. Wang S, Charbonnier L-M, Rivas MN*, et al.* Myd88 adaptor-dependent microbial sensing by regulatory t cells promotes mucosal tolerance and enforces commensalism. Immunity. 2015;43(2):289-303.
207. Dosler S, Mataraci E. *In vitro* pharmacokinetics of antimicrobial cationic peptides alone and in combination with antibiotics against methicillin resistant *Staphylococcus aureus* biofilms. Peptides. 2013;49(8):53-58.
208. de la Fuente-Núñez C, Reffuveille F, Haney EF*, et al.* Broad-spectrum anti-biofilm peptide that targets a cellular stress response. Public Library of Science Pathology. 2014; 10(5):1-12.
209. de la Fuente-Núñez C, Reffuveille F, Mansour SC*, et al.* D-enantiomeric peptides that eradicate wild-type and multidrug-resistant biofilms and protect against lethal *Pseudomonas aeruginosa* infections. Chemistry and Biology. 2015;22(2):196-205.
210. Reffuveille F, de la Fuente-Núñez C, Mansour S*, et al.* A broad-spectrum antibiofilm peptide enhances antibiotic action against bacterial biofilms. Antimicrobial Agents and Chemotherapy. 2014;58(9):5363-5371.
211. Fleming D, Rumbaugh KP. Approaches to dispersing medical biofilms. Microorganisms. 2017;5(2):1-16.
212. Waters CM, Bassler BL. Quorum sensing: Cell-to-cell communication in bacteria. Annual Review of Cell and Developmental Biology. 2005;21(1):319-346.
213. Yan H, Hancock RE. Synergistic interactions between mammalian antimicrobial defense peptides. Antimicrobial Agents and Chemotherapy. 2001;45(5):1558-1560.
214. Berditsch M, Jäger T, Strempel N*, et al.* Synergistic effect of membrane-active peptides polymyxin b and gramicidin s on multidrug-resistant strains and biofilms of *Pseudomonas aeruginosa*. Antimicrobial Agents and Chemotherapy. 2015;59(9):5288-5296.
215. Gordya N, Yakovlev A, Kruglikova A*, et al.* Natural antimicrobial peptide complexes in the fighting of antibiotic resistant biofilms: *Calliphora vicina* medicinal maggots. Public Library of Science One. 2017;12(3):1-19.
216. Mishra NM, Briers Y, Lamberigts C*, et al.* Evaluation of the antibacterial and antibiofilm activities of novel cramp–vancomycin conjugates with diverse linkers. Organic and Biomolecular Chemistry. 2015;13(27):7477-7486.
217. Eckert R, Brady KM, Greenberg EP*, et al.* Enhancement of antimicrobial activity against *Pseudomonas aeruginosa* by coadministration of g10khc and tobramycin. Antimicrobial Agents and Chemotherapy. 2006;50(11):3833-3838.
218. Guo Y, Xun M, Han J. A bovine myeloid antimicrobial peptide (bmap-28) and its analogs kill pan-drug-resistant *Acinetobacter baumannii* by interacting with outer membrane protein a (ompa). Medicine (Baltimore). 2018;97(42):12832-12832.
219. Orlando F, Ghiselli R, Cirioni O*, et al.* Bmap-28 improves the efficacy of vancomycin in rat models of gram-positive cocci ureteral stent infection. Peptides. 2008;29(7):1118-1123.
220. Ribeiro SM, de la Fuente-Núñez C, Baquir B*, et al.* Antibiofilm peptides increase the susceptibility of carbapenemase-producing *Klebsiella pneumoniae* clinical isolates to β-lactam antibiotics. Antimicrobial Agents and Chemotherapy. 2015;59(7):3906-3912.

221. Wu X, Wang Y, Tao L. Sulfhydryl compounds reduce *Staphylococcus aureus* biofilm formation by inhibiting pia biosynthesis. Federation of European Microbiological Societies Microbiology Letters. 2011;316(1):44-50.
222. Ahire JJ, Dicks LM. Nisin incorporated with 2, 3-dihydroxybenzoic acid in nanofibers inhibits biofilm formation by a methicillin-resistant strain of *Staphylococcus aureus*. Probiotics and Antimicrobial Proteins. 2015;7(1):52-59.
223. Lin M-H, Shu J-C, Huang H-Y*, et al.* Involvement of iron in biofilm formation by *Staphylococcus aureus*. Public Library of Science One. 2012;7(3):1-7.
224. Jones EA, McGillivary G, Bakaletz LO. Extracellular DNA within a nontypeable *Haemophilus influenzae*-induced biofilm binds human beta defensin-3 and reduces its antimicrobial activity. Journal of Innate Immunity. 2013;5(1):24-38.
225. Balaban N, Gov Y, Giacometti A*, et al.* A chimeric peptide composed of a dermaseptin derivative and an rna iii-inhibiting peptide prevents graft-associated infections by antibiotic-resistant *Staphylococci*. Antimicrobial Agents and Chemotherapy. 2004;48(7):2544-2550.
226. Brackman G, Cos P, Maes L*, et al.* Quorum sensing inhibitors increase the susceptibility of bacterial biofilms to antibiotics *in vitro* and *in vivo*. Antimicrobial Agents and Chemotherapy. 2011;55(6):2655-2661.
227. Han R, Wang S. Mechanisms of antimicrobial peptides as characterized by solid-state NMR. Magnetic Resonance Letters. 2022;2(2):119-129.
228. Alamri MA, Tahir ul Qamar M, Afzal O*, et al.* Discovery of anti-mers-cov small covalent inhibitors through pharmacophore modeling, covalent docking and molecular dynamics simulation. Journal of Molecular Liquids. 2021;330(1):1-9.
229. Venkatesan SK, Shukla AK, Dubey VK. Molecular docking studies of selected tricyclic and quinone derivatives on trypanothione reductase of *Leishmania infantum*. Journal of Computational Chemistry. 2010;31(13):2463-2475.
230. Altharawi A, Ahmad S, Alamri MA*, et al.* Structural insight into the binding pattern and interaction mechanism of chemotherapeutic agents with sorcin by docking and molecular dynamic simulation. Colloids and Surfaces B: Biointerfaces. 2021;208:1-7.
231. Balogh G, Gyöngyösi T, Timári I*, et al.* Comparison of carbohydrate force fields using gaussian accelerated molecular dynamics simulations and development of force field parameters for heparin-analogue pentasaccharides. Journal of Chemical Information and Modeling. 2019;59(11):4855-4867.
232. Campagne S, Krepl M, Sponer J*, et al.* Combining NMR spectroscopy and molecular dynamic simulations to solve and analyze the structure of protein–RNA complexes. Methods in Enzymology. 614: Elsevier; 2019. p. 393-422.
233. Damjanovic J, Miao J, Huang H*, et al.* Elucidating solution structures of cyclic peptides using molecular dynamics simulations. Chemical Reviews. 2021;121(4):2292-2324.
234. Ziarek JJ, Baptista D, Wagner G. Recent developments in solution nuclear magnetic resonance (NMR)-based molecular biology. Journal of Molecular Medicine (Berlin). 2018;96(1):1-8.
235. Philippopoulos M, Lim C. Exploring the dynamic information content of a protein NMR structure: Comparison of a molecular dynamics simulation with the NMR and x-ray structures of *Escherichia coli* ribonuclease hi. Proteins: Structure, Function, and Bioinformatics. 1999;36(1):87-110.
236. Markwick PR, Malliavin T, Nilges M. Structural biology by NMR: Structure, dynamics, and interactions. Public Library of Science Computational Biology. 2008;4(9):1-7.
237. Wang Y, Chen CH, Hu D*, et al.* Spontaneous formation of structurally diverse membrane channel architectures from a single antimicrobial peptide. Nature Communications. 2016;7(1):1-9.
238. Nevins N, Cicero D, Snyder JP. A test of the single-conformation hypothesis in the analysis of NMR data for small polar molecules: A force field comparison. The Journal of Organic Chemistry. 1999;64(11):3979-3986.
239. Wennberg CL, Murtola T, Hess B*, et al.* Lennard-jones lattice summation in bilayer simulations has critical effects on surface tension and lipid properties. Journal of Chemical Theory and Computation. 2013;9(8):3527-3537.
240. Palmer N, Maasch J, Torres MDT*, et al.* Molecular dynamics for antimicrobial peptide discovery. Infection and Immunity. 2021;89(4):1-10.
241. Westerfield J, Gupta C, Scott HL*, et al.* Ions modulate key interactions between phlip and lipid membranes. Biophysical Journal. 2019;117(5):920-929.
242. MacKerell Jr AD. Empirical force fields for biological macromolecules: Overview and issues. Journal of Computational Chemistry. 2004;25(13):1584-1604.
243. Essmann U, Perera L, Berkowitz ML*, et al.* A smooth particle mesh ewald method. The Journal of Chemical Physics. 1995;103(19):8577-8593.
244. Song C, de Groot BL, Sansom MS. Lipid bilayer composition influences the activity of the antimicrobial peptide dermcidin channel. Biophysical Journal. 2019;116(9):1660.
245. Penna MJ, Biggs MJ. The binding mechanism of an experimentally identified platinum-binding peptide by molecular dynamics simulation. Chemeca 2010: Engineering at the edge; 26-29 September 2010, Hilton Adelaide, South Australia: Engineers Australia; 2010. p. 289-298.

246. Vallet-Regí M, Balas F. Silica materials for medical applications. Open Biomedical Engineering Journal. 2008;2:1-9.
247. Hildebrand N, Köppen S, Derr L*, et al.* Adsorption orientation and binding motifs of lysozyme and chymotrypsin on amorphous silica. The Journal of Physical Chemistry C. 2015;119(13):7295-7307.
248. Brancolini G, Kokh DB, Calzolai L*, et al.* Docking of ubiquitin to gold nanoparticles. American Chemical Society Nano. 2012;6(11):9863-9878.
249. Monti S, Barcaro G, Sementa L*, et al.* Dynamics and self-assembly of bio-functionalized gold nanoparticles in solution: Reactive molecular dynamics simulations. Nano Research. 2018;11(4):1757-1767.
250. Mihailescu D, Smith JC. Atomic detail peptide-membrane interactions: Molecular dynamics simulation of gramicidin s in a dmpc bilayer. Biophysical Journal. 2000;79(4):1718-1730.
251. Duay SS, Sharma G, Prabhakar R*, et al.* Molecular dynamics investigation into the effect of zinc(ii) on the structure and membrane interactions of the antimicrobial peptide clavanin a. Journal of Physical Chemistry B. 2019;123(15):3163-3176.
252. Prinsloo L, Naidoo A, Serem J*, et al.* Structural and functional characterization of peptides derived from the carboxy-terminal region of a defensin from the tick *Ornithodoros savignyi*. Journal of Peptide Science. 2013;19(5):325-332.
253. Taute H, Bester MJ, Neitz AWH*, et al.* Investigation into the mechanism of action of the antimicrobial peptides Os and Os-c derived from a tick defensin. Peptides. 2015;71:179-187.
254. Malan M. Anti-inflammatory properties of peptides derived from the carboxy-terminal region of a defensin from the tick *Ornithodoros savignyi* 2015.
255. Maritz-Olivier C, Stutzer C, Jongejan F*, et al.* Tick anti-hemostatics: Targets for future vaccines and therapeutics. Trends in Parasitology. 2007;23(9):397-407.
256. Olivier NA. Isolation and cahracterization of antibacterial peptides from hemolymph of the soft tick, *Ornithodoros savignyi* 2013.
257. Charrel RN, Fagbo S, Moureau G*, et al.* Alkhurma hemorrhagic fever virus in *Ornithodoros savignyi* ticks. Emerging Infectious Diseases. 2007;13(1):153-155.
258. Hoogstraal H. Argasid and nuttalliellid ticks as parasites and vectors. Advances in Parasitology. 1985;24(1):135-238.
259. Taute H, Bester MJ, Neitz AW*, et al.* Investigation into the mechanism of action of the antimicrobial peptides Os and Os-c derived from a tick defensin. Peptides. 2015;71(1):179-187.
260. Ramafoko S. The effect of tryptophan end-tagging on the function of antimicrobial peptide, Os-c, derived from the tick *Ornithodoros savignyi* [MSc Biochemistry]. Pretoria: University of Pretoria; 2018.
261. Christensen GD, Simpson WA, Bisno AL*, et al.* Adherence of slime-producing strains of *Staphylococcus epidermidis* to smooth surfaces. Infectious Immunity. 1982;37(1):318-326.
262. Mirzaei R, Alikhani MY, Arciola CR*, et al.* Highly synergistic effects of melittin with vancomycin and rifampin against vancomycin and rifampin resistant *Staphylococcus epidermidis*. Frontiers in Microbiology. 2022;13:6-11.
263. Akbari R, Hakemi Vala M, Hashemi A*, et al.* Action mechanism of melittin-derived antimicrobial peptides, mdp1 and mdp2, de novo designed against multidrug resistant bacteria. Amino Acids. 2018;50(9):1231-1243.
264. Lamichhane TN, Abeydeera ND, Duc A-CE*, et al.* Selection of peptides targeting helix 31 of bacterial 16s ribosomal rna by screening m13 phage-display libraries. Molecules. 2011;16(2):1211-1239.
265. Rautenbach M, Gerstner GD, Vlok NM*, et al.* Analyses of dose–response curves to compare the antimicrobial activity of model cationic α-helical peptides highlights the necessity for a minimum of two activity parameters. Analytical Biochemistry. 2006;350(1):81-90.
266. Shang D, Liu Y, Jiang F*, et al.* Synergistic antibacterial activity of designed trp-containing antibacterial peptides in combination with antibiotics against multidrug-resistant *Staphylococcus epidermidis*. Frontiers in Microbiology. 2019;10(11):1-15.
267. Eucast definitive document e.Def 1.2, may 2000: Terminology relating to methods for the determination of susceptibility of bacteria to antimicrobial agents. Clinical Microbiology and Infection. 2000;6(9):503-508.
268. Foster TJ. Surface proteins of *Staphylococcus epidermidis*. Frontiers in Microbiology. 2020;11(7):1829-1829.
269. Hancock IC, Baddiley J. Biosynthesis of the bacterial envelope polymers teichoic acid and teichuronic acid. The enzymes of biological membranes: Springer US : Boston, MA; 1985. p. 279-307.
270. Neuhaus FC, Baddiley J. A continuum of anionic charge: Structures and functions of alanyl-teichoic acids in gram-positive bacteria. Microbiology and Molecular Biology Reviews. 2003;67(4):686-723.
271. Candeias LP, MacFarlane DPS, McWhinnie SLW*, et al.* The catalysed NADH reduction of resazurin to resorufin. Journal of the Chemical Society, Perkin Transactions 2. 1998(11):2333-2334.
272. Yuwen L, Sun Y, Tan G*, et al.* Mos2@polydopamine-ag nanosheets with enhanced antibacterial activity for effective treatment of *Staphylococcus aureus* biofilms and wound infection. Nanoscale. 2018;10(35):16711-16720.
273. Boukamp P, Petrussevska RT, Breitkreutz D*, et al.* Normal keratinization in a spontaneously immortalized aneuploid human keratinocyte cell line. Journal of Cell Biology. 1988;106(3):761-771.

274. Chacon E, Acosta D, Lemasters JJ. 9 - primary cultures of cardiac myocytes as *in vitro* models for pharmacological and toxicological assessments. In: Castell JV, Gómez-Lechón MJ, editors. *In vitro* methods in pharmaceutical research. San Diego: Academic Press; 1997. p. 209-223.
275. Camproux A-C, Gautier R, Tuffery P. A hidden markov model derived structural alphabet for proteins. Journal of Molecular Biology. 2004;339(3):602.
276. Praprotnik M, Delle Site L, Kremer K. Adaptive resolution molecular-dynamics simulation: Changing the degrees of freedom on the fly. The Journal of Chemical Physics. 2005;123(22):3-4.
277. Marrink SJ, De Vries AH, Mark AE. Coarse grained model for semiquantitative lipid simulations. The Journal of Physical Chemistry B. 2004;108(2):751.
278. Maupetit J, Derreumaux P, Tuffery P. Pep-fold: An online resource for de novo peptide structure prediction. Nucleic Acids Research. 2009;37(1):500-502.
279. Van Gunsteren WF, Berendsen HJ. Computer simulation of molecular dynamics: Methodology, applications, and perspectives in chemistry. Angewandte Chemie International Edition in English. 1990;29(9):1003.
280. Wang C-W, Fischer WB. Rotational dynamics of the transmembrane domains play an important role in peptide dynamics of viral fusion and ion channel forming proteins—a molecular dynamics simulation study. Viruses. 2022;14(4):699.
281. Brooks BR, Bruccoleri RE, Olafson BD*, et al.*: A program for macromolecular energy, minimization, and dynamics calculations. Journal of Computational Chemistry. 1983;4(2):187-212.
282. Brooks BR, Brooks CL, 3rd, Mackerell AD, Jr.*, et al.* Charmm: The biomolecular simulation program. Journal of Computational Chemistry. 2009;30(10):3-5.
283. Kluyver T, Ragan-Kelley B, Pérez F*, et al.* Jupyter notebooks-a publishing format for reproducible computational workflows. 2 ed2016.
284. Anaconda software distribution 2016 [Computer software]. Available from: https://www.anaconda.com/.
285. Maupetit J, Derreumaux P, Tufféry P. A fast method for large-scale de novo peptide and miniprotein structure prediction. Journal of Computational Chemistry. 2010;31(4):726-738.
286. Shen Y, Maupetit J, Derreumaux P*, et al.* Improved pep-fold approach for peptide and miniprotein structure prediction. Journal of Chemical Theory and Computation. 2014;10(10):4745-4758.
287. Thévenet P, Shen Y, Maupetit J*, et al.* Pep-fold: An updated de novo structure prediction server for both linear and disulfide bonded cyclic peptides. Nucleic Acids Research. 2012;40(5):288-293.
288. Tuffery P, Derreumaux P. Dependency between consecutive local conformations helps assemble protein structures from secondary structures using go potential and greedy algorithm. Proteins: Structure, Function, and Bioinformatics. 2005;61(4):734.
289. Tuffery P, Guyon Fdr, Derreumaux P. Improved greedy algorithm for protein structure reconstruction. Journal of Computational Chemistry. 2005;26(5):508.
290. Lilkova E, Petkov P, Ilieva N*, et al.* The pymol molecular graphics system. Schrödinger & LLC; 2015.
291. Schrodinger L. The axpymol molecular graphics plugin for microsoft powerpoint, version 1.8. Schrödinger, LLC, New York, NY. 2015.
292. Schrodinger L. The jymol molecular graphics development component. Version. 2015;1:8.
293. Eisenberg D, Weiss RM, Terwilliger TC*, et al.*, editors. Hydrophobic moments and protein structure. Faraday Symposia of the Chemical Society; 1982: Royal Society of Chemistry.
294. Kraml J, Kamenik AS, Waibl F*, et al.* Solvation free energy as a measure of hydrophobicity: Application to serine protease binding interfaces. Journal of Chemical Theory and Computation. 2019;15(11):5872-5882.
295. Jorgensen WL, Chandrasekhar J, Madura JD*, et al.* Comparison of simple potential functions for simulating liquid water. The Journal of Chemical Physics. 1983;79(2):926-935.
296. Mark P, Nilsson L. Structure and dynamics of the tip3p, spc, and spc/e water models at 298 k. The Journal of Physical Chemistry A. 2001;105(43):9954-9960.
297. Hoover WG. Canonical dynamics: Equilibrium phase-space distributions. Physical Review A. 1985;31(3):1695-1697.
298. Nosé S. A molecular dynamics method for simulations in the canonical ensemble. Molecular Physics. 1984;52(2):255-268.
299. Fossi M, Oschkinat H, Nilges M*, et al.* Quantitative study of the effects of chemical shift tolerances and rates of sa cooling on structure calculation from automatically assigned noe data. Journal of Magnetic Resonance. 2005;175(1):92-102.
300. Lee J, Cheng X, Swails JM*, et al.* Charmm-gui input generator for namd, gromacs, amber, openmm, and charmm/openmm simulations using the charmm36 additive force field. Journal of Chemical Theory and Computation. 2016;12(1):405-413.
301. Manzo G, Ferguson PM, Gustilo VB*, et al.* Minor sequence modifications in temporin b cause drastic changes in antibacterial potency and selectivity by fundamentally altering membrane activity. Scientific Reports. 2019;9(1).
302. Manzo G, Ferguson PM, Hind CK*, et al.* Temporin l and aurein 2.5 have identical conformations but subtly distinct membrane and antibacterial activities. Scientific Reports. 2019;9(1):1-13.

303. Barber KE, Smith JR, Ireland CE*, et al.* Evaluation of ceftaroline alone and in combination against biofilm-producing methicillin-resistant *Staphylococcus aureus* with reduced susceptibility to daptomycin and vancomycin in an *in vitro* pharmacokinetic/pharmacodynamic model. Antimicrobial Agents and Chemotherapy. 2015;59(8):4497-4503.
304. Ciofu O, Rojo-Molinero E, Macià MD*, et al.* Antibiotic treatment of biofilm infections. Apmis. 2017;125(4):304-319.
305. Fujimura S, Sato T, Hayakawa S*, et al.* Antimicrobial efficacy of combined clarithromycin plus daptomycin against biofilms-formed methicillin-resistant *Staphylococcus aureus* on titanium medical devices. Journal of Infection and Chemotherapy. 2015;21(10):756-759.
306. Nis Pedersen J, Skovdal SM, Meyer RL*, et al.* Rifampicin-containing combinations are superior to combinations of vancomycin, linezolid and daptomycin against *Staphylococcus aureus* biofilm infection *in vivo* and *in vitro*. Pathogens and Disease. 2016;74(4):1-7.
307. Shi J, Mao N-F, Wang L*, et al.* Efficacy of combined vancomycin and fosfomycin against methicillin-resistant *Staphylococcus aureus* in biofilms *in vivo*. Public Library of Science One. 2015;9(12):1-14.
308. Odendaal C. Structure-function studies of peptide fragments derived from a defensin of the tick *Ornithodoros savignyi* [Masters Dissertation]. Pretoria: University of Pretoria; 2013.
309. Lovero G, De Giglio O, Montagna O*, et al.* Epidemiology of candidemia in neonatal intensive care units: A persistent public health problem. Annali di igiene: Medicina Preventiva e di Comunità. 2016;28(4):282-287.
310. Viscoli C, Girmenia C, Marinus A*, et al.* Candidemia in cancer patients: A prospective, multicenter surveillance study by the invasive fungal infection group (ifig) of the european organization for research and treatment of cancer (eortc). Clinical Infectious Diseases. 1999;28(5):1071-1079.
311. Lomakin IB, Gagnon MG, Steitz TA. Antimicrobial peptides targeting bacterial ribosome. Oncotarget. 2015;6(22):18744-18745.
312. Shapiro JA, Nguyen VL, Chamberlain NR. Evidence for persisters in *Staphylococcus epidermidis* rp62a planktonic cultures and biofilms. Journal of Medical Microbiology. 2011;60(7):950-960.
313. Mirzaei R, Alikhani MY, Arciola CR*, et al.* Highly synergistic effects of melittin with vancomycin and rifampin against vancomycin and rifampin resistant *Staphylococcus epidermidis*. Frontiers in Microbiology. 2022;13(6):1-19.
314. Bergeron MG, Simard P, Provencher P. Influence of growth medium and supplement on growth of *Haemophilus influenzae* and on antibacterial activity of several antibiotics. Journal of Clinical Microbiology. 1987;25(4):650-655.
315. Jaśkiewicz M, Neubauer D, Kamysz W. Comparative study on anti-*Staphylococcal* activity of lipopeptides in various culture media. Antibiotics (Basel). 2017;6(3):1-11.
316. Choi JH, Jang AY, Lin S*, et al.* Melittin, a honeybee venom-derived antimicrobial peptide, may target methicillin-resistant *Staphylococcus aureus*. Molecular Medicine Reports. 2015;12(5):6483-6490.
317. Maitip J, Mookhploy W, Khorndork S*, et al.* Comparative study of antimicrobial properties of bee venom extracts and melittins of honey bees. Antibiotics. 2021;10(12):1-14.
318. Khemaissa S, Walrant A, Sagan S. Tryptophan, more than just an interfacial amino acid in the membrane activity of cationic cell-penetrating and antimicrobial peptides. Quarterly Reviews of Biophysics. 2022;55:1-22.
319. Basri DF, Xian LW, Abdul Shukor NI*, et al.* Bacteriostatic antimicrobial combination: Antagonistic interaction between epsilon-viniferin and vancomycin against methicillin-resistant *Staphylococcus aureus*. BioMed Research International. 2014;2014(8):1-8.
320. Mull RW, Brennan AA, Russ BR*, et al.* Attenuating the selection of vancomycin resistance among enterococci through the development of peptide-based vancomycin antagonists. American Chemical Society Infectious Diseases. 2020;6(11):2913-2925.
321. Mao C, Wang Y, Yang Y*, et al.* Cec4-derived peptide inhibits planktonic and biofilm-associated methicillin resistant *Staphylococcus epidermidis*. Microbiology Spectrum. 2022;10(6):1-17.
322. Agerberth B, Gunne H, Odeberg J*, et al.* Fall-39, a putative human peptide antibiotic, is cysteine-free and expressed in bone marrow and testis. Proceedings of the National Academy of Sciences. 1995;92(1):197-198.
323. Agier J, Efenberger M, Brzezińska-Błaszczyk E. Cathelicidin impact on inflammatory cells. Central European Journal of Immunology. 2015;40(2):1-11.
324. Zanetti M. Cathelicidins, multifunctional peptides of the innate immunity. Journal of Leukocyte Biology. 2004;75(1):1-10.
325. Liang Y, Wang J-X, Zhao X-f*, et al.* Molecular cloning and characterization of cecropin from the housefly (musca domestica), and its expression in *Escherichia coli*. Developmental and Comparative Immunology. 2006;30(3):249-257.
326. Bernier SP, Lebeaux D, DeFrancesco AS*, et al.* Starvation, together with the sos response, mediates high biofilm-specific tolerance to the fluoroquinolone ofloxacin. Public Library of Science Genetics. 2013;9(1):1-14.

327. Kaplan JB. Antibiotic-induced biofilm formation. The International Journal of Artificial Organs. 2011;34(9):737-751.
328. Kaplan JB, Izano EA, Gopal P*, et al.* Low levels of β-lactam antibiotics induce extracellular DNA release and biofilm formation in *Staphylococcus aureus*. mBio. 2012;3(4):198-212.
329. Popat R, Crusz SA, Messina M*, et al.* Quorum-sensing and cheating in bacterial biofilms. Proceedings of the Royal Society B: Biological Sciences. 2012;279(1748):4765-4771.
330. Vasilchenko AS, Rogozhin EA. Sub-inhibitory effects of antimicrobial peptides. Frontiers in Microbiology. 2019;10:1-13.
331. Mirzaei R, Alikhani MY, Arciola CR*, et al.* Prevention, inhibition, and degradation effects of melittin alone and in combination with vancomycin and rifampin against strong biofilm producer strains of methicillin-resistant *Staphylococcus epidermidis*. Biomedicine and Pharmacotherapy. 2022;147(1):1-15.
332. Gerayelou G, Khameneh B, Malaekeh-Nikouei B*, et al.* Dual antibiotic and diffusible signal factor combination nanoliposomes for combating *Staphylococcus epidermidis* biofilm. Advanced Pharmaceutical Bulletin. 2021;11(4):687-688.
333. Gerke C, Kraft A, Süssmuth R*, et al.* Characterization of the n-acetylglucosaminyltransferase activity involved in the biosynthesis of the *Staphylococcus epidermidis* polysaccharide intercellular adhesin. Journal of Biological Chemistry. 1998;273(29):18586-18593.
334. Gera S, Kankuri E, Kogermann K. Antimicrobial peptides–unleashing their therapeutic potential using nanotechnology. Pharmacology and Therapeutics. 2021;323(9):1-23.
335. Moretta A, Scieuzo C, Petrone AM*, et al.* Antimicrobial peptides: A new hope in biomedical and pharmaceutical fields. Frontiers in Cellular and Infection Microbiology. 2021;11(6):1-26.
336. Narayana JL, Chen J-Y. Antimicrobial peptides: Possible anti-infective agents. Peptides. 2015;72(5):88-94.
337. Schmidtchen A, Ringstad L, Kasetty G*, et al.* Membrane selectivity by w-tagging of antimicrobial peptides. Biochimica et Biophysica Acta (BBA)-Biomembranes. 2011;1808(4):1082-1089.
338. Schmidtchen A, Pasupuleti M, Mörgelin M*, et al.* Boosting antimicrobial peptides by hydrophobic oligopeptide end tags. Journal of Biological Chemistry. 2009;284(26):17587-17589.
339. Drechsler S, Andrä J. Online monitoring of metabolism and morphology of peptide-treated neuroblastoma cancer cells and keratinocytes. Journal of Bioenergetics and Biomembranes. 2011;43(3):275-285.
340. Bai Y, Liu S, Li J*, et al.* Progressive structuring of a branched antimicrobial peptide on the path to the inner membrane target. Journal of Biological Chemistry. 2012;287(32):26606-26617.
341. Tran DP, Tada S, Yumoto A*, et al.* Using molecular dynamics simulations to prioritize and understand ai-generated cell penetrating peptides. Scientific Reports. 2021;11(1):1-9.
342. Krieger F, Möglich A, Kiefhaber T. Effect of proline and glycine residues on dynamics and barriers of loop formation in polypeptide chains. Journal of the American Chemical Society. 2005;127(10):3346-3352.
343. Casier R, Duhamel J. The effect of amino acid size on the internal dynamics and conformational freedom of polypeptides. Macromolecules. 2020;53(22):9811-9822.
344. Barik S. The uniqueness of tryptophan in biology: Properties, metabolism, interactions and localization in proteins. International Journal Molecular Science. 2020;21(22):1-22.
345. Olson CA, Shi Z, Kallenbach NR. Polar interactions with aromatic side chains in α-helical peptides: Ch···o h-bonding and cation−π interactions. Journal of the American Chemical Society. 2001;123(26):6451-6452.
346. Dougherty DA. Cation-pi interactions in chemistry and biology: A new view of benzene, phe, tyr, and trp. Science. 1996;271(5246):163-168.
347. Saravanan R, Li X, Lim K*, et al.* Design of short membrane selective antimicrobial peptides containing tryptophan and arginine residues for improved activity, salt-resistance, and biocompatibility. Biotechnology and Bioengineering. 2014;111(1):37-49.
348. Shao C, Li W, Lai Z*, et al.* Effect of terminal arrangement of tryptophan on biological activity of symmetric α-helix-forming peptides. Chemical Biology and Drug Design. 2019;94(6):2051-2063.
349. Pokhrel R, Bhattarai N, Baral P*, et al.* Molecular mechanisms of pore formation and membrane disruption by the antimicrobial lantibiotic peptide mutacin 1140 electronic supplementary information (esi) available. See doi: 10.1039/c9cp01558b. Physical Chemistry Chemical Physics. 2019;21(23):12530-12539.
350. Heimburg T. Lipid ion channels. Biophysical Chemistry. 2010;150(1-3):2-22.
351. Sani MA, Whitwell TC, Gehman JD*, et al.* Maculatin 1.1 disrupts *Staphylococcus aureus* lipid membranes via a pore mechanism. Antimicrobial Agents and Chemotherapy. 2013;57(8):3593-3600.
352. Santo KP, Irudayam SJ, Berkowitz ML. Melittin creates transient pores in a lipid bilayer: Results from computer simulations. The Journal of Physical Chemistry B. 2013;117(17):3035-3036.
353. Spohn R, Daruka L, Lázár V*, et al.* Integrated evolutionary analysis reveals antimicrobial peptides with limited resistance. Nature Communications. 2019;10(1):9-10.
354. Kim S, Lieberman TD, Kishony R. Alternating antibiotic treatments constrain evolutionary paths to multidrug resistance. Proceedings of the National Academy of Sciences USA. 2014;111(40):14494-14499.
355. Huang J, Hao D, Chen Y*, et al.* Inhibitory effects and mechanisms of physiological conditions on the activity of enantiomeric forms of an α-helical antibacterial peptide against bacteria. Peptides. 2011;32(7):1488-1493.

356. Torcato IM, Huang Y-H, Franquelim HG*, et al.* Design and characterization of novel antimicrobial peptides, r-bp100 and rw-bp100, with activity against gram-negative and gram-positive bacteria. Biochimica et Biophysica Acta (BBA)-Biomembranes. 2013;1828(3):944-955.
357. White SH, Wimley WC. Membrane protein folding and stability: Physical principles. Annual Review of Biophysics and Biomolecular Structure. 1999;28(1):319-365.
358. Nandi PK, Robinson DR. Effects of salts on the free energy of the peptide group. Journal of the American Chemical Society. 1972;94(4):1299-1308.
359. Strömstedt AA, Pasupuleti M, Schmidtchen A*, et al.* Evaluation of strategies for improving proteolytic resistance of antimicrobial peptides by using variants of efk17, an internal segment of ll-37. Antimicrobial Agents and Chemotherapy. 2009;53(2):593-602.
360. Zhao Z, Corredig M. Changes in the physico-chemical properties of casein micelles in the presence of sodium chloride in untreated and concentrated milk protein. Dairy Science and Technology. 2015;95(1):87-99.
361. Younes E. Structural properties of casein miscelles in milk, the effect of salt, temperature, and ph. Int J Biotechnology and Bioengineering. 2017;3(6):202-215.
362. Horne DS. Casein micelle structure: Models and muddles. Current Opinion in Colloid and Interface Science. 2006;11(2-3):148-153.
363. Tang C, Qiu F, Zhao X. Molecular design and applications of self-assembling surfactant-like peptides. Journal of Nanomaterials. 2013;2013(8):1-7.
364. Rhoades E, Gafni A. Micelle formation by a fragment of human islet amyloid polypeptide. Biophysical Journal. 2003;84(5):3480-3487.
365. Elmore DT, Sovago I, Farkas E*, et al.* Amino acids, peptides and proteins: Volume 362007.
366. Zhao Y, Zhang M, Qiu S*, et al.* Antimicrobial activity and stability of the d-amino acid substituted derivatives of antimicrobial peptide polybia-mpi. AMB Express. 2016;6(1):1-11.
367. Berthold N, Czihal P, Fritsche S*, et al.* Novel apidaecin 1b analogs with superior serum stabilities for treatment of infections by gram-negative pathogens. Antimicrobial Agents and Chemotherapy. 2013;57(1):402-409.